CZECH UNIVERSITY OF LIFE SCIENCES PRAGUE

FACULTY OF ECONOMICS AND MANAGEMENT

Department of Systems Engineering

Dissertation Thesis

Computer simulations for economic evaluation of land recovery following radionuclide contamination

Author: Ing. Bc. Anna Selivanova

Supervisor: doc. Ing. Igor Krejčí, Ph.D.

Prague 2025

Acknowledgements

I wish to express my gratitude to my supervisor, doc. Ing. Igor Krejčí, Ph.D., for his invaluable supervision of this dissertation, expert consultations, and support. Sincere thanks are also extended to doc. Ing. Milan Houška, Ph.D. Further appreciation is owed to Tereza Sedlářová-Nehézová and to my family for their unwavering support and encouragement.

Computer simulations for economic evaluation of land recovery following radionuclide contamination

Abstract

The present study is dedicated to the development of a mathematical model for the recovery of areas affected by radionuclide releases. It focuses on mathematical modelling, with particular emphasis on atmospheric dispersion, radiation transport, and decontamination strategies. The recovery model was developed using the System Dynamics approach, which is well-suited for analysing complex systems demonstrating non-linear behaviour, e.g., radioactive decay. The recovery model was created using Vensim software.

The proposed model integrates dosimetry assessments with economic evaluations. It addresses the decontamination of various urban and rural objects, including buildings, agricultural land, forests, and transportation infrastructure. To obtain the necessary input parameters, simulations were performed using specialized tools, namely JRODOS and MCNP. Furthermore, empirical data concerning the demographic structure of Czechia, building characteristics, and land-use were incorporated.

Consequently, a cost-benefit analysis of relevant countermeasures was conducted, reflecting the current conditions in Czechia. In scenarios involving low atmospheric releases, extensive decontamination would not be required. In contrast, in the case of severe accidents, the simulated decontamination outcomes were consistent with empirical data obtained from the Chernobyl and Fukushima clean-up experience. Subsequently, sensitivity analyses were performed to identify critical parameters and relevant thresholds. The results of the study provide a valuable basis for decision-making by policymakers and other stakeholders engaged in emergency preparedness and response.

Keywords: accident, atmospheric dispersion, cost-benefit analysis, decontamination, modelling, Monte Carlo simulations, nuclear power plant, radiation, radionuclide release, System Dynamics.

Počítačové simulace pro ekonomické hodnocení nápravy území po kontaminaci radionuklidy

Abstrakt

Tato studie je věnována vývoji matematického modelu pro nápravu oblastí zasažených úniky radionuklidů. Práce se zaměřuje na matematické modelování se zvláštním důrazem na atmosférickou disperzi, transport záření a dekontaminační strategie. Model nápravy byl vyvinut s využitím metodologie systémové dynamiky, která je vhodná pro analýzu složitých systémů vykazujících nelineární chování, např. radioaktivní přeměnu. Model nápravy byl vytvořen v softwaru Vensim.

Navržený model spojuje dozimetrické výpočty s ekonomickým hodnocením. Model se zabývá dekontaminací různých městských a venkovských objektů, včetně budov, zemědělské půdy, lesů a dopravní infrastruktury. Pro získání nezbytných vstupních parametrů byly provedeny simulace pomocí specializovaných nástrojů, JRODOS a MCNP. Dále byla do modelu zahrnuta empirická data týkající se demografické struktury Česka, charakteristik budov a využití území.

Následně byla provedena analýza nákladů a přínosů příslušných opatření, která odráží aktuální podmínky v Česku. V případě malých atmosférických úniků by rozsáhlá dekontaminace nebyla nutná. Naopak v případě závažných havárií byly simulované výsledky dekontaminace v souladu s empirickými daty získanými při nápravě po haváriích v Černobylu a Fukušimě. Poté byly provedeny analýzy citlivosti za účelem identifikace kritických parametrů a relevantních prahových hodnot. Výsledky této práce poskytují podklady pro rozhodování tvůrců politik a dalších zainteresovaných subjektů zapojených do přípravy na mimořádné události a reakce na ně.

Klíčová slova: atmosférická disperze, cost-benefit analýza, dekontaminace, havárie, jaderná elektrárna, modelování, Monte Carlo simulace, radiace, Systémová dynamika, únik radionuklidů.

Contents

1 Introduction

Practical knowledge in the recovery of areas affected by nuclear/radiation accidents (e.g., the Chernobyl accident, the Fukushima Daiichi accident, or the Kyshtym accident) or nuclear testing (e.g., Bikini Atoll) has led to the development of decontamination techniques, new technologies, and countermeasure strategies (IAEA, 2014, 2013a, 2013b). Various decontamination methods developed during the decommissioning of nuclear facilities or during the remediation of uranium mining areas have also widely contributed to the current state of the art (IAEA, 2013b, 1999).

Based on the collected experience, particularly from the Chernobyl cleanup, elaborate guidelines and handbooks with detailed descriptions of different decontamination techniques have been published. For example, various recovery methods for inhabited areas can be found in the guide "*Generic handbook for assisting in the management of contaminated inhabited areas*" (Nisbet et al., 2010) and in its updated version, which reflects the Fukushima accident, "*UK Recovery Handbooks for Radiation Incidents 2015. Inhabited Areas Handbook*" (Nisbet and Watson, 2018).

After the Fukushima disaster, the U.S. Environmental Protection Agency (U.S. EPA) released a report titled "*Current and Emerging Post-Fukushima Technologies, and Techniques, and Practices for Wide Area Radiological Survey, Remediation, and Waste Management*" (U.S. EPA, 2016). This document outlines the technologies and decontamination methods that were employed. Similarly, the International Atomic Energy Agency (IAEA) has offered a range of recommendations and shared practical experiences on site recovery in numerous publications. Notable among these are e.g., the "*Guidelines for Remediation Strategies to Reduce the Radiological Consequences of Environmental Contamination*" (IAEA, 2013b) or "*Guidelines for Agricultural Countermeasures Following an Accidental Release of Radionuclides*" (IAEA, 1994).

To support decision-making in the recovery of affected areas, various software solutions have been developed to suggest the most appropriate strategies. These solutions have primarily focused on dosimetry estimates, for instance, the ERMIN model (Charnock et al., 2016) and the AgriCP model (Calábria and Morais, 2017). However, these models are integral components of decision support systems (DSS) such as JRODOS (Java-based Real-time On-line Decision Support) and ARGOS (Accident Reporting and Guiding Operational System) (Hoe et al., 2009; Raskob et al., 2011; Schneider et al., 2017). For the economic

evaluation of recovery strategies, the Multi-Criteria Decision Analysis (MCDA) tool is available. It utilizes the outputs from these models for comprehensive assessments (Müller et al., 2020).

1.1 Novelty of the Research

Unlike existing software solutions that separate physics and economic assessments, a unique approach utilizing System Dynamics methods can be adopted. The System Dynamics approach is capable of modeling complex systems with a wide range of parameters and variables that demonstrate non-linear behavior patterns over time (Sterman, 2000). Thus, the novelty of this research resides in applying System Dynamics methods to analyze recovery cases from various perspectives simultaneously.

Due to challenges in acquiring real, detailed input data, the required information was supplemented through simulations using various software solutions. The JRODOS tool was utilized for simulating initial contamination, specifically surface activities (Raskob et al., 2011). Additionally, the Monte Carlo radiation transport MCNP code was employed to calculate conversion coefficients for the surface activity to doses (Goorley et al., 2013). Therefore, this work encapsulates the current state-of-the-art in numerical simulations, covering radiation transport, atmospheric dispersion of contaminants, and associated tasks.

1.2 Funding

The research was supported by the project 2021B0003 “System approach to cost-benefit analysis of recovery of habitation and adjacent areas after a nuclear or radiation accident” of The Internal Grant Agency of Faculty of Economics and Management CZU Prague (IGA FEM).

2 Objectives and Methodology

2.1 Main Aim

The main aim of the work presented is to introduce a comprehensive mathematical model of decontamination that captures the **multidisciplinary** nature of recovering affected areas through the System Dynamics approach. The model is independent of other software solutions; however, it can be coupled with various codes. Both the model and the results derived from simulations aim to contribute to decision-making in the field of radiation protection.

2.2 Objectives

The research conducted within the dissertation focuses on developing resource materials for planning recovery efforts after large-scale radioactive contamination under the conditions of the Czech Republic. Partial objectives of the research are:

1) **Affected areas**. The specific goal is to assess potential surface deposition following a radionuclide release from a selected nuclear power plant in the Czech Republic.
2) **Mathematical Model**. The specific objective is to develop a mathematical model of recovery, validate it, and design decontamination scenarios.
3) **Economic analyses**. By simulating the proposed scenarios, cost-benefit and sensitivity analyses will be conducted. Scenarios will then be compared based on these assessments. The simulation results will also be compared with knowledge from the Chernobyl and Fukushima Daiichi accidents.

2.3 Methodology

This chapter outlines the methodology used in the overall research, including the development of the mathematical model and the preparation of its inputs. The research tasks were segmented into distinct steps, which are explained in the paragraphs that follow. A flow chart illustrating the methodology is presented in Fig. 1. As shown in the diagram, three software programs were utilized: JRODOS (Raskob et al., 2011), MCNP6.1 (Goorley et al., 2013) and Vensim (Ventana Systems, 2023a). Independent inputs included population data, information about buildings, and the input costs of items necessary for decontamination.

The mathematical model of recovery was developed using Vensim (Ventana Systems, 2023a). Simulations of proposed decontamination scenarios were also conducted using this tool. A substantial amount of input data for the Recovery model was obtained from simulations performed in JRODOS, e.g., the extent of contaminated areas and surface contamination levels (Ievdin et al., 2019). Thereafter, a set of simulation tasks was created for various conditions, including different accident scenarios and meteorological conditions, utilizing automation scripts. The results of these simulations were subsequently assessed and prepared for use as inputs for the Recovery model.

Several input parameters, i.e., the required conversion coefficients, were obtained from Monte Carlo simulations performed using the MCNP (Monte Carlo N-Particle Transport) code (Goorley et al., 2013). In the Monte Carlo simulations, a three-dimensional representation of anticipated geometries for hypothetical radiation sources, i.e., selected types of contaminated objects, was developed. Consequently, the required conversion coefficients for the proposed conditions were derived from the Monte Carlo simulations.

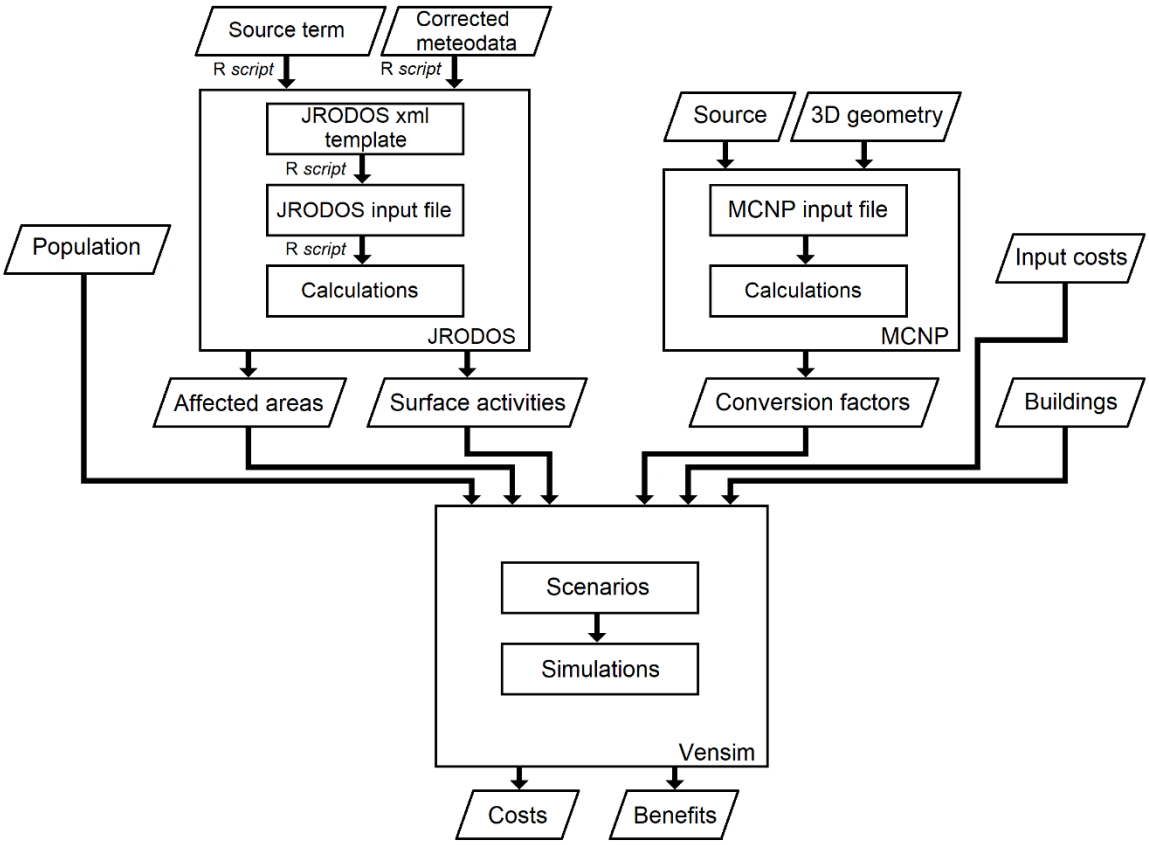

Fig. 1. Flow chart of simulations and analyses (source: Selivanova et al., 2025: 3)

2.3.1 Initial Release

In order to prepare input data for the recovery model, assessments of input contamination (i.e., surface activities) and affected areas were required. Such estimations were performed using the JRODOS tool (Raskob et al., 2011).

For simulations in JRODOS, input data such as meteorological information and the source term were required (Ievdin et al., 2019). Meteorological data for Czechia can be provided, e.g., by the Czech Hydrometeorological Institute (CHMI, 2022) or by the NOAA Operational Model Archive and Distribution System (NOMADS) (Rutledge et al., 2003). Detailed weather data from CHMI, including historical records for Nuclear Power Plant Dukovany, have already been analyzed and used in JRODOS simulations of long-term discharges (Selivanova et al., 2025, 2022b).

The source term can be defined as the amount of radioactivity released following radiation or nuclear accidents. The source term parameters include the radionuclide composition, its chemical and physical form, the release mode (separate puffs or a continuous release), the release height, duration, and other factors (IAEA, 2008a; Pappas et al., 2014).

The source terms can be calculated using the severe accident code MELCOR (Methods of Estimation of Leakages and Consequences of Releases) if a detailed description of the reactor is available (Di Giuli et al., 2022; Humphries et al., 2017). The calculated source term can then be utilized in JRODOS simulations (Selivanova et al., 2022a). In the absence of detailed information about the release or reactors, the JRODOS library of source terms can be used for indicative assessments (Ievdin et al., 2019; Raskob et al., 2011).

Iodines

Source terms can include iodine isotopes (IAEA, 2012, 2008a; Khalil et al., 2006). Depending on the chemical form (e.g., aerosol CsI, organic CH_3I or HI, and elemental I_2), iodines demonstrate varying behaviors concerning their contribution to dry and wet deposition, as well as deposition velocity (IAEA, 2012; Kim et al., 2020). Therefore, information regarding the chemical form can influence dose assessments (Kim et al., 2020).

Considering accidents in nuclear reactors, iodines released from the fuel are predominantly expected in the gaseous form as elemental iodines. Upon interacting with cesium in the reactor or hydrogen in the atmosphere, iodines can form CsI (aerosol form) or

HI (organic form). Organic iodines are less susceptible to removal processes (e.g., washout) compared to elemental iodines or aerosols (IAEA, 2008a; Kim et al., 2020).

Reports by the U.S. Nuclear Regulatory Commission (U.S. NRC, 2023, 2003) have specified iodine fractions; however, these data differ significantly. In the case of releases of iodine from the reactor coolant system (RCS) into the containment, as well as from the fuel gap and pellets, approximately 5% corresponds to aerosols, 91% is attributed to elemental iodine, and 4% to organic iodine in accordance with Regulatory Guide 1.195 (U.S. NRC, 2003). A similar distribution is anticipated for releases from fuel pins in fuel handling accidents (FHAs) and from fuel pins through the RCS during design basis accidents (DBAs), excluding FHAs or loss-of-coolant accidents (LOCAs).

According to Regulatory Guide 1.183 (U.S. NRC, 2023), 95% of iodine is attributed to aerosols (CsI), 4.85% corresponds to elemental iodine, and 0.15% to organic iodine for releases from the RCS into the containment and from the fuel gap/pellets. However, the iodine fractions may be altered during transport from the fuel, as noted in both the current and previous versions of the guide (U.S. NRC, 2023, 2003).

Regarding source terms in JRODOS, the system's library already includes information on iodine fractions. In cases where such information is missing, e.g., when creating custom source terms, the default setting assigns 100% of iodine to elemental iodine.

Due to such significant differences in data regarding iodine composition in general, as well as due to the short half-lives of iodine isotopes (particularly in comparison to the typical durations of recovery following large-scale accidents), iodine isotopes were excluded from this study, although some estimates are available. Nevertheless, iodine isotopes can significantly contribute to the exposure of inhabitants and workers in the short term following the initial release. In contrast, cesium isotopes are more relevant over the long term due to their greater environmental persistence and sustained contribution to exposure.

2.3.2 Site Selection

Considering Czech nuclear power plants (NPP), four units of VVER-440/V213 (NPP Dukovany) and two units of VVER-1000/V320 (NPP Temelín) are currently operated (ČEZ Group, 2023a). In JRODOS, eleven design basis accident (DBA) source terms for the VVER-440/V213 type of reactors are described, while for VVER-1000/V320, there is a limited number of source terms.

Anticipating severe (SEV) accidents, for VVER-440/V213, nine source terms are added to the JRODOS library. For reactors of the same type as in NPP Dukovany, significantly more detailed information is available. Additionally, the construction of new units in Dukovany is being planned (ČEZ Group, 2022), which may lead to the need for new or updated safety analyses.

Therefore, the location of the release at NPP Dukovany in Czechia was chosen based on the available input data: the source term (released radionuclides), detailed historical meteorological conditions from CHMI, and due to the need for new safety analyses.

2.3.3 Dosimetry

In order to calculate irradiation of inhabitants in the vicinity of the NPP, dose assessments were prepared. Consequently, surface activities were converted to dose rates (Ahn et al., 2014; Andersson et al., 2002). Considering various surface types, different equations were utilized that include different weathering rates and different conversion factors (Andersson et al., 2002; Andersson and Roed, 2006).

In the case of unknown conversion factors, the missing information was obtained using Monte Carlo simulation in the MCNP6.1 radiation transport code (Goorley et al., 2013) for simplified geometries of contaminated objects, where the exponential distribution of activities in the upper layer of the object was anticipated (UNSCEAR, 2000). The obtained raw data additionally required subsequent recalculations (ICRP, 1997). Then, the dose rates were integrated over a selected period, employing the dynamic simulations in the Vensim software (Ventana Systems, 2023a).

2.3.4 Validation

In order to validate dosimetry calculations, the results of simulations conducted using Vensim software (Ventana Systems, 2023a) were compared with analytical assessments based on empirical formulas (Andersson and Roed, 2006). Therefore, the analytical integration of dose accumulation in simplified scenarios should yield results very similar to those obtained with Vensim. Small deviations from the reference analytical integration (< 1%) could be accepted due to rounding during calculations in Vensim.

Another method to validate the model involved tracking the dose rate changes over time to determine whether they correspond with the implemented dose rate reduction coefficient/decontamination factor (Nisbet et al., 2010; U.S. EPA, 2016).

In addition, a comparison between the simulations and a simplified approach was also conducted. By employing the simplified approach, doses were derived from surface activities using conversion factors for different time intervals as provided in published tables, i.e., without the need for integrations (Nisbet et al., 2010). However, in this case, more significant differences could be expected.

2.3.5 Dimensional Analysis

To ensure dimensional consistency and to identify potential errors, missing data, or mistyped characters in the equations, the *Units Check* feature was utilized. The *Units Check* is an inbuilt diagnostic tool in Vensim software that allows for quick and effective model evaluation at any time (Ventana Systems, 2023b). This test also provides information regarding the variables used in the model, indicating whether the corresponding units of measurement are specified.

2.3.6 Countermeasures

The identification of decontamination techniques applicable to urban and agricultural areas was essential for the selection of suitable countermeasures. Parameters such as decontamination effectiveness expressed as decontamination factors (DF) or dose rate reduction (DRR), working speeds, waste production, and the required personnel and technical resources were assessed (Nisbet et al., 2010; Severa and Bár, 1985; U.S. EPA, 2016). Additionally, the limitations of selected countermeasures were examined, including changes in decontamination effectiveness over time from the initial contamination and the impact of weather conditions on the applicability of different techniques (Nisbet et al., 2010; U.S. EPA, 2016). This investigation provided a theoretical basis for the creation of recovery scenarios. Subsequently, the chosen countermeasures were integrated into decontamination scenarios in accordance with general recommendations.

2.3.7 Population

The NPP Dukovany emergency planning zone (EPZ) is divided into 16 regular sectors. The outer radius of the EPZ is 20 km, with inner rings having radii of 5 km and 10 km (Amec Foster Wheeler s.r.o., 2017; Kubanyi et al., 2008). Using the results of simulations in JRODOS, the affected sectors and inner segments of the EPZ were assessed.

Thereafter, information about the inhabitants in the corresponding localities was required. This information was provided by the Czech Statistical Office (CZSO, 2024). The demographic data were utilized to estimate the collective effective doses of irradiated inhabitants, which served as the basis for a financial expression of benefits and for the subsequent cost-benefit analyses of proposed scenarios (ICRP, 2006).

2.3.8 Buildings

To propose appropriate decontamination scenarios in the EPZ, information about buildings and their parameters (e.g., building materials, number of floors, spatial dimensions, etc.) in the affected localities was required. The most typical parameters were assessed, along with their range. These source data were extracted from the database of the State Administration of Land Surveying and Cadastre (ČÚZK, 2022).

2.3.9 Costs

To assess the total costs of recovery, it was necessary to estimate the costs of items required for decontamination. The total costs included labor costs, fuel and material consumption, costs of waste bags and other auxiliary tools. Wear-off of fixed capital was also factored into the assessments, following the methodology of Roed et al. (1998).

Due to the rapid increase in the inflation rate, all costs were adjusted for inflation (CZSO, 2022; Peníze.cz, 2023). During the model development, additional attention was given to the creation of the waste handling sub-model, following available recommendations and clean-up expertise (Andersson et al., 2000).

2.3.10 Analyses

Within the analyses of the Recovery model, a sensitivity analysis was conducted to identify critical parameters. To estimate the applicability of the scenarios, thresholds of selected parameters were determined and compared with published data. For each scenario, applicability was evaluated using cost-benefit analysis (ICRP, 2006; SÚJB, 2016).

3 Limitations of the Study

Due to the overall complexity of the study, the scope of the research has been delimited, with certain tasks to be addressed in future studies. The research itself was therefore guided by the availability of source data, necessitating the simplification or omission of several aspects as required (e.g., neglecting of iodines during the recovery). Consequently, the methods employed may differ slightly from the recommendations in Czech legislation, e.g., in the parameters for the representative person (SÚJB, 2016).

It should be emphasized that this study does not address early protective measures such as sheltering, evacuation, or the implementation of iodine prophylaxis. Furthermore, the implementation of temporary relocation or permanent resettlement was beyond the scope of this research. Additionally, restrictions on food and water consumption/production were excluded from the study, as was the management of potentially or actually contaminated livestock.

The main focus of the presented research aligns with tasks within the framework of probabilistic safety assessment (PSA). For example, in Level 3 PSAs, evaluations of the effectiveness of remedial countermeasures, associated economic aspects, risk assessments to the public, and environmental impacts should be conducted (IAEA, 1996). Consequently, the analyses performed and results obtained in this study could potentially contribute to future Level 3 PSAs. However, under current Czech legislation, Level 3 PSAs have not yet been addressed or required (SÚJB, 2010).

Another limitation is related to the scale of the estimates. In this study, the recovery estimates were conducted only for the EPZ of NPP Dukovany due to the availability of detailed source data. Regarding dosimetry assessments, the proposed recovery model assumes external irradiation only. Internal irradiation (i.e., ingestion and inhalation) has not yet been included in the model due to the lack of input data. The model's limitations also pertain to waste management. While the handling of solid waste has been successfully implemented, the management of liquid waste has been omitted due to a lack of information on current Czech conditions.

Additionally, the management and decontamination of contaminated water bodies (e.g., ponds, rivers, lakes, and others) were excluded from the study due to insufficient input data.

The final limitation is related to the assessment of initial contamination following different nuclear or radiation accidents. The source terms employed in the evaluations do

not fully correspond to the Design Extension Conditions (DEC). DECs are categorized into two groups: DEC-A (prevention of severe fuel damage) and DEC-B (mitigation after severe fuel damage) (WENRA, 2014). Nevertheless, all of the mentioned limitations of the present study can be addressed as independent tasks in future research.

4 Research Gap Identification

To identify research gaps, databases such as the Web of Science (WOS) and the System Dynamics Bibliography (SDB) were utilized (Clarivate, 2023; System Dynamics Society, 2023), using keywords like “System Dynamics”, “nuclear”, “decontamination” and others.

4.1 Web of Science

Using keywords “System Dynamics” and “nuclear” together, fewer than 100 records were found in the WOS database. The most relevant results were contributions by Selivanova (Selivanova, 2022, 2021, 2020a) in conference proceedings, which originated from the presented research. These contributions focused on the development of the mathematical model of recovery, including the incorporation of new decontamination strategies following nuclear/radiation accidents, various model improvements, and testing. The remaining records primarily addressed nuclear energy issues. For example, the restart of approval of new coastal nuclear projects and its economic impacts on nuclear power development in China were simulated by Guo et al. (2016).

After the Fukushima Daiichi accident, nuclear energy issues in Belgium occurred (Kunsch and Friesewinkel, 2014). According to Kunsch et al. (2014), the vast majority of domestically produced electricity was generated by nuclear power plants. Therefore, the Belgian nuclear phase-out could potentially lead to urgent economic challenges due to the lack of capacity-replacement plans (Kunsch and Friesewinkel, 2014). The development of electric power in Taiwan was analyzed by Hsiao et al. (2018), while nuclear energy issues in Singapore were addressed by Chia et al. (2015).

Other results of the survey were related to additional analyses for NPPs. The System Dynamics approach was applied, for example, to the following cases: analyses of human failure events (J. Liu et al., 2021) and safety assessments for a new type of cooling systems (Kim and Woo, 2017). Another topic successfully addressed using System Dynamics methods was related to nuclear/radioactive waste (Ju and Hwang, 2018) and to the nuclear fuel cycle, including studies of the global uranium market (Rooney et al., 2015).

Ju et al. (2018) analyzed the probability of human intrusion into a deep geological repository containing radioactive waste or spent nuclear fuel. Rooney et al. (2015) simulated the effects on uranium prices and the uranium mining industry. Additionally, some papers were dedicated to simulations of environmental impacts, such as modeling the Fukushima

accident (Woo, 2014) or investigating climate change due to the use of nuclear energy (Woo, 2018).

Using the keyword “decontamination” and “System Dynamics” together, three papers focused on decontamination were identified (Selivanova, 2022, 2021, 2020a), all of which are directly connected with the current thesis. Subsequently, a survey using the keywords “System Dynamics” and “radioecology” was conducted, resulting in only one work devoted to modeling of food chains after severe nuclear accidents and to assessing the related radiation risks (Kang and Jae, 2008).

For completeness, keywords such as “contaminated sites” and “System Dynamics” were used as a new search query. This search revealed three records related to contaminated groundwater issues addressed using System Dynamics methods. For example, assessments of human health and ecological risks due to releases of contaminants into groundwater and soil were conducted by McKnight et al. (2010; 2013). Groundwater remediation scenarios and their sustainability were investigated by Naseri-Rad et al. (2022).

According to WOS (Clarivate, 2023), the System Dynamics approach has not been widely applied to cases of decontamination following radiological accidents.

4.2 System Dynamics Bibliography

Exploring the SDB database, approximately 40 records were identified with titles or descriptions including the word “nuclear”. Most of these records focused on energy market cases (Bennett et al., 2017; Taylor et al., 2012; Wade et al., 2006), nuclear fuel cycle issues (Jacobson et al., 2010; Rooney et al., 2015) or problems related to radioactive waste (Glazner et al., 2011; Woodham et al., 2016). For the word “radioactive”, only four records were found. The most relevant record was a conference contribution on decontamination, which originated from the current work (Selivanova et al., 2022c).

The remaining three publications were dedicated to radioactive waste issues (Cave et al., 2016; Maloney and Sterman, 1982; Woodham et al., 2016). Therefore, almost no records on recovery and decontamination of affected areas after nuclear/radiation were found in the SDB database (System Dynamics Society, 2023). Consequently, System Dynamics methods have not been frequently utilized to analyze and to solve decontamination or radiological emergency cases, which is consistent with the survey results from the WOS database (Clarivate, 2023).

5 Literature Review

5.1 Czech NPPs

In Czechia, two nuclear power plants (NPP), Dukovany and Temelín, with a total of six nuclear power reactors, are currently in operation (IAEA, 2021a). Both NPPs are operated by the ČEZ Group (2023a). The NPPs accounted for approximately 40% of the total electricity production in Czechia in 2020 (IAEA, 2021a). At Temelín, two production units with VVER-1000/V320 type pressurized-water reactors (Water-Water Energetic Reactor) are located (ČEZ Group, 2023b). The total installed power at NPP Temelín is 2110 MWe (IAEA, 2021a). NPP Dukovany consists of four production units with VVER-440/V213 type reactors (ČEZ Group, 2023c). The overall installed capacity at NPP Dukovany is 2040 MWe (IAEA, 2021a).

According to the IAEA Advisory Mission in 2021, both NPPs passed the inspection, and nuclear security in Czechia is well-established (SÚJB, 2021). The probability of any significant accidents at both NPPs is **extremely low** (IAEA, 2021a). Therefore, the proposed model for the recovery of affected areas after radiation or nuclear accidents, as presented in the current work, can be applied to Czech conditions **for demonstration purposes only**. Additionally, ČEZ is planning the construction of new units at NPP Dukovany (ČEZ Group, 2022), which will require various studies and analyses. For example, estimates of new potential sampling sites in the Emergency Planning Zone of NPP Dukovany were presented in a study on routine discharges by Selivanova et al. (2022b).

5.2 Probabilistic Safety Assessments

Probabilistic safety assessments (PSA) methods and techniques are utilized within the safety evaluations of nuclear power plants. PSA provide comprehension of the safety aspects and performance of nuclear power plants. PSA can be used for assessments of postulated accidents and potential environmental impacts. The PSA study includes the identification of risk contributors and possibilities for risk reduction. It provides a consistent framework for the decision-making process (IAEA, 1996).

PSA should be conducted for all nuclear facilities that include a nuclear reactor, including research facilities. In Czechia, the PSA study should describe and model the actual conditions and the current state of a specific nuclear power plant (SÚJB, 2010).

Considering international practice, three levels of PSA have been defined (IAEA, 1996; SÚJB, 2010):

- Level 1: assessments of nuclear power plant failures from the perspective of core melting or nuclear fuel damage at the nuclear power plant. It also includes determination of core damage frequency.
- Level 2: assessments of the containment response to accident scenarios from Level 1, including the determination of the frequency of radionuclide releases outside the containment and hermetically sealed areas of the nuclear power plant. This PSA additionally evaluates their qualitative and quantitative characteristics.
- Level 3: assessments based on the results of Level 2, including the evaluation of the consequences of radionuclide releases outside the NPP premises and their impact on the population and the environment. Level 3 also includes assessments of risks to the public.

Level 1 PSA has already been conducted at most nuclear power plants worldwide. Level 1 PSA identifies weaknesses in the plant design and methods to prevent core damage. Core damage is the event that precedes accidents involving significant radionuclide releases, which may have potential health and environmental consequences (IAEA, 1996). The license holder of a given nuclear facility is responsible for the completeness, quality, and conclusions of the PSA. The PSA is prepared, documented, and maintained in accordance with the license holder's quality management system (SÚJB, 2010).

Level 2 PSA provides additional analyses of accident sequences leading to core damage. It focuses on the severity of radioactive releases, weaknesses in the containment design, and improvements in the mitigation and management of severe accidents (IAEA, 1996).

Level 3 PSA provides insights into accident prevention and mitigation measures. It includes assessments of impacts on public health, impacts of contamination of land, air, water, and food, as well as economic impacts (IAEA, 1996). Level 3 PSA also estimates the effectiveness of emergency response planning and off-site accident management. So far, Level 3 PSA has been developed for only a few nuclear power plants, in Korea and the Netherlands (NEA, 2018). Level 3 PSA is not currently relevant in Czechia (SÚJB, 2010).

5.3 Phases of Emergency Responses

In the context of emergency responses to nuclear or radiation accidents, three general phases can be specified (DHS, 2008; FEMA, 2011; NCRP, 2014):

- *Short-term/early* (hours–days): This phase involves emergency response actions aimed at protecting the public and workers, activation of recovery organizations, assessments of the damage extent, and the provision of first aid. This phase is sometimes referred to as the "emergency" phase (NCRP, 2014; NRC, 2014);
- *Intermediate* (weeks–months): During this phase, the radiation source is under control or radionuclide releases have ceased. Protective actions are based on the monitoring of radioactivity levels (DHS, 2008).
- *Long-term/late (*months–years); This phase is sometimes defined as "recovery" and focuses on the revitalization and repopulation of affected areas (NCRP, 2014; NRC, 2014).

Additionally, a preparedness or planning phase is often defined as an ongoing phase before the incident (FEMA, 2011). All phases tend to overlap during the course of the incident (FEMA, 2011; NCRP, 2014), as illustrated in Fig. 2. However, the definitions and descriptions of these phases may vary to some extent across relevant publications, e.g., in terminology, duration, etc. (NCRP, 2014).

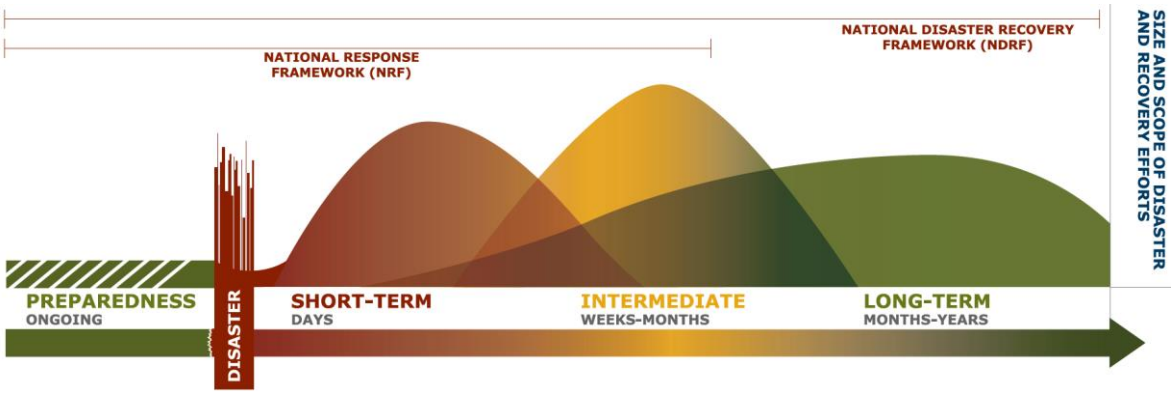

Fig. 2. Recovery continuum – overlapping of phases (source: FEMA, 2011: 8)

Moreover, alternative approaches to accident management exist. For example, the German Federal Office for Radiation Protection – Bundesamt für Strahlenschutz (BfS, 2023) defines five phases: uncertain situation, pre-release phase, release phase, transition phase (post-emergency phase), and long-term post-accident phase. These phases can be aggregated into two broader phases: the urgency phase and the post-accident phase. The urgency phase, lasting several hours to days, involves early protective measures such as

iodine prophylaxis, sheltering, and evacuation. The post-accident phase pertains to the period following the release of radioactivity. This phase includes the preparation and implementation of recovery countermeasures and can extend for decades (BfS, 2023).

According to the National Council on Radiation Protection and Measurements (NCRP, 2014), the recovery phase encompasses all response actions that are coordinated to achieve the overall recovery objectives. These actions should be proposed in accordance with established criteria to reduce or eliminate radiation exposure to the population. The recovery process must consider aspects such as public health and safety, key public services, economic conditions of the affected area, and the restoration of critical infrastructure.

5.4 Response to Nuclear and Radiation Accidents

In response to nuclear or radiation accidents, urgent protective actions should be taken immediately to protect the public. These actions primarily include sheltering, evacuation, and iodine prophylaxis (if radioactive iodine is released) (IAEA, 2007). The implementation of early countermeasures is determined by dose levels[1]. In Czechia, the criteria for implementing urgent protective actions are as follows (SÚJB, 2016):

- Sheltering: averted effective dose of 10 mSv/2 days,
- Evacuation: averted effective dose of 100 mSv/7 days,
- Iodine prophylaxis: averted committed dose equivalent to the thyroid of 100 mSv,

where the averted dose is the dose saved up as a result of the implementation of the protective action (ICRP, 2007).

Considering longer-term countermeasures, measures such as the relocation of residents or restrictions on the consumption of food, feed, and drinking water may be required (SÚJB, 2016):

- Restriction on the use of food, water, and feed contaminated with radionuclides: averted annual committed effective dose exceeds 1 mSv.
- Relocation: effective dose exceeds 20 mSv per 12 months after return of residents to the affected area.

Other sources mention not only temporary relocation but also permanent resettlement as a longer-term protective measure (IAEA, 1993). Permanent resettlement may be required

[1] Dose levels are expressed in millisieverts (mSv). Sievert (Sv) is the unit used to measure effective, equivalent, and operational doses. It quantifies the irradiation of biological tissues (ICRP, 2007).

in cases of high contamination levels with long-lived radionuclides when effective doses remain excessively high. Such a protective action would require significant resources to cover the transportation of inhabitants and their property, the construction of new infrastructure, and compensation for income losses incurred during the development of new infrastructure. The generic intervention levels for permanent resettlement are (IAEA, 1993):

- Averted effective dose of 1 Sv in a lifetime,
- Averted effective doses ≥ 10 mSv/month persisting for more than 1–2 years.

In the case of radioactive contamination of food, the maximum permitted levels of specific activities are summarized in Table 1 (EURATOM, 2016).

Table 1. Maximum permitted levels in food (source: EURATOM, 2016: 8)

Isotopes	Infant food (Bq/kg)	Dairy produce and liquid food (Bq/kg)	Other food except minor food (Bq/kg)
Sum of strontium isotopes, Sr-90	75	125	750
Sum of iodine isotopes, I-131	150	500	2 000
Sum of alpha-emitting isotopes of plutonium/transplutonium elements, Pu-239 and Am-241	1	20	80
Sum of all other nuclides of half-life ≥10 days, Cs-134 and Cs-137	400	1 000	1 250

5.5 Classification of Radiation and Nuclear Accidents

Major nuclear/radiation accidents may lead to significant radionuclide releases, contamination of large areas, and public exposure, necessitating various countermeasures and decontamination strategies (NCRP, 2014; Nisbet et al., 2010; U.S. EPA, 2016). These accidents can occur at nuclear facilities (e.g., the Chernobyl accident, the Fukushima Daiichi accident, or the Kyshtym accident) or involve abandoned or stolen medical or industrial sources (e.g., the Goiânia accident). Detailed information about these accidents and the recovery or clean-up strategies implemented in the affected areas is provided in the following paragraphs.

Radiological and nuclear terrorism should also be considered, including the potential use of nuclear weapons (cause an explosion through an uncontrolled chain reaction), radiological dispersal devices (RDDs) (which contain radioactive material but do not involve a nuclear detonation, also known as “dirty bombs”), or improvised nuclear devices (INDs) (which contain nuclear or fissile material and cause a nuclear explosion) (Bland et al., 2018; NCRP, 2014). Such incidents can also result in surface contamination and will necessitate

appropriate countermeasures, as well as urgent protective actions. However, no accidents involving RDDs have been reported to date (Bland et al., 2018).

Another type of radiological threat involves the use of radiological exposure devices (REDs), where radioactive material is not dispersed but hidden, causing inconspicuous irradiation of victims (Bland et al., 2018). For example, Vladimir Kaplun, a Russian businessman, was killed by irradiation from a radioactive source placed in his chair in 1993. Another case is that of Alexander Litvinenko, who was poisoned with ^{210}Po in 2006 (Bland et al., 2018; Harrison et al., 2017). However, unintended ^{210}Po contamination of some buildings in London occurred, leading to response actions such as monitoring these locations and conducting urine sampling of potentially contaminated individuals (Ham, 2009).

5.5.1 INES Scale

For the classification of nuclear and radiological events, the International Nuclear and Radiological Event Scale (INES) is utilized (IAEA, 2013c). INES is intended as a tool to consistently share information about nuclear and radiological events with the public at local, national, and international levels. The scale applies to events in the civil nuclear industry as well as those associated with the use, transport, and storage of radiation sources. However, military applications and malicious irradiation are beyond the scope of this scale (IAEA, 2013c).

The INES scale is logarithmic and describes the safety significance of events, which are divided into levels 1 to 7 according to increasing severity (IAEA, 2013c). The levels are as follows: anomaly, incident, serious incident, accident with local consequences, accident with wider consequences, serious accident, and major accident. Level 1 corresponds to an “anomaly”, while Level 7 corresponds to a “major accident”. Level 0, or “below scale” refers to events without safety significance. A general description of the INES levels (IAEA, 2008b) is presented in Table 2. Examples of the INES rankings of selected nuclear and radiation accidents can be found in Paragraph 5.6.

INES considers three fields of impact: people and the environment (e.g., amounts of released radioactive material and exposure), radiological barriers and controls at facilities (e.g., damage to fuel), and defense in depth (e.g., common cause failures, issues with procedures or safety culture).

The INES scale should not be used within the planning of the emergency responses, as well as the implemented emergency actions should not be used for the INES ranking (IAEA,

2013c). Therefore, the INES classification is applied **retrospectively** (ENSI, 2011; Webb et al., 2006). IAEA maintains an online system, USIE (Unified System for Information Exchange in Incidents and Emergencies), for international communication about nuclear and radiological events (IAEA, 2010). INES national officers, designated by the Member States, share relevant information on this web portal (IAEA, 2013c, 2010).

Table 2. General description of INES levels (source: IAEA, 2013: 3)

INES Level	People and Environment	Radiological Barriers and Control	Defense-in-Depth
Major Accident Level 7	Major release of radioactive material with widespread health and environmental effects requiring implementation of planned and extended countermeasures	–	–
Serious Accident Level 6	Significant release of radioactive material likely to require implementation of planned countermeasures	–	–
Accident with Wider Consequences Level 5	• Limited release of radioactive material likely to require implementation of some planned countermeasures • Several deaths from radiation	• Severe damage to reactor core • Release of large quantities of radioactive material within an installation with a high probability of significant public exposure. This could arise from a major criticality accident or fire	–
Accident with Local Consequences Level 4	• Minor release of radioactive material unlikely to result in implementation of planned countermeasures other than local food controls • At least one death from radiation	• Fuel melt or damage to fuel resulting in more than 0.1% release of core inventory • Release of significant quantities of radioactive material within an installation with a high probability of significant public exposure	–
Serious Incident Level 3	• Exposure in excess of ten times the statutory annual limit for workers • Non-lethal deterministic health effect (e.g., burns) from radiation	• Exposure rates of more than 1 Sv/h in an operating area • Severe contamination in an area not expected by design, with a low probability of significant public exposure	• Near accident at a nuclear power plant with no safety provisions remaining • Lost or stolen highly radioactive sealed source • Misdelivered highly radioactive sealed source without adequate procedures in place to handle it
Incident Level 2	• Exposure of a member of the public in excess of 10 mSv • Exposure of a worker in excess of the statutory annual limits	• Radiation levels in an operating area of more than 50 mSv/h • Significant contamination within the facility into an area not expected by design	• Significant failures in safety provisions but with no actual consequences • Found highly radioactive sealed orphan source, device or transport package with safety provisions intact • Inadequate packaging of a highly radioactive sealed source
Anomaly Level 1	–	–	• Overexposure of a member of the public in excess of statutory annual limits • Minor problems with safety components with significant defense-in-depth remaining • Low activity lost or stolen radioactive source, device or transport package

5.5.2 Radiation Hazard Scale

In addition to the INES Scale, which is solely dedicated to accidents in civilian applications of ionizing radiation, another approach has been developed. The Radiation Hazard Scale, prepared by the U.S. Centers for Disease Control and Prevention (CDC, 2021) and covers all radiation emergencies, including, for example, an explosion of an RDD. Similar to the INES Scale, the Radiation Hazard Scale serves as a communication tool during radiation emergencies.

The Radiation Hazard Scale is specifically applicable to radiation emergencies and to short-term exposures. The Scale outlines the immediate impacts of accidents, with its categories varying based on the locations of inhabitants (CDC, 2021). A description of the categories is provided in Table 3. The categories utilize suggested dose levels[2].

Table 3. General description of Radiation Hazard Scale categories (source: CDC, 2021)

Category	Impacts	Suggested Dose Guide
5	Death may occur in days to weeks	2 Gy
4	Increased risk of radiation sickness, but death is not likely (symptoms may appear in hours to days)	1 Gy
3	Increased risk of cancer later in life (symptoms may take decades to appear)	20 mSv
2	Above the range of normal, everyday radiation levels, but no health effects expected	Location specific
1	Within the range of normal, everyday radiation levels	–

5.6 Selected Nuclear and Radiation Accidents

This chapter summarizes selected nuclear and radiation accidents that resulted in significant radionuclide dispersion and widespread contamination of large territories. Various aspects, including the quantities of radioactive material released, affected areas, surface deposition of radionuclides, protective measures, decontamination techniques, countermeasures, and the resulting radioactive waste, have been considered.

The selected decontamination techniques are described in detail in subsequent chapters. Archived photographs of certain countermeasures are included to illustrate the scale of the impacts of these nuclear and radiation accidents.

[2] Gray (Gy) is a defined unit of doses absorbed in matter (ICRP, 2007).

Based on these historical data and the corresponding recovery experience, suitable countermeasures and their parameters were identified to be optimized and included in the developed mathematical model of recovery.

5.6.1 Chernobyl Accident

The Chernobyl accident occurred on 26.4.1986 at the 4th unit of the Chernobyl nuclear power plant (NPP) near Pripyat (Ukraine) during a scientific experiment (UNSCEAR, 1988). The core of reactor #4 (RBMK-1000 type) was destroyed and large amounts of radioactive materials were released into the atmosphere: inert gases, isotopes of cesium, tellurium, iodine, strontium, other radionuclides and fuel particles. For example, a total activity of the released ^{137}Cs (half-life of 30 years) was estimated to be 85 PBq. In case of ^{131}I (half-life of 8 days), a total released amount was about 1 760 PBq (IAEA, 2006). The fallout was spread over large areas of the Soviet Union, European countries and also occurred in the northern hemisphere. This accident was the most severe accident related to the use of nuclear energy and was rated as the major accident, or Level 7, according to the INES Scale (IAEA, 2013c; UNSCEAR, 1988).

The duration of radionuclide releases was more than 10 days (UNSCEAR, 1988). Dispersed radioactive material affected > 200 000 km^2 of European territory (IAEA, 2008c). For example, surface activities of ^{137}Cs deposited in the Russian Federation, Belarus and Ukraine exceeded 1 480 kBq·m^{-2} (IAEA, 2006, 2001). Such high surface activities led to the implementation of early countermeasures (sheltering, iodine prophylaxis, evacuation) and long-term countermeasures (resettlement of inhabitants, decontamination and foodstuff restrictions) (IAEA, 2001).

Decontamination of affected areas started at the end of May 1986 (IAEA, 2001). Due to the large extent of contaminated areas, the overall recovery process **is still ongoing** (Cholteeva, 2020; IAEA, 2001). During the decontamination process, the following techniques were utilized: removal of contaminated soil (manually and using agricultural machinery) and subsequent use of non-contaminated soil instead, asphalting roads, dismantling of objects that were not able to be decontaminated, water hosing buildings and roads, demolition of buildings, temporary storage of produced waste etc. (IAEA, 2014, 2001; Nisbet et al., 2010). The soil removal using heavy machinery is depicted in Fig. 3 (IAEA, 2011). The manual topsoil removal can be found in Fig. 4 (Uatom, 2023). Washing of buildings is shown in Fig. 5 (Uatom, 2023).

Considering recovery actions, large amounts of radioactive waste were produced during the Chernobyl clean-up (IAEA, 2001; Napier et al., 2007). Large volumes of contaminated waste were then placed in temporary storages and disposal facilities of trench and landfill type. These burial sites (roughly 800 facilities) were built up to 15 km from Chernobyl NPP, without any detailed documentation or safety analyses. Therefore, the largest amounts of produced waste are located in the Chernobyl Exclusion Zone (CEZ). The total area of temporary storages is approximately 8 km^2, where the total waste volume exceeds 10^6 m^3. Typical concentrations of ^{137}Cs and ^{90}Sr in the waste are 10^5 $Bq \cdot kg^{-1}$. Due to missing description of many facilities, only half of the storages are known, as well as their inventories (Napier et al., 2007).

In Czechoslovakia, surface activities of deposited ^{137}Cs after the Chernobyl accident were substantially lower and were approximately ≤ 81 $kBq \cdot m^{-2}$ (Rulík and Helebrant 2011). Considering early countermeasures, the most conservative estimates of irradiation of the population in Czechoslovakia were significantly below intervention levels and decontamination was not required (Bučina et al., 1996). Except for the iodine prophylaxis of shepherds in mountain regions of Slovakia, no early countermeasures (i.e. sheltering or evacuation) were implemented. Selective restrictions in the foodstuff/feedstuff consumption were additionally applied to minimize the impact on daily life, such as adjustments in cattle feeding, milk production and sampling (Bučina et al., 1996).

Fig. 3. Topsoil removal using heavy machinery in Chernobyl (source: IAEA, 2011 – Imagebank)

Fig. 4 Manual topsoil removal in Chernobyl (source: Uatom, 2023)

Fig. 5. Washing of buildings in Chernobyl (source: Uatom, 2023)

5.6.2 Fukushima Daiichi Accident

The Fukushima Daiichi accident on 11.3.2011 was caused by a massive earthquake and a subsequent tsunami that led to damage to power supply lines and infrastructure of the Fukushima Daiichi NPP (FDNPP), Japan (IAEA, 2015a). The damage of FDNPP caused the loss of power supply, resulting in the loss of cooling of operating units #1–3 (BWR type of reactors) and pools with the spent fuel. Due to the loss of cooling, units #1–3 overheated, causing the melting of cores and breaches of containment vessels. The hydrogen releases from reactor pressure vessels (RPV) then occurred resulting in explosions in the reactor buildings of units #1, #3 and #4. Thereafter, radionuclide releases into the atmosphere and into the sea happened (IAEA, 2015a). For the FDNPP accident, the INES ranking was progressively changed from Level 3 to Level 7 (ENSI, 2011).

Considering ^{137}Cs, atmospheric releases were in a range of 7–50 PBq, while for ^{131}I this interval was 90–700 PBq (IAEA, 2015b). Areas affected by the FDNPP accident were estimated to 13 000 km^2 (National Research Council, 2014). Surface activities of ^{137}Cs and ^{134}Cs were in a range from 300 kBq·m^{-2} (and less) to 30 MBq·m^{-2} at the end of April 2011, in accordance with results of airborne measurements up to 80 km from FDNPP (MEXT, 2011).

The nature of affected areas after the Fukushima accident was mainly forest and agricultural (U.S. EPA, 2016). Therefore, for agricultural lands, decontamination techniques similar to the techniques employed during the Chernobyl clean-up were implemented, e.g., vegetation and topsoil removal, collection of leaves or plowing. For urban/industrial regions, e.g. Fukushima City, such decontamination methods as high-pressure washing, wiping or various techniques of surface removal were used (U.S. EPA, 2016). The vegetation and leaves removal process is depicted in Fig. 6 (Uatom, 2023). Examples of decontamination of playgrounds, e.g. using turf removal (upper photographs), wiping (down, to the left) and high pressure washing (down, to the right) can be found in Fig. 7 (MOE, 2013; U.S. EPA, 2016).

The Fukushima decontamination works are **still in progress**, i.e. more than 10 years after the accident (Schreurs, 2021). According to available data[3], the total cleanup costs were

[3] In 2022, 4 trillion yen was approximately equivalent to 29 billion EUR (European Central Bank, 2025), or 31 billion USD (Exchange-Rates.org, 2025), or 713 billion CZK (CNB, 2025b), based on average exchange rates.

above 4 trillion yen (up to 2022), while the predicted costs of ongoing decontamination in future are expected to be of the same orders of magnitude (Hanawa, 2023).

During the Fukushima clean-up, 70 000 workers participated in the decontamination works, where millions of m^3 of radioactive waste (mainly contaminated topsoil) were produced (The Guardian, 2019). Photographs of bags containing radioactive waste are presented in Fig. 8 (The Japan Times, 2015). For example, in Fukushima prefecture, the volume of waste temporarily located at 830 sites is 8 460 m^3 (The Asahi Shimbun, 2022). The radioactive waste packed into bags will be moved to the temporary interim storages and stored up to 2045, then the waste will be placed in a permanent site (The Asahi Shimbun, 2022; The Guardian, 2019). The area of the temporary interim storage will reach 1 600 ha (or 16 km^2), allowing holding 14 million m^3 of contaminated soil (The Japan Times, 2022).

In comparison with the Chernobyl accident, releases from FDNPP were significantly lower, as well as measured values of concentrations in the air in the Czech Republic (Steinhauser et al., 2014; SÚJB, 2020a). Therefore, no countermeasures/local food restrictions were required to be implemented for territories of the Czech Republic (Zemanová et al., 2011).

Fig. 6. Removal of vegetation and leaves in Fukushima (source: Uatom, 2023)

Fig. 7. Decontamination of playgrounds in Fukushima (source: U.S. EPA, 2016: 37)

Fig. 8. Bags with radioactive waste at a temporary storage site in Tomioka, Fukushima Prefecture (source: The Japan Times, 2015)

5.6.3 Kyshtym Accident

The Kyshtym accident happened on 29.9.1957 at the Mayak fuel reprocessing plant near Kyshtym (Chelyabinsk Oblast, Russian Federation) (Akleyev et al., 2017; IAEA, 2013a). The reprocessing plant contained underground storage tanks for liquid high-level radioactive waste (primarily nitrate compounds), including circulatory water cooling, ventilation and monitoring systems. Each tank was surrounded by an individual reinforced cell (Akleyev et al., 2017; Batorshin and Mokrov, 2018).

The accident was caused by technical failures that led to evaporation of water in one tank (cell #14), heating of nitrate salts inside (70–80 t), chemical explosion of cell #14 and the subsequent atmospheric release of all fission products (Akleyev et al., 2017; IAEA, 2014). For the Kyshtym accident, the INES ranking corresponds to Level 6 (serious accident, with a significant release of radioactive material) (IAEA, 2014).

The total activity of the fission products in the waste in the tank was approximately 740 PBq (Akleyev et al., 2017; IAEA, 2014). 90% of this amount was released and deposited up to 5 km from the plant. The rest of the release (i.e. 10%) was dispersed mainly up to 300 km from the site in the north-northeast wind direction, forming the East Urals Radioactive Trace (EURT) (Akleyev et al., 2017; Batorshin and Mokrov, 2018).

The radionuclide composition of the atmospheric release consisted primarily of $^{144}Ce/^{144}Pr$ (65.8%), $^{95}Zr/^{95}Nb$ (24.8%), $^{90}Sr/^{90}Y$ (5.4%), $^{106}Ru/^{106}Rh$ (3.7%), $^{137}Cs/^{137m}Ba$ (0.35%) and traces. Contrary to the Chernobyl accident, the contribution of long-lived radionuclides originated mainly from $^{90}Sr/^{90}Y$, while the ^{137}Cs contribution was almost negligible. ^{137}Cs had been radiochemically extracted earlier, for the production of radionuclide sources (Akleyev et al., 2017; Batorshin and Mokrov, 2018).

The area of EURT was delineated in regions, where the ^{90}Sr contamination was below 3.7 $kBq \cdot m^{-2}$, or 0.1 $Ci \cdot km^{-2}$. Such activities were measured in areas of roughly 15 000–20 000 km^2, or in the zone of 30–50 km × 300 km (Batorshin and Mokrov, 2018; IAEA, 2014). Considering this area, 270 000 inhabitants lived there, in 217 settlements (Akleyev et al., 2017). Using a threshold of 74 $kBq \cdot m^{-2}$ (or 2 $Ci \cdot km^{-2}$) of ^{90}Sr, protective measures of population were required in areas of about 1 000 km^2, or 8–9 km × 100 km. The highest surface activity of ^{90}Sr there was 150 $MBq \cdot m^{-2}$ (or 4 $kCi \cdot km^{-2}$) (Batorshin and Mokrov, 2018).

Within the site decontamination and remediation, following options were implemented: top soil removal, covering with a clean soil, deep ploughing, addition of fertilizers, demolition of highly contaminated buildings, washing of roads and others (Batorshin and Mokrov, 2018; IAEA, 2014, 2013a). The decontamination of adjacent areas of the production site was finished in March 1958, when 320 000 m^3 of soil were removed (Batorshin and Mokrov, 2018).

5.6.4 Windscale Pile Accident

The Windscale Pile accident occurred on 10–11.10.1957 in the nuclear reactor Pile 1 (one of two) used for the plutonium production in the United Kingdom (Garland and Wakeford, 2007). In the reactor (air-cooled graphite-moderated nuclear reactor type), the annealing operation of the core graphite was conducted, when part of the core overheated and then led to fire (Garland and Wakeford, 2007; Webb et al., 2006). As a result, the atmospheric radionuclide release of fission and activation products from the core happened, having been dispersed over territories of the United Kingdom, Wales and Northern Europe (Crick and Linsley, 1984). The corresponding INES Level is #5, or an accident with wider consequences (IAEA, 2008b; Webb et al., 2006).

Considering the released activities, various estimates had been performed (Garland and Wakeford, 2007). Nevertheless, the vast majority of the release was comprised of ^{131}I, or **the short-lived radionuclide** with a half-life of 8 days (Crick and Linsley, 1984; Dunster et al., 2007; Webb et al., 2006). According to Garland and Wakeford (2007), activities of ^{131}I were assessed to be from 740 to 1 800 TBq (the best estimate), while the ^{137}Cs activity was from 22 to 180 TBq (the best estimate). Assuming the protective measures, restrictions in the milk consumption only were implemented in the adjacent area of 520 km^2, while the other foodstuffs (e.g. eggs or vegetables) were not included in the ban, as well as other countermeasures (Crick and Linsley, 1984; Webb et al., 2006). An example of pouring away of radioactive milk is in Fig. 9 (The Guardian, 2012).

Fig. 9. Pouring away of contaminated milk in Cumbria, near Windscale (source: The Guardian, 2012)

5.6.5 Goiânia Accident

The Goiânia accident was caused by a stolen radiotherapy source in 1987, Brazil (IAEA, 1988). According to the INES scale, the corresponding Level is #5 (IAEA, 2008b). The ^{137}Cs teletherapy unit was abandoned during moving of a local radiotherapy institute to new buildings. The source activity was approximately 51 TBq (IAEA, 1988; Rosenthal et al., 1991). The unit was then found and dismantled by two persons due to its possible scrap value. ^{137}Cs was placed inside the source capsule, which ruptured during the dismantling (IAEA, 2008b, 1988).

Owing to the physical properties of the cesium chloride salts (blue glow), the source was shown and distributed to other people (mainly friends and relatives). Metal parts of the source assembly were sold to the scrapyard (IAEA, 1988). Therefore, subsequent contamination of several persons and the environment occurred. In the contaminated area, 85 houses demonstrated higher levels of radiation. Estimates of the ^{137}Cs activity involved in the contamination were 44 TBq (IAEA, 1988; Rosenthal et al., 1991). Thereafter, several deaths were caused by the irradiation from the source (IAEA, 2008b, 1988).

Within the remedial actions in the affected areas, such public places as roads and buildings (e.g. bars) were required to be decontaminated. The following decontamination techniques were primarily used: demolition of highly contaminated buildings, washing of houses and roofs with high-pressure water jets, vacuum cleaning inside contaminated buildings, chemical decontamination of various surfaces, topsoil removal in gardens and covering with clean soil/concrete (IAEA, 1988). Photographs of the demolition process are shown in Fig. 10: a) contaminated rubble soon after demolition, b) the site after removal of contaminated waste (IAEA, 1988).

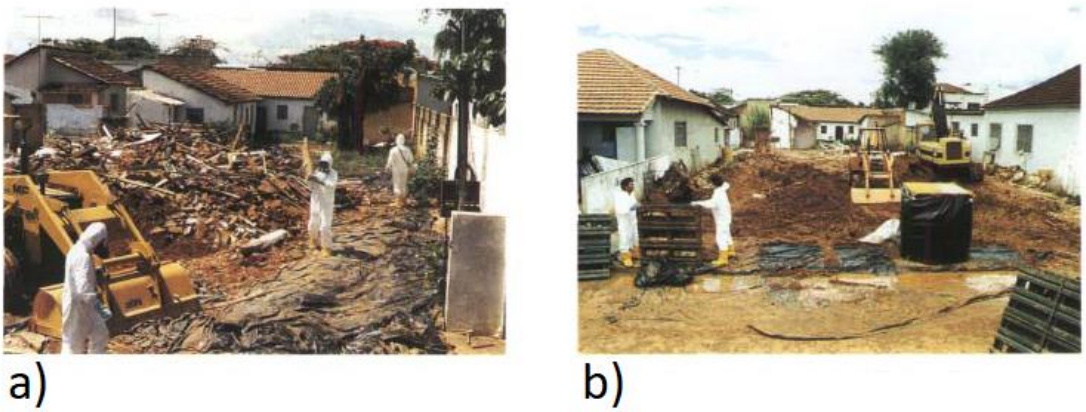

Fig. 10. Demolition process in Goiânia (source: IAEA, 1988: 101)

The remedial process was conducted under strong pressure of politicians and inhabitants. Hence, action levels for the decontamination were significantly lower than the expected values from the optimization (IAEA, 1988).

Considering waste management, a temporary storage was selected 20 km far from Goiânia. The storage capacity was 4 000–5 000 m^3 of waste (IAEA, 1988). The waste was divided into 3 categories (IAEA, 1988):

- Non-radioactive (massic activity of 74 $kBq \cdot kg^{-1}$),
- Low level (dose rates < 2 $mSv \cdot h^{-1}$),
- Medium level (dose rates 2–20 $mSv \cdot h^{-1}$).

The total volume of the radioactive waste originated from the decontamination was 3 500 m^3 (more than 275 lorry loads). The produced waste was packed into metal drums, boxes, containers and concrete packaging. The photographs of the packed waste and the waste storage are in Fig. 11, a) and b), respectively.

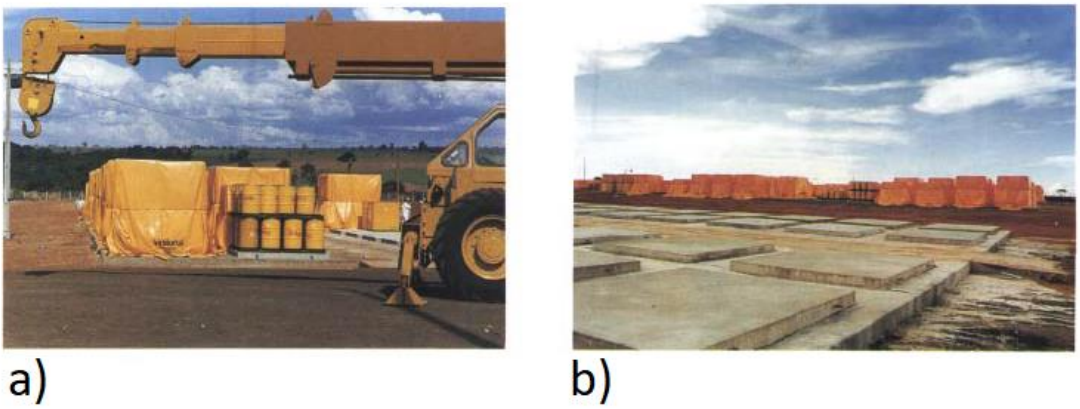

Fig. 11. Waste storage in Goiânia (source: IAEA, 1988: 106)

5.7 Decontamination Techniques

Following the Chernobyl accident, large-scale recovery efforts were conducted over several years. The decontamination process involved various methods, including the cleanup of residential areas, washing of buildings, and removal of vegetation and soil. Additionally, the decontamination of water bodies was also required (U.S. EPA, 2016).

The decontamination of affected areas must be carefully planned in advance. It should be carried out in a top-down manner to prevent secondary contamination of lower surfaces. When planning the decontamination schedule, priority should be given to agricultural lands and forests, followed by large buildings and residential houses, and finally, roads (Masayuki, 2012; U.S. EPA, 2016).

According to the U.S. EPA (2016), decontamination techniques can be classified into non-destructive and destructive categories. Non-destructive methods include techniques such as vacuum cleaning, wiping, and washing. The effectiveness of washing depends on the type of equipment used (e.g., varying water pressure), the use of detergents, and other factors. Destructive technologies range from minimally to fully destructive methods. Minimally destructive techniques include grass cutting and plowing (U.S. EPA, 2016). In contrast, fully destructive methods involve topsoil removal, roof replacement, and building demolition (Nisbet et al., 2010; U.S. EPA, 2016).

Many decontamination technologies depend significantly on the time elapsed since the initial contamination. However, many methods demonstrate the highest effectiveness when applied shortly after contamination occurs. For example, grass cutting is highly efficient only within a few days following contamination. In contrast, regarding soil contamination, the most effective decontamination methods involve soil stripping or

removing the upper soil layers, which remains effective even long after the initial contamination (Nisbet et al., 2010; U.S. EPA, 2016).

Another factor influencing decontamination efficiency is the prevailing meteorological conditions during deposition, particularly whether it occurred under dry or wet conditions (e.g., rain or snow) (Nisbet et al., 2010). In the case of dry deposition, conventional methods such as street washing and cleaning, removal of grass, leaves, and branches, and soil plowing are both cost-effective and efficient. Similarly, washing buildings, particularly walls and roofs, can substantially reduce dose levels; however, these methods are typically more expensive and require significant human resources. For wet deposition, priority should be given to decontaminating small grass-covered areas in residential zones, such as gardens and lawns. Removing contaminated vegetation in these areas can result in a substantial dose reduction. Fast, efficient, and cost-effective methods for this purpose include mowing, trimming, pruning, and related techniques (Nisbet et al., 2010; U.S. EPA, 2016).

In accordance with IAEA (2006) and the U.S. EPA (2016), simple long-term decontamination methods include the following options:

- Topsoil removal: in residential areas, 5–10 cm of soil or turf should be removed, with the thickness depending on the distribution of radioactivity in the soil. This method is suitable for courtyards, areas near public buildings (including schools and kindergartens), roadsides, and fruit or vegetable gardens.
- Plowing: this technique is appropriate for private fruit and vegetable gardens as well as small grass-covered areas.
- Covering with clean material: decontaminated surfaces in residential areas, such as courtyards or roadsides, can be covered with a layer of sand or gravel to reduce residual radiation.
- Cleaning of buildings: this method includes washing or cleaning walls and roofs, as well as replacing roofs when necessary. However, potential damage to private property should be considered during decontamination planning.

In rural areas and on contaminated farmland, effective and suitable countermeasures include plowing (which dilutes contamination within the soil volume), reseeding, and applying fertilizers such as lime, phosphorus and potassium. In forests, decontamination is generally less efficient, more labor-demanding, slower, and significantly more expensive (IAEA, 2006; U.S. EPA, 2016).

Additionally, recovery measures include administrative restrictions such as limiting physical access, prohibiting hunting, fishing, and logging, as well as implementing fire prevention strategies to reduce the resuspension of radioactive dust/particles (U.S. EPA, 2016).

In the case of water body contamination, water treatment processes should be employed for drinking water supplies to remove soluble radioactive contaminants. Filtering methods such as activated charcoal and zeolite filtration systems can be applied. Following the Chernobyl accident, additional measures were implemented, including the dredging of water bodies and the construction of zeolite-containing dykes. However, these methods proved insufficient due to water flows and the solubility of contaminants (IAEA, 2006; U.S. EPA, 2016).

For large contaminated areas, the most commonly applied decontamination technologies involve washing contaminated surfaces using high-pressure techniques and physically removing contaminated materials such as surface layers or debris. These methods effectively reduce dose rates and external surface radioactivity levels in inhabited areas (U.S. EPA, 2016). During recovery planning, the following factors should be considered: associated costs, time requirements, and the volumes of radioactive waste generated (U.S. EPA, 2016). Another important aspect to address during decontamination planning is the decontamination of workers and equipment (Andersson et al., 2000; Nisbet and Watson, 2018). Consequently, the most widely used decontamination techniques are outlined in the subsequent sections.

5.7.1 Decontamination Effectiveness

In assessing decontamination effectiveness, specialized units can be utilized to evaluate decontamination techniques. The most commonly used units are summarized below. The decontamination factor (DF) quantifies the effectiveness of decontamination efforts and is defined by the following equation (Roed et al., 1998; Severa and Bár, 1985):

$$DF = \frac{A_0}{A_d}, \tag{1}$$

where A_0 is the surface activity before decontamination, and A_d is the surface activity after decontamination.

Decontamination factors describe the effectiveness of decontamination methods; however, these values may change over time from the initial contamination due to factors such as the weather conditions, and other environmental effects (Nisbet and Watson, 2018).

Another approach to evaluating decontamination effectiveness is the dose rate reduction (DRR), which indicates the extent to which dose rates decrease following decontamination. DRR is defined by the following equation (Severa and Bár, 1985):

$$DRR = 1 - DF^{-1}. \quad (2)$$

5.7.2 Access Restriction

Restricting public access is a highly effective countermeasure for reducing external irradiation from contaminated surfaces and the inhalation of radioactive particles. It can significantly decrease the irradiation of inhabitants, potentially approaching 100% (Nisbet and Watson, 2018). This countermeasure is applicable to all types of radionuclides and can be implemented at any scale. However, it may necessitate specific legislation due to restrictions on access to land and private properties (Nisbet and Watson, 2018).

A disadvantage of this countermeasure is that contamination will persist in the restricted areas. Another challenge lies in the need for an effective public information and communication strategy. The implementation of such a measure (i.e., demarcation) requires the installation of warning signs, information boards, tapes, fences, and barriers (Nisbet and Watson, 2018). An example of the access restriction is depicted in Fig. 12 and originates from Belarus following the Chernobyl accident (Lidovky.cz, 2016).

Fig. 12. Access restriction (source: Reuters/Lidovky, 2016)

5.7.3 Grass Removal

Grass cutting and removal helps reduce external gamma and beta irradiation, as well as the inhalation of radioactive material from outdoor surfaces. This method is applicable to any grassed area at any scale, depending on the equipment used (e.g., lawn mowers, tractors) (Nisbet and Watson, 2018). It is suitable for gardens, parks, playgrounds, large open areas, and agricultural land (Nisbet and Watson, 2018; U.S. EPA, 2016).

The decontamination effectiveness of this countermeasure is particularly high shortly after deposition under dry conditions. In such cases, the DF can reach a value of 3. Grass removal is also more effective when applied to mature plants, as the migration of radionuclides into the soil occurs at a slower rate (Nisbet and Watson, 2018).

The implementation of grass removal is not feasible under severe cold meteorological conditions. Another limitation is the potential risk of damage to private property. Additionally, the disposal of collected organic material contaminated with radionuclides must be addressed. The waste production (organic waste) is approximately 0.1–0.7 $l \cdot m^{-2}$ (Nisbet and Watson, 2018).

The grass removal process is shown in Fig. 13, originating from the Fukushima clean-up (U.S. EPA, 2016).

Fig. 13. Grass removal (source: U. S. EPA, 2016: 37)

5.7.4 Turf Harvesting

Turf harvesting is an effective countermeasure for removing radionuclide contamination from grassed and soil areas. During this process, a thin layer of turf is skimmed off. The thickness of the removed layer is approximately 1 cm, though it may reach several centimeters, and is collected into rolls or slabs. Prior to the removal of the upper turf/soil layers, grass, plants, and shrubs should be cut. Turf harvesting may require subsequent reseeding or returfing (Nisbet and Watson, 2018).

This countermeasure is suitable for gardens, parks, playgrounds, and other grassed areas. For its implementation, the areas to be decontaminated must have a mature root mat (Nisbet and Watson, 2018). This technique is also unsuitable during cold weather due to frozen soil (Andersson et al., 2000).

The implementation of this method requires turf harvesters and spades/shovels (Andersson et al., 2000; Nisbet and Watson, 2018). Therefore, this technique cannot be applied to soil containing stones or rocks, as they may damage turf harvesters (Nisbet and Watson, 2018). As with the grass removal, potential risks of damage to private property must be considered. Additionally, the collection, handling, and disposal of solid radioactive waste generated by turf harvesting must be addressed (Nisbet and Watson, 2018). The corresponding waste production is approximately 20–50 $l \cdot m^{-2}$ (U.S. EPA, 2016).

Considering the corresponding decontamination factors, values differ in a range of 1.7–10, depending on weather conditions and implementation periods (Nisbet et al., 2010; Nisbet and Watson, 2018; U.S. EPA, 2016).

The method is illustrated in Fig. 14, which depicts the Fukushima clean-up (Masayuki, 2012; Selivanova, 2019).

Water tie-down

During turf harvesting, the use of a water tie-down or the spraying of solidifying/fixation agents is recommended to prevent the resuspension of radioactive dust and to dampen the soil. For decontaminating large areas, a winding hose reel, a water sprinkler with a tripod, and a tractor are required (Nisbet and Watson, 2018). The process of soil solidification is depicted in Fig. 15 (Miyahara et al., 2012).

Fig. 14. Turf harvesting (source: Masayuki, 2012: 45)

Fig. 15. Soil solidification (source: Miyahara et al., 2012: 13)

5.7.5 Soil Stripping

Topsoil removal (soil stripping) is similar to turf harvesting (Nisbet and Watson, 2018; U.S. EPA, 2016). However, in this decontamination method, the upper soil layers (up to 5 cm) are removed. Consequently, waste production (solid waste) is higher, reaching approximately 50 $l \cdot m^{-2}$. The associated decontamination factors are also higher, ranging from 5 to 30. This method remains highly effective even several years after the initial contamination (Nisbet and Watson, 2018; U.S. EPA, 2016).

Topsoil removal has nearly the same limitations and recommendations (e.g., plant removal and water tie-down) as turf harvesting. This method is not applicable in areas with extreme slopes. For larger areas requiring decontamination, the use of excavators is recommended. Additionally, decontaminated areas should not be tilled, as this would mix contaminated upper soil layers with deeper, uncontaminated layers. For small areas, manual topsoil removal can be used instead of heavy agricultural machinery (Nisbet and Watson, 2018). The process of topsoil removal during the Fukushima clean-up is depicted in Fig. 16 (Miyahara et al., 2012).

Fig. 16. Topsoil removal (source: Miyahara et al., 2012: 13)

5.7.6 Shrub Removal and Tree Pruning

Shrub removal, tree pruning, and branch trimming (or clipping) are countermeasures suitable for the decontamination of vegetated outdoor areas (Nisbet and Watson, 2018; U.S. EPA, 2016). The clipping process during decontamination efforts following the Fukushima accident is shown in Fig. 17 and Fig. 18 (Miyahara et al., 2012).

During the implementation of this method, leaves and branches are cut using cutters, axes, chainsaws, and forage harvesters. Considering tall trees, ladders may be required (Nisbet and Watson, 2018). This method is highly effective soon after deposition, when the corresponding decontamination factor can reach up to 50. However, its effectiveness decreases over time due to weathering and the migration of radionuclides into the soil, similar to grass removal.

Regarding contaminated waste production, the generated waste (i.e., vegetation and wood) ranges from 2 to 10 $kg \cdot m^{-2}$. All generated waste should be carefully collected and disposed of. In the case of contaminated tree replacement, tree saplings would be required (Nisbet and Watson, 2018).

Fig. 17. Clipping of shrubs (source: Miyahara et al., 2012: 12)

Fig. 18. Clipping of tall trees (source: Miyahara et al., 2012: 12)

5.7.7 High-Pressure Washing of Roads

High-pressure washing of roads and paved areas is an effective method for removing surface contamination (Nisbet and Watson, 2018). The maximum benefits of this decontamination technique can be achieved if implemented shortly after the initial contamination. However, high-pressure hosing remains effective for several years following deposition. The corresponding decontamination factors typically range from approximately 2 to 10 (Nisbet and Watson, 2018).

The method has certain restrictions related to weather conditions, as it cannot be implemented during severe cold weather. There is also a potential risk of damage to private property. Additionally, an important aspect to consider is the collection of contaminated water and its subsequent management following decontamination. However, in cases of lower contamination, the use of public sewers or highway drainage systems may be accepted (Nisbet and Watson, 2018; U.S. EPA, 2016).

The method can be implemented at any scale, either manually or with the use of large vehicles. In terms of technical equipment, pressure washers, road sweepers, pumps, water tanks, brushes, and other tools can be utilized (Nisbet and Watson, 2018; U.S. EPA, 2016).

The application of this method is illustrated in Fig. 19 and Fig. 20, based on examples from the Fukushima clean-up (Masayuki, 2012; Miyahara et al., 2012).

Fig. 19. High-pressure washing of roads using large vehicles (source: Masayuki, 2012: 52)

Fig. 20. Manual high-pressure washing of paved areas (source: Miyahara et al., 2012: 15)

5.7.8 High-Pressure Washing of Buildings

High-pressure washing of external building surfaces includes the decontamination of walls and roofs. This method shares similarities with high-pressure washing of roads, particularly regarding risks such as potential damage to private property and the careful collection of liquid waste. However, compared to building surfaces, radionuclide penetration is less significant on asphalt. Consequently, delays in road decontamination may be less critical than those for buildings (Nisbet and Watson, 2018; U.S. EPA, 2016).

Decontamination effectiveness for buildings is highest shortly after the initial contamination, with decontamination factors reaching up to 10 (Nisbet and Watson, 2018). Regarding application constraints, several factors should be considered, including building materials, the number of windows, water jet angles, worker expertise, and other relevant aspects. For example, roof tiles, bricks, and limestone components tend to retain more contamination, requiring greater decontamination efforts. Additionally, moss on roofs accumulates radionuclides and should be removed. For access to higher floors and roofs, scaffolding, ladders, or mobile lifts should be used as supplementary equipment (Nisbet and Watson, 2018). The process is depicted in Fig. 21 (Miyahara et al., 2012).

Fig. 21. High-pressure washing of buildings (source: Miyahara et al., 2012: 14)

5.8 Cost-Benefit Analysis (CBA)

Cost-benefit analysis (CBA) is a recognized formal technique for economic evaluation in decision-making. CBA allows the assessment of the worthiness and constraints of analyzed projects (Mishan and Quah, 2020). It has been applied across various research fields and in government decision-making, including economics and social policy, to optimize the allocation of financial resources (Brent, 2006; Robinson, 1993).

The main difference between CBA and other approaches originates from its ability to express both inputs and outcomes (costs and benefits, respectively) in monetary terms (Robinson, 1993). CBA can utilize net benefits (i.e., the difference between benefits and costs) and the benefit-cost ratio (i.e., benefits divided by costs) (Jiang and Marggraf, 2021). However, the implementation of selected activities is justified only if the benefits exceed the costs. Otherwise, such activities should be restricted (Brent, 2006).

Another aspect of CBA is the maximization of net benefits while considering relevant constraints (Brent, 2006). It reflects the efficiency of the activities under consideration. In the absence of constraints (except for production possibilities), activities with positive net benefits should be approved. However, benefits and costs can be further adjusted using distributional weights to account for key factors and impacts (Brent, 2006).

5.8.1 Data Envelopment Analysis (DEA) in CBA

Data Envelopment Analysis (DEA) is a method used to assess the relative efficiency of decision making units (DMUs). The DEA framework captures the relations between multiple inputs and outputs (Charnes et al., 1978). Considering coupling with CBA, DEA interprets costs as inputs and benefits as outputs, enabling the application of benefit-cost ratios as performance indicators (Womer et al., 2006). For completeness, a brief overview of this approach is provided below.

In assessing the efficiency of a DMU, the objective is to maximize the ratio of weighted outputs to weighted inputs, subject to the constraint that the corresponding ratios for all other DMUs do not exceed unity. The corresponding weights are determined by solving an optimization problem that can be transformed into a linear program (LP) (Charnes et al., 1978; Womer et al., 2006). The following equation can be then used (Charnes et al., 1978):

$$\max h_0(u, v) = \frac{\sum_{r=1}^{s} u_r y_{r0}}{\sum_{i=1}^{m} v_i x_{i0}} \tag{3}$$

subject to:

$$\frac{\sum_{r=1}^{s} u_r y_{rj}}{\sum_{i=1}^{m} v_i x_{ij}} \leq 1, j = 1, \ldots, n,$$

$$u_r, v_i \geq 0, r = 1, \ldots, s, i = 1, \ldots, m,$$

where y_{rj} and x_{ij} are outputs and inputs, respectively, and u_r and v_i are the corresponding weights.

5.8.2 Uncertainties in CBA

Within CBA, uncertainties should be taken into account. These uncertainties may arise within parameter values (e.g., distributional weights) or may pertain to the measurement of outcomes (e.g., costs). Uncertainties in value parameters can be examined through sensitivity analysis (SA), which involves varying input parameters to assess their effect on the outputs (or their sensitivity) (Borgonovo and Plischke, 2016; Brent, 2006). Uncertainties in the outcomes can be identified using a probabilistic framework for decision-making (Brent, 2006). An example of such a framework is the PSA framework for nuclear facilities, as described in Chapter 5.2. PSA studies should identify risks and propose options for their mitigation within the decision-making process (IAEA, 1996).

Regarding SA methods in the context of System Dynamics, the internal features of Vensim software, including Monte Carlo simulations, can be utilized (Ventana Systems, 2025). SA techniques help identify which input data have the most significant impact on the model's behavior. Based on these analyses, effective policies can be proposed for resource allocation (Bier, 2011). SA can be used to identify leverage points in the model, or parts where even small changes can significantly influence the results (Meadows, 1999). Additionally, SA methods can be applied to assess the model's robustness. Consequently, the model can be simplified by reducing components that have minimal impact on the results (Bier, 2011).

5.8.3 CBA in Radiation Protection

Considering the application of CBA in radiation protection, the simplest implementation of CBA involves converting individual factors affecting the examined system into monetary equivalents, then grouping costs and benefits on different sides (ICRP, 2006). In terms of radiation protection and the corresponding CBA, the monetary value of the man-sievert,

manSv[4], (collective effective dose) is used (ICRP, 2006). This factor expresses the benefit (reduction in the collective effective dose – referred to as the averted dose) of the implemented measure in financial terms, allowing comparison with associated costs (ICRP, 2006; SÚJB, 2016).

Mathematical Representation of Costs

The economic costs Y associated with a collective effective dose can be described using the following equation (ICRP, 2006):

$$Y = \sum_j \alpha_j \cdot S_j, \tag{4}$$

where:

- α_j: monetary equivalent of the collective effective dose for the j-th group (e.g., the public or workers), or health detriment.
- S_j: collective effective dose received by the exposed group.

In the context of the Czech regulatory framework, monetary equivalent values α_j for various exposure scenarios are specified in Decree 422/2016 Sb. issued by the State Office for Nuclear Safety (SÚJB, 2016).

Optimizing Total Costs

Total costs for each alternative measure are determined as the sum of associated costs of protection X and the economic costs of collective exposure (or detriment) Y, as defined by the equation above (ICRP, 2006). The optimal alternative is identified by minimizing the total costs, where marginal protection costs equal the marginal price of one unit of averted collective effective dose. The optimal solution is visually represented in Fig. 22, showing the relationship between costs and benefits in the context of cost-benefit analysis (ICRP, 2006).

[4] The man-sievert (manSv) represents the irradiation of a group of inhabitants, also referred to as the collective effective dose (CED) (ICRP, 2006).

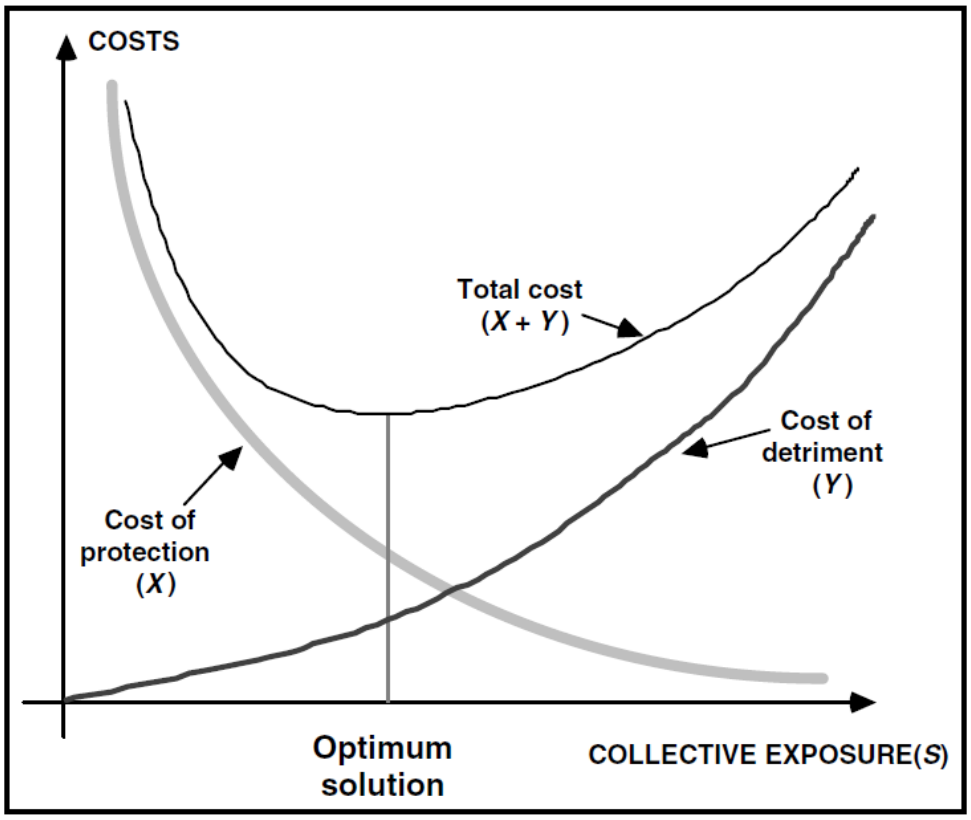

Fig. 22 Cost-Benefit Analysis (source: ICRP, 2006: 97)

5.9 Existing Software Solutions

This chapter summarizes the most widely recognized software solutions and mathematical models/codes dedicated to the analysis of recovery and countermeasure strategies. All of the described tools were subsequently integrated into the JRODOS/ARGOS software systems (Schneider et al., 2017). Some models no longer exist as independent tools or have been completely discontinued. The National Radiation Protection Institute[5] (SÚRO) employs the JRODOS tool for simulating atmospheric radionuclide transport (Raskob et al., 2011). Therefore, the atmospheric dispersion calculations performed in JRODOS were utilized in the present research.

5.9.1 JRODOS

The JRODOS Decision Support System (DSS) was developed in Germany following the Chernobyl accident to simulate the atmospheric transport of radionuclides during accident releases and to propose early countermeasures, such as the distribution of iodine

[5] National Radiation Protection Institute (SÚRO), Bartoškova 1450/28, 140 00, Prague, Czechia, https://www.suro.cz/.

tablets, sheltering, evacuation, and relocation (Raskob et al., 2016, 2011). JRODOS includes a database of nuclear power plants (NPPs) and their corresponding units, and it allows for the integration of GIS functionalities, such as working with various map layers (Ievdin et al., 2019; Raskob et al., 2011). For such simulations, JRODOS employs an atmospheric dispersion module (ADM) (Ievdin et al., 2019).

Considering recent radionuclide releases, JRODOS was used, for example, to estimate affected areas following the Fukushima Daiichi accident in 2011 (Ievdin et al., 2012; Kovalets et al., 2014; Landman et al., 2014). JRODOS was also utilized to estimate a potential source of the unknown origin of ^{106}Ru in 2017 using forward/backward simulations (Kovalets et al., 2020).

Additionally, simulations in JRODOS can be applied to assess the impacts on the agricultural sector following radionuclide releases, as investigated in the study dedicated to assessing potential consequences after a severe accident at NPP Zaporizhzhya (Selivanova et al., 2022a). Another example of the application of JRODOS is its use in the case of routine discharges from NPP Dukovany (Selivanova et al., 2022b), where the JRODOS tool was extended using scripts in R language (R Core Team, 2022) and the cUrl POST method (Hostetter et al., 1997; Ievdin et al., 2017).

5.9.2 ERMIN

The ERMIN (European Model for Inhabited Areas) tool is dedicated to the analysis of remediation strategies for inhabited areas and is implemented within the JRODOS/ARGOS software (Charnock et al., 2016; Raskob et al., 2011; Schneider et al., 2017). The model addresses areas contaminated by radioactive fallout. Users define the grid of interest and specify contaminated objects (e.g., different types of buildings, grassed or industrial areas) along with the corresponding fractions, levels of contamination, and types of deposition (Charnock et al., 2016; RODOS team, 2013). Countermeasure zones must then be defined, with selected decontamination strategies (e.g., grass cutting, ploughing) assigned accordingly. ERMIN also employs an additional strategy, "*no further action*" (NFAS), as a reference scenario. ERMIN outputs include, for example, information on public doses, surface and air concentrations, worker irradiation, total costs, total waste generated, and other relevant data (RODOS team, 2013).

5.9.3 AgriCP

The AgriCP (Agricultural Countermeasure Program) model focuses on agricultural countermeasures (i.e., for livestock, food, and crop production) and is integrated into the JRODOS/ARGOS systems (Gering et al., 2010; Jacobsen et al., 2010). The AgriCP model operates on the same principle as ERMIN: the user defines the grid of interest on the map and then selects appropriate countermeasures, such as food processing, removing animals from contaminated feed, adding sorbents, adjusting slaughter times, and others. The results include information on foodstuff and feedstuff activities, food ban areas and their corresponding ban durations, worker irradiation, and basic cost assessment (Gering et al., 2010).

5.9.4 Web-HIPRE

For economic assessments of the ERMIN/AgriCP outputs, the Web-HIPRE (Hierarchical preference analysis software) tool was previously utilized (Bertsch et al., 2007; Hämäläinen and Mustajoki, 2007; Mustajoki and Hämäläinen, 2000). Web-HIPRE, derived from the HIPRE 3+ decision support software, was an Internet Java applet designed to facilitate Multi-Criteria Decision Analysis (MCDA) (Hämäläinen and Kettunen, 1994; Mustajoki and Hämäläinen, 2000). This online software was proposed to support decision-making, employing prioritization methods based on Multi-Attribute Value Theory (MAVT) and on the Analytic Hierarchy Process (AHP) (Mustajoki and Hämäläinen, 2000).

According to the experiences from simulations using JRODOS (which includes ERMIN/AgriCP models), many users indicated that a simple MCDA tool would be highly beneficial for scenario estimation, particularly during real emergency situations (Bertsch et al., 2007). To meet these requirements, JRODOS was enhanced with an option that allowed for the generation of files containing attribute trees. These files could then be read, modified, and evaluated within the Web-HIPRE tool. For example, JRODOS outputs, such as countermeasure sets for agricultural and urban environments, could be assessed using Web-HIPRE (Bertsch et al., 2007).

Compatibility issues have arisen between the latest versions of the software and new information systems. **As Web-HIPRE is no longer supported**, new MCDA software is currently being developed to replace it in the future (Müller et al., 2020).

5.9.5 MCDA/HELDA

The MCDA tool enhances JRODOS by evaluating countermeasure strategies proposed in models such as ERMIN and AgriCP, thereby facilitating the selection of the optimal recovery strategy within radiological crisis management (Duranova et al., 2020). Compared to the Web-HIPRE model, the MCDA tool has been improved to handle uncertainties (Duranova et al., 2020; Müller et al., 2021, 2020).

The MCDA software is employed to analyze sets of alternatives (i.e., countermeasure strategies), wherein the advantages and disadvantages of each selected strategy are aggregated, expressed as a numerical value, and subsequently ranked (Müller et al., 2021). For example, the tool was tested in two case studies under actual conditions in the Netherlands and Slovakia, where hypothetical nuclear accidents were simulated in JRODOS, and subsequent countermeasure strategies were proposed using the ERMIN2 model (Asselt et al., 2021). The recovery strategies included options such as:

1) No further action,
2) Grass removal and vacuum cleaning of roads,
3) Cleaning of roofs and interior spaces, removal of vegetation, and waste removal,
4) The previous strategy (i.e., #3) extended with soil and vegetation rotovation,
5) Replacement of roofs, vacuum cleaning of interior spaces, and soil/vegetation removal.

The ERMIN outputs, particularly health effects, costs, and waste amounts, were evaluated using the MCDA software. According to the results obtained, these tools can serve as supportive measures, with the final decisions to be made by trained experts following discussions with stakeholders (Duranova et al., 2020).

Since 2024, the MCDA tool has been developed under a new name – HELDA (Helmholtz MCDA Tool) (KIT, 2025, 2024). Currently, HELDA incorporates the following aggregation methods: weighted sum, weighted product, weighted rank, TOPSIS, and VIKOR. The implementation of PROMETHEE I and II as well as ELECTRE III methods is planned in the near future (KIT, 2025).

Considering weighting methods, AHP, SWING, SMART, and direct weight assignment are already available. HELDA also enables uncertainty analysis on input data, using probability distributions and Monte Carlo simulations (KIT, 2025).

The primary reason for not employing the MCDA/HELDA software in this study is that its main objective was to develop a dynamic model capable of handling a large number of

various parameters. Additionally, the application of MCDA would necessitate input from a team of experienced specialists and the engagement of stakeholders, which exceeds the scope of this work.

5.9.6 MOIRA-PLUS

The decision support system (DSS) MOIRA-PLUS (MOdel-based Computerised System for Management Support to Identify Optimal Remedial Strategies for Restoring Radionuclide Contaminated Aquatic Ecosystems and Drainage Areas) was originally an independent tool developed for the management of contaminated freshwater ecosystems (Monte et al., 2009, 1999).

MOIRA was applied to water bodies contaminated with radionuclides or heavy metals, where concentrations of isotopes such as ^{137}Cs and ^{90}Sr could be calculated, along with dosimetry and economic assessments (Hofman et al., 2011; Monte et al., 2009). An example of dose assessment for fish is presented in Fig. 23. MOIRA enabled the evaluation of potential countermeasure strategies for contaminated rivers and lakes, including options such as potash treatment, fertilization, removal of contaminated sediments, or bans on fish consumption (Monte et al., 2009).

The MOIRA hydrological model was also integrated into the JRODOS system, while the development of the original tool was discontinued (Schneider et al., 2017). JRODOS now additionally incorporates the Hydrological Dispersion Module (HDM) (Zheleznyak et al., 2002), which includes models such as RIVTOX (Zheleznyak et al., 2003), THREETOX (Margvelashvily et al., 1997), or POSEIDON (Bezhenar et al., 2016). However, these models primarily focus on the transport of contaminants in water bodies.

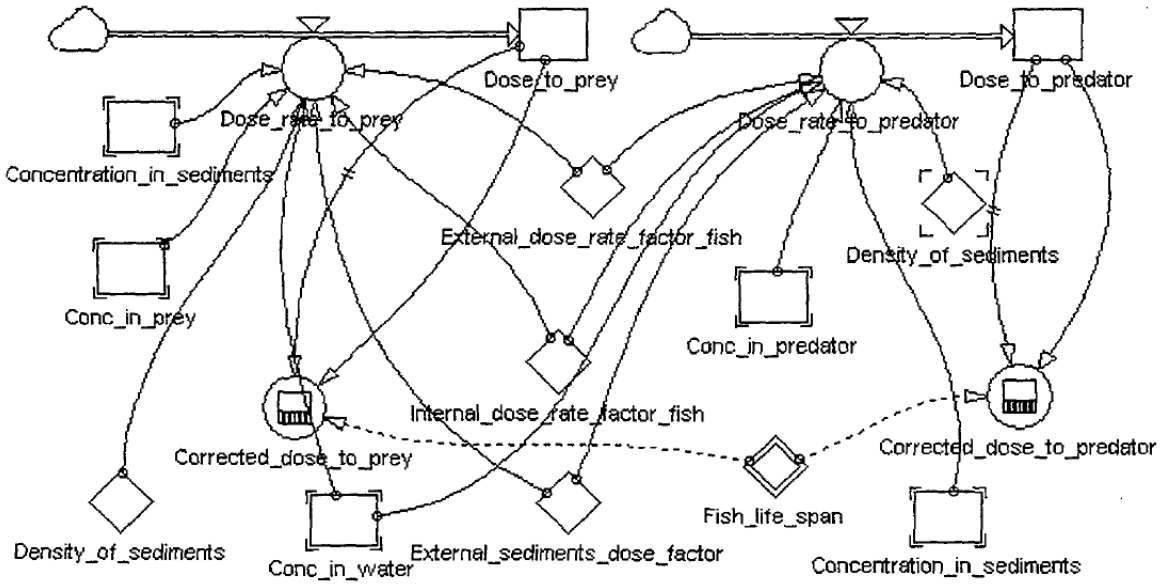

Fig. 23. MOIRA: assessments of doses to fish (source: Monte et al., 1999: 139)

5.9.7 POSEIDON

POSEIDON is a dynamic marine box model that simulates the migration of radionuclides from sediments to marine organisms (Bezhenar et al., 2016; Lepicard et al., 2004). In this model, water bodies, such as seas and oceans (and their parts in certain cases), are represented as distinct cells. POSEIDON is integrated into JRODOS within the HDM. Input data on surface contamination required for the POSEIDON model can be utilized from previous simulations using ADM models. Consequently, POSEIDON can incorporate simulations from conventional atmospheric dispersion models in JRODOS and can be connected with models such as the "Emergency" model chain (Ievdin et al., 2019; Lepicard et al., 2004).

In POSEIDON, the marine environment is described as a system of compartments, including the water column, bottom sediments, and biota (Bezhenar et al., 2016). POSEIDON provides assessments of activity concentrations in water, living organisms (e.g., fish, molluscs, zooplankton), and in the top sediment layers (Lepicard et al., 2004).

5.10 System Dynamics Approach

5.10.1 Description

The System Dynamics is an approach used to address complex problems with non-linear behavior (Sterman, 2000). It was developed by Jay W. Forrester at the Massachusetts Institute of Technology to support decision-making processes (Forrester, 1961; Sterman,

2000). The System Dynamics approach can be applied to enhance the performance and outcomes of complex systems across various fields by proposing effective policies (Assas and Gass, 2011; System Dynamics Society, 2024). This method involves computer simulations, where mathematical models are represented by differential equations (Forrester, 1961; Sterman, 2000). One of the most well-known works on the System Dynamics approach is the report by Meadows et al. (1972), which presents a computer model of exponential economic and population growth.

The System Dynamics method can be applied across a wide range of fields, including social, environmental, economic, and management sciences, as well as many other disciplines (Bossel, 2007a, 2007b, 2007c; System Dynamics Society, 2024). It facilitates the understanding and explanation of business and social system behaviors by utilizing concepts from feedback control theory (Assas and Gass, 2011).

Such multidisciplinary problems can be represented as complex systems composed of various parameters and mutually interconnected variables. These intricate interrelations often result in non-linear system behavior. Such dynamic behavior emerges from the interactions within closed structures, or feedback loops (Sterman, 2000).

Feedback loops can be classified as self-reinforcing (positive) or self-correcting (balancing, goal-seeking or negative). In a self-reinforcing feedback loop, a change in one variable reinforces itself through interactions with other variables within the overall structure, leading to overall system growth (Sterman, 2000). A common example of a self-reinforcing feedback loop is exponential population growth (Meadows and Wright, 2008).

In contrast, balancing feedback loops show the opposite behavior. These loops regulate self-limiting processes, driving the system toward equilibrium (Sterman, 2000). An example of the balancing feedback loop is radioactive decay (Albin, 2001), in which activity decreases exponentially over time.

System behavior can also be influenced by delays in interactions between its subcomponents. For example, a delay may occur between the initial release of contaminants and the contamination of groundwater, as the transport of contaminants from the source to the affected area takes a specific amount of time (Meadows and Wright, 2008). In balancing feedback loops, such delays can induce oscillations and contribute to the system's unstable behavior (Sterman, 2000).

Multiple interacting feedback loops contribute to the dynamic complexity of systems. The key properties of such systems include (Sterman, 2000, p. 22):

- *Dynamic behavior*: changes within the system occur across multiple time scales, which may interact with one another.
- *Tight interconnections*: all variables strongly interact within the system and with the external environment.
- *Feedback presence*: due to strong interconnections between elements (or variables), any action generates feedback, influencing the system's dynamics.
- *Non-linearity*: outcomes are rarely proportional to initial actions; moreover, local changes in one part of the system do not necessarily affect distant regions.
- *History- and path-dependency*: past actions are irreversible and shape the system's current state.
- *Self-organization*: system behavior emerges spontaneously from feedback interactions among its components.
- *Adaptability*: the system evolves over time in response to its capabilities and applied decisions.
- *Counter-intuitiveness*: in complex systems, causes and effects are not always obvious and may manifest over extended time and space.
- *Policy resistance*: apparent solutions may be ineffective due to system complexity and can even lead to unintended consequences.
- *Need for trade-offs*: the system's long-term responses may differ from its short-term reactions. High-leverage policies may initially cause setbacks before yielding improvements, whereas low-leverage policies often provide only temporary benefits.

5.10.2 Representation of Systems

The model structure can be represented using two types of diagrams: Causal Loop Diagrams (CLD) and Stock and Flow Diagrams (SFD) (Mildeová and Vojtko, 2008; Sterman, 2000). Both types of diagrams can be sketched using the Vensim software (Ventana Systems, 2023a). A detailed description of each diagram type is provided below.

CLDs

CLDs are useful for illustrating interdependencies and feedback processes within a model. They are employed to depict relationships between different components of the model and to identify feedback loops. This type of diagram is primarily used for communication, problem representation, and the identification of critical factors; however, it does not include

the equations used in the model. Another limitation of CLDs is their inability to represent the stock-and-flow structure of systems (Sterman, 2000).

CLDs consist of variables connected by arrows that represent causal relationships. Each arrow has its polarity. Polarities can be positive (+) or negative (-) (Fig. 24). Links with polarities define the structure of the system rather than the behavior of the variables. Polarities indicate how the dependent variable responds to changes in the independent variable (Sterman, 2000).

A positive link shows that changes in the cause and effect occur in the same direction: an increase in the cause results in an increase in the effect, and vice versa. Conversely, a negative link denotes that changes in the cause and effect occur in opposite directions: an increase in the cause leads to a decrease in the effect, and vice versa (Sterman, 2000).

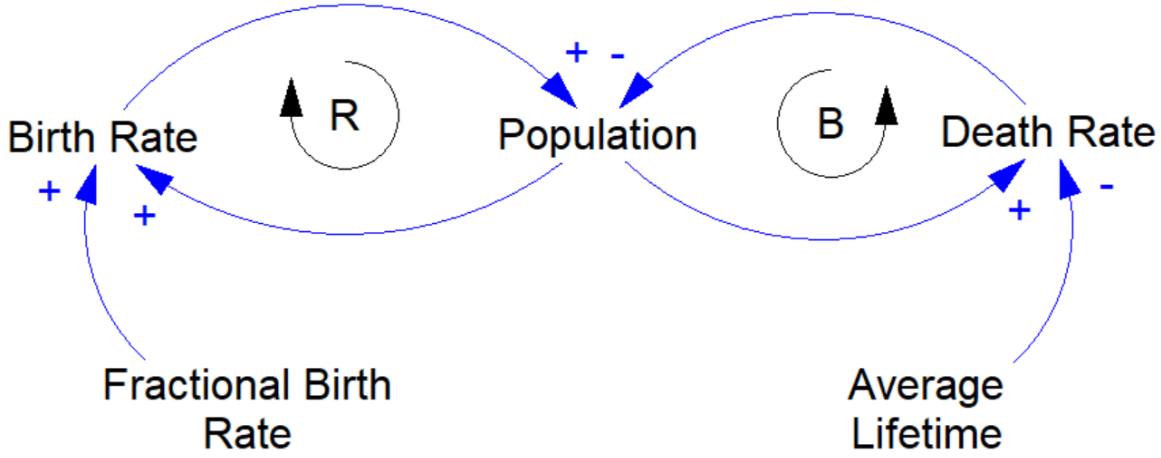

Fig. 24. Example of CLD (source: Sterman, 2000:138, adapted)

The feedback loops can then be identified using a loop indicator that specifies their type (Fig. 24). Self-reinforcing feedback loops are denoted by a '+' or 'R', while balancing feedback loops are represented by a '-' or 'B' (Sterman, 2000). An example of a reinforcing feedback loop can be found in Fig. 24. The reinforcing feedback loop consists of such variables as birth rate and population. The birth rate is affected by the fractional birth rate and by the population. Additionally, a balancing feedback loop is also depicted in Fig. 24. This feedback loop includes variables such as death rate and population. The death rate is determined by the average lifetime and also by the population (Sterman, 2000).

SFDs

SFDs are used to mathematically represent the structure of the investigated model, using stock and flow variables. Stocks and flows, including feedback loops, are fundamental

concepts in System Dynamics theory. Stocks (also referred to as levels) are time-dependent variables that correspond to definite integrals (Sterman, 2000). An example of a stock variable is the activity of a radionuclide (Albin, 2001). Stock variables indicate accumulations and define the current state of the system. The history- and path-dependency of a system are determined by stock variables (Sterman, 2000).

Stocks can be represented graphically as rectangles or boxes (Fig. 25). The rates of change in stocks are flows. Stocks accumulate flows, serving as their integrals. Flows are controlled using valves (Fig. 25). An increase in a stock is depicted as an inflow, represented by a filling pipe connected to the box, whereas a decrease in a stock can be shown as an outflow, represented by a draining pipe (Fig. 25). Stocks can produce delays by accumulating the difference between inflows and outflows in the examined processes (Sterman, 2000).

A simple representation of the relationship between stocks and flows can be expressed using the integral equation below (Sterman, 2000):

$$Stock(t_1) = Stock(t_0) + \int_{t_0}^{t_1} (Inflow(t) - Outflow(t))dt, \quad (5)$$

where *Stock*(t_1) is the integral of the difference between the *Inflow* and the *Outflow* rates, including the initial state *Stock*(t_0).

The corresponding differential equation is presented below (Sterman, 2000):

$$\frac{d(Stock)}{dt} = Inflow(t) - Outflow(t). \quad (6)$$

The boundaries of the model are graphically represented by clouds, which denote sources and sinks for flows outside the model's boundaries (Fig. 25). Sources and sinks are considered to have unlimited capacity and impose no constraints on the flows they facilitate (Sterman, 2000).

An example of an SFD is shown in Fig. 25. The same variables as in the CLD depicted in Fig. 24 are used. Population corresponds to the stock variable, while the birth rate and death rate represent the inflow and outflow, respectively.

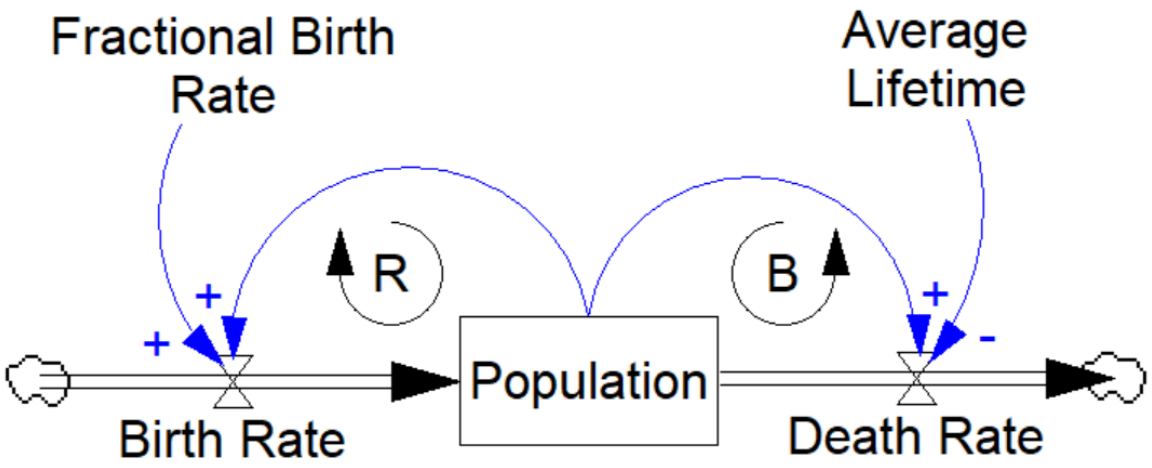

Fig. 25. Example of SFD (source: own efforts)

5.10.3 Environmental Cases

The System Dynamics approach has already been applied to various environmental contamination-related tasks. Selected cases are presented below. Moreover, System Dynamics methods were employed in the DSS MOIRA (Hofman et al., 2011; Monte et al., 2009), which is described in paragraph 5.9.6.

Transport of Radionuclides in Food Chains

The System Dynamics approach has been utilized to describe the transport of radionuclides in food chains (Kang and Jae, 2008). In this study, the Vensim software was used to develop a mathematical model. Using this model, the magnitude of radionuclide releases during severe nuclear accidents and their offsite consequences were evaluated. The modeling of atmospheric dispersion is presented in Fig. 26. The created model reflects the Korean environment and was developed to assess radiological consequences following short-term radioactive releases.

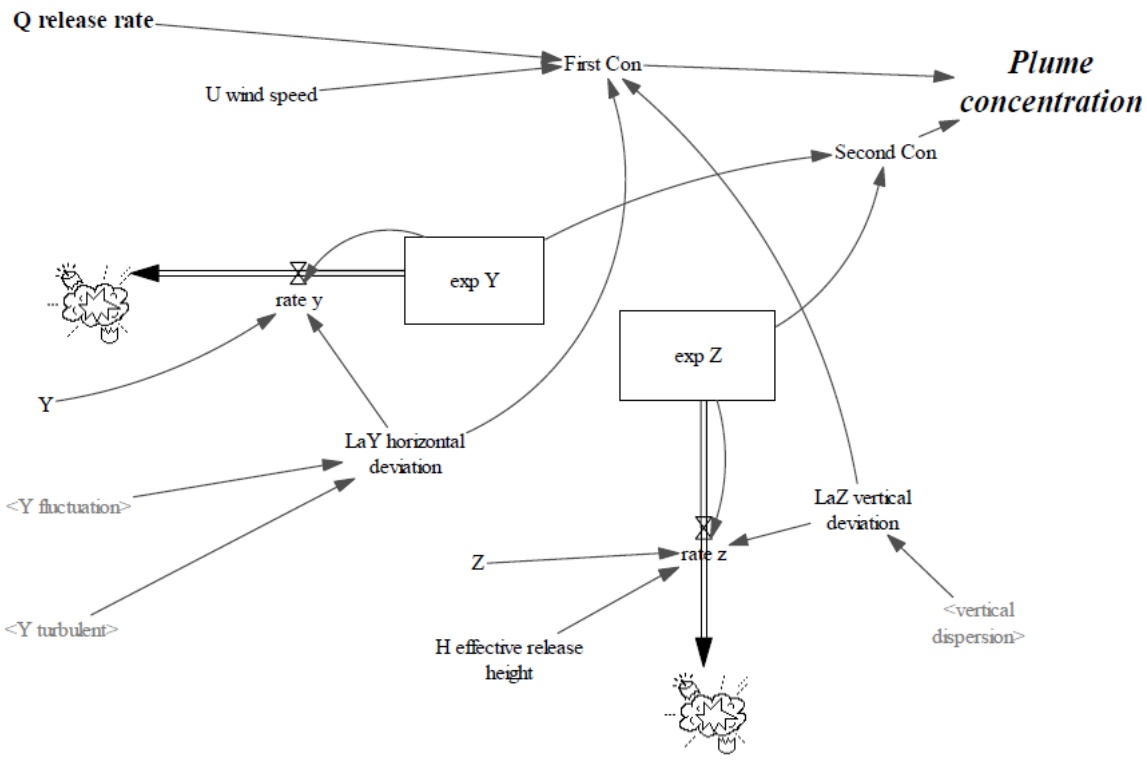

Fig. 26. Gaussian plume model (source: Kang et al., 2008: 729)

The proposed methodology included description of time-dependent behaviors, feedback loops, and uncertainties in complex physical systems. The developed model considered multiple environmental factors, such as deposition, weathering, washout, resuspension, and biological processes in soil and plants (Fig. 27). Nevertheless, it should be mentioned that several principles of model correctness should be fulfilled. For example, stock variables can be changed solely by flows (rule #6) (Lai and Wahba, 2001).

The model simulated radionuclide transport through rangeland-grazing, human-food crops, and pasture systems. It accounted for the transport of radionuclides in various environmental compartments, including vegetation, soil, and agricultural products such as fruits, vegetables, grains, meat, milk, and eggs. Additionally, the model improved predictions of long-term exposure risks (Kang and Jae, 2008).

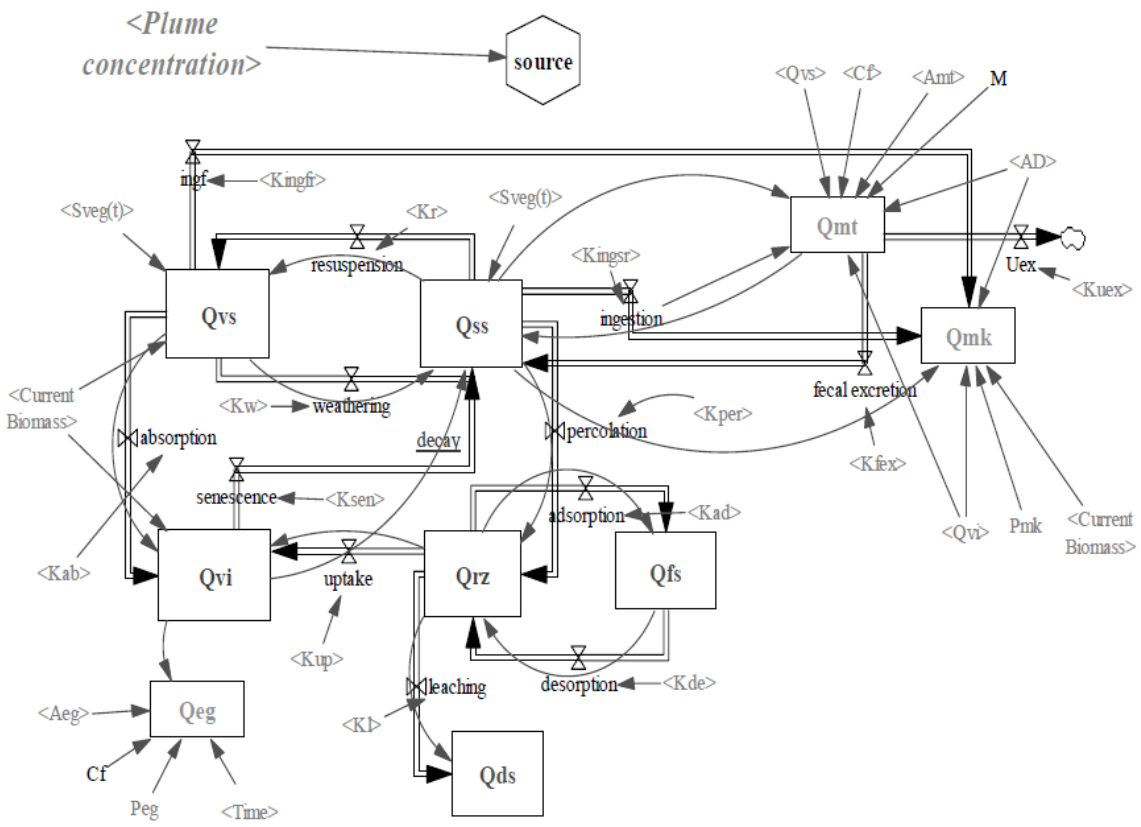

Fig. 27. Ingestion model (source: Kang and Jae, 2008: 729)

Groundwater Contamination

McKnight et al. (2010) developed an integrated model to assess the risks of trichloroethylene (TCE) contamination in groundwater (Fig. 28). Their system combined the CARO-PLUS decision-support system with the AQUATOX aquatic ecosystem model, allowing for the evaluation of both human health and ecological risks.

The study found that although TCE concentrations in surface water were below human health risk thresholds, volatilization processes played a significant role in attenuating contamination levels, emphasizing the importance of understanding groundwater-surface water interactions. Within the uncertainty assessments, hydraulic conductivity revealed was the most significant site-specific parameter.

In a subsequent study, McKnight and Finkel (2013) expanded on their previous work by developing a system dynamics model for long-term human health risk assessment at contaminated sites. The CARO-PLUS model was applied to assess risks associated with non-aqueous phase liquids (NAPLs) in groundwater, emphasizing the need for early-stage decision-making tools. The study highlighted the benefits of using Monte Carlo simulations

to account for uncertainties in contaminant transport and exposure scenarios, improving the reliability of risk assessments.

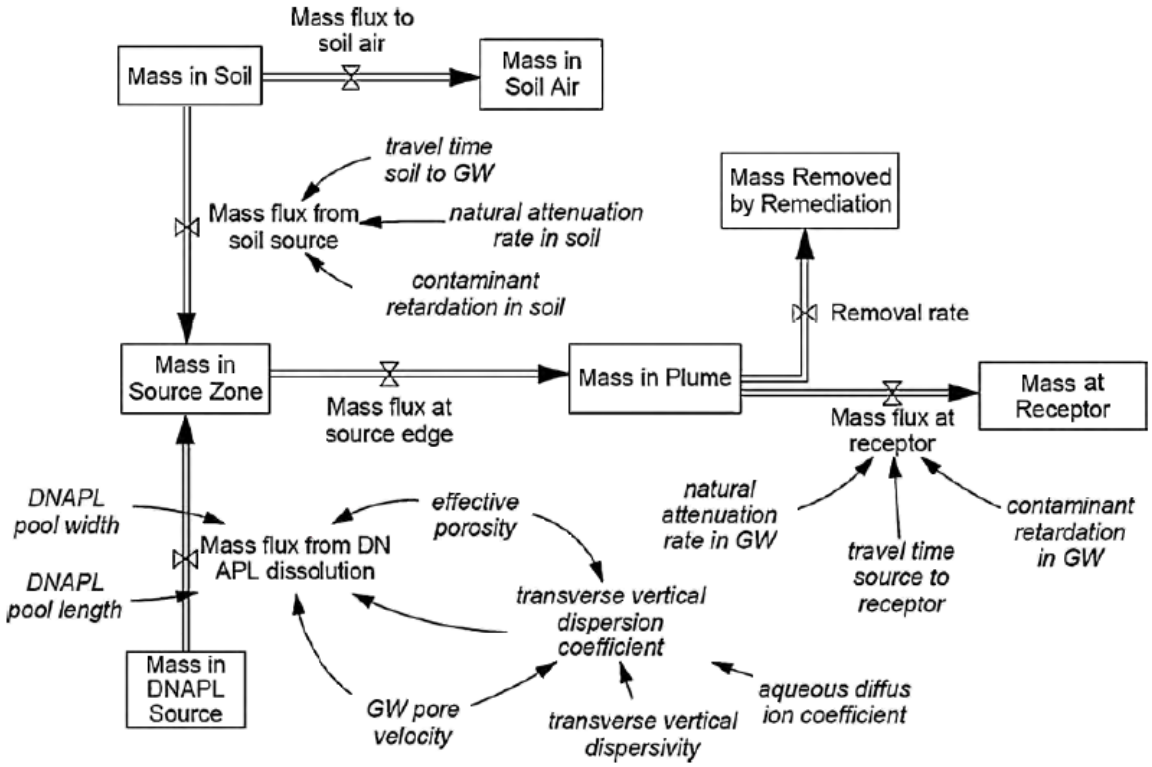

Fig. 28. Model for the release and transport of contaminants (source: McKnight et al., 2010: 1129)

Consequently, Naseri-Rad et al. (2022) introduced DynSus, a decision-support system for assessing sustainability in groundwater remediation. This tool integrates a contaminant fate and transport model with sustainability indicators, enabling the evaluation of various remediation scenarios. Their study demonstrated that although passive methods, such as monitored natural attenuation, may be initially favorable, more active approaches, like bioremediation, would provide better long-term sustainability outcomes.

5.10.4 The Most Recent Applications

The most recent findings (since 2021) on the use of System Dynamics methods are summarized below, excluding radionuclide transport. Selected studies focus on areas such as risk management, decision-making support, and the modelling of physical, and to some extent, biological processes, which are relevant to the current research.

J. Liu et al. (2021) explored the dependencies among performance shaping factors (PSFs) in human reliability analysis (HRA) using the System Dynamics approach. The study aimed to improve the Standardized Plant Analysis of Risk-Human Reliability Analysis (SPAR-H) method by modeling the dynamic and nonlinear interdependencies of PSFs. By

integrating mutual information theory and the analytic hierarchy process, the research enhanced the accuracy of human error probability (HEP) estimation. The methodology was tested on three human failure events in a nuclear power plant, demonstrating its robustness and practical applicability.

Naeem et al. (2024) proposed the System Dynamics model to solve water resource management (WRM) challenges in Qatar. The model integrates policy scenario analysis and decision-support systems to simulate water supply and demand dynamics from 2021–2070. The findings indicated that the "business-as-usual" policy can sustain water balance for only 32 years, while the optimized policy could extend sustainability up to 50 years. The WRD model is depicted in Fig. 29. The study also revealed groundwater conservation as a critical strategy for long-term water security.

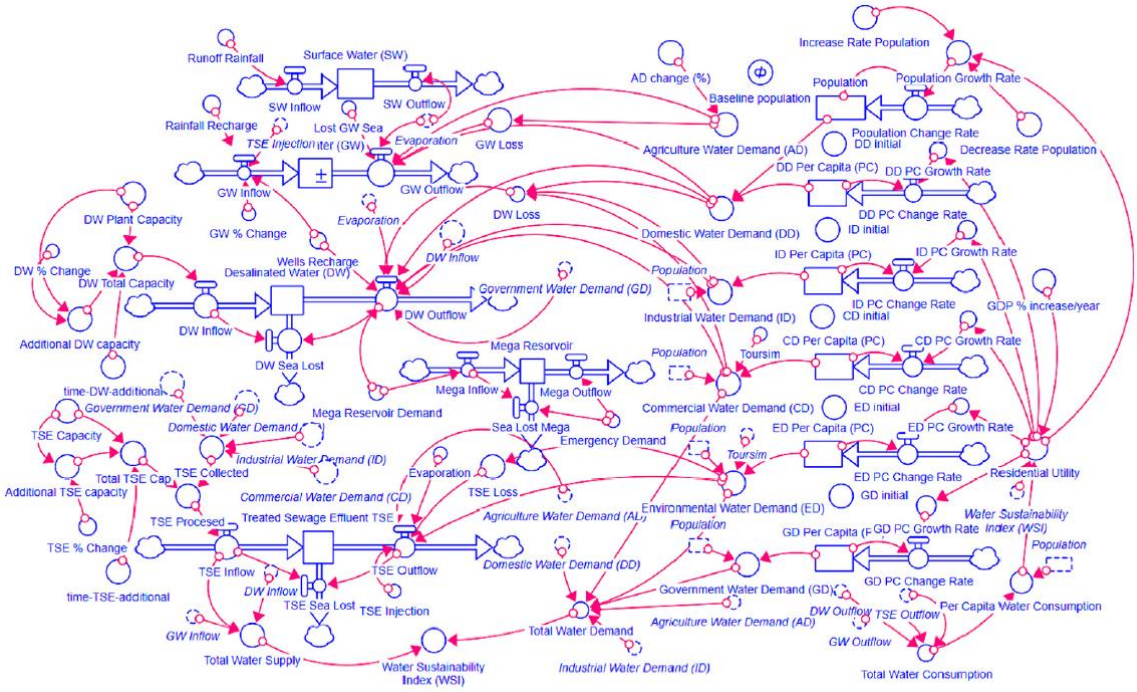

Fig. 29. Qatar's WRM model (source: Naeem et al., 2024: 738)

Meng et al. (2022) proposed a hybrid approach for the economic evaluation of predictive maintenance technologies. Their study developed an integrated system dynamics and evolutionary game theory (SD-EGT) model to assess the cost-benefit analysis (CBA) of predictive maintenance adoption. The model was applied to lithium-ion batteries, examining the trade-offs between failure risk reduction and investment costs. The research optimized investment strategies for stakeholders and highlighted the importance of information asymmetry in decision-making. The results offered valuable insights into subsidy strategies and the economic feasibility of predictive maintenance implementation.

Park et al. (2024) developed the System Dynamics model to assess the performance of safety management systems (SMS) in petrochemical plants. The article addressed the limitations of traditional safety approaches by incorporating feedback loops and time delays. The model established relationships within SMS and was validated through scenario-based simulations. Results highlighted the significant impact of senior management on safety performance. The model can be used by decision-makers with insights on how to optimize safety policies and how improve risk management in process industries.

Qiao et al. (2024) focused on modeling human reliability in extreme environments, particularly in manned submarine diving tasks. The study extended the traditional IDA (Intelligent Data Analysis) team cognitive model by incorporating team performance shaping factors (Team-PSFs) and human time performance based on the Weibull function. The research employed dynamic risk assessment techniques to quantify decision-making errors in high-risk cooperative scenarios. Through simulations, the proposed model demonstrated its accuracy in predicting operator performance, thereby improving the reliability of risk assessment in extreme operational settings. The developed approach was validated using simulations of manned submarine.

He et al. (2025) developed the System Dynamics model to optimize safety investments in chemical industrial parks (CIPs). Based on an analysis of 203 major accidents from 2000–2023, the study identified key accident causes and proposed targeted safety investment strategies. The model was validated using a provincial CIP case study, showing that safety management had the highest impact on safety improvement, followed by training, protection, and assessment measures. The study emphasized the need for dynamic investment strategies to maximize safety enhancements with limited financial resources.

Ismail et al. (2022) applied the System Dynamics approach to optimize the management of the Indian mackerel (IM) fishery. The study provided a holistic framework for balancing ecological preservation with economic viability in open-access fisheries. The developed model integrated biological, economic, and management sub-models to evaluate the impact of different fishing policies (Fig. 30). The study thus well demonstrated that the System Dynamics approach is highly suitable for addressing complex tasks from multiple perspectives.

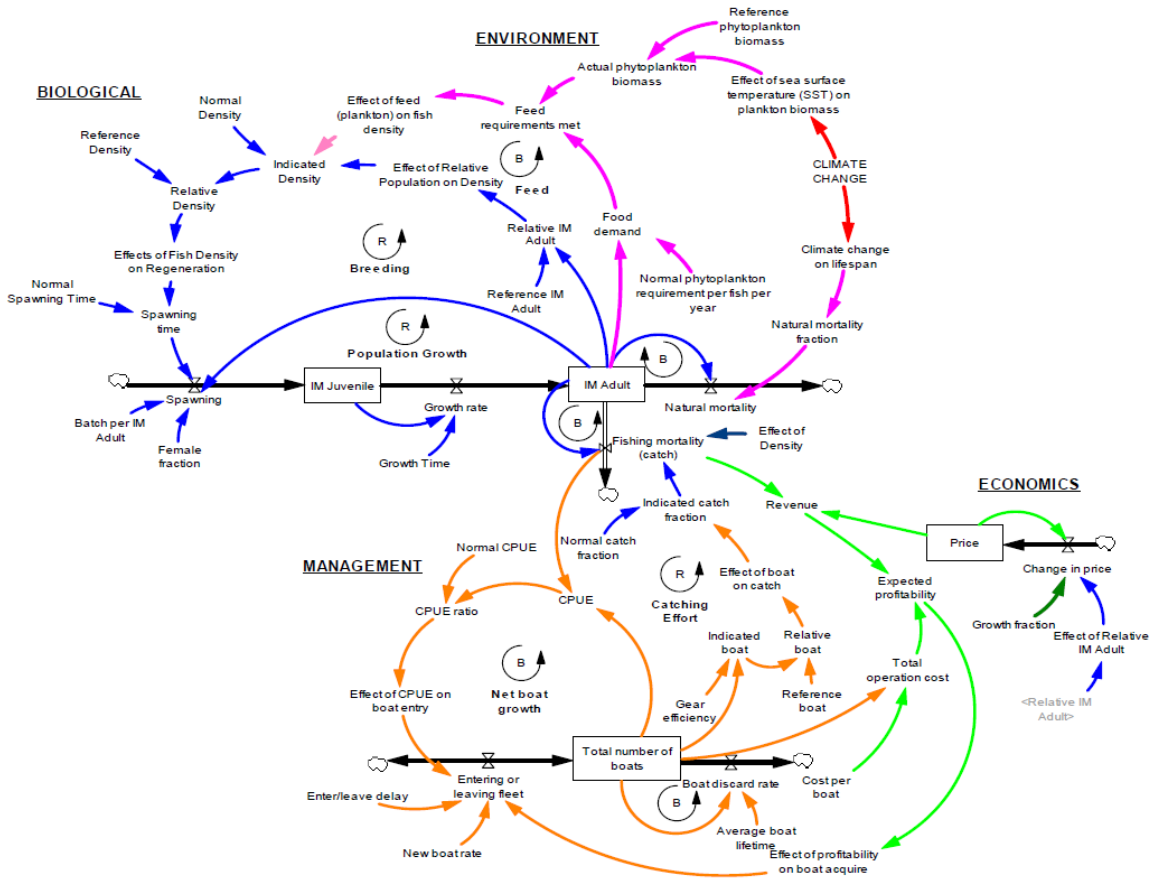

Fig. 30. Model of IM fishery (source: Ismail et al., 2022: 7)

A. Liu et al. (2021) proposed a dynamic risk assessment model for buried gas pipelines, addressing the limitations of static risk models. The research integrated system dynamics with failure probability calculations and accident consequence analysis. By simulating risk evolution over time, the study demonstrated that corrosion-related failures required proactive risk mitigation measures. The model was tested on a natural gas pipeline in Zhuhai, China, revealing its effectiveness in predicting spatial and temporal risk trends and supporting preemptive safety interventions.

Gong et al. (2025) examined the long-term vulnerability evolution of critical infrastructures (CIs) by integrating environmental, physical, and socio-economic factors into a system dynamics model. The study introduced four key vulnerability components: risk exposure, physical fragility, environmental sensitivity, and recovery capacity. Through case simulations, the research revealed that CI vulnerability follows a nonlinear growth pattern influenced by long-term environmental feedback loops. The findings provided a framework for optimizing vulnerability mitigation strategies and enhancing infrastructure resilience against emerging risks.

6 Material and Methods

This chapter outlines the overall process of preparing input data and corresponding modeling tasks, developing the Recovery model, conducting tests and validations, designing recovery scenarios, and performing related analyses. The main findings from this chapter, along with those from Chapter 7, which focuses on the obtained results, have been recently published by Selivanova et al. (2025).

6.1 Atmospheric Release

To obtain input information about the initial contamination, i.e., its scale and surface activities, a set of 110 simulation tasks was performed using JRODOS. The simulations were conducted for several source terms of changing magnitudes and for the most typical meteorological conditions in the area of interest. Due to the large number of simulation tasks, the processes of task creation and auto-launching of the corresponding xml-files were automated utilizing scripts in R language (R Core Team, 2022; Selivanova et al., 2023).

6.1.1 Basic Set-up

The release point was located in NPP Dukovany. The simulation radius in JRODOS was set to 40 km to ensure complete coverage of an area of interest, or the emergency planning zone (EPZ) of NPP Dukovany. The EPZ is located within a circle with a radius of 20 km, including inner radii of 10 km and 5 km (Kubanyi et al., 2008). The EPZ consists of 16 sectors and inner segments, categorized according to their distance from the NPP (i.e., 10 km or 20 km). The spatial resolution varied from 0.1 km to 1.6 km, depending on the distance from the release point (the standard JRODOS grid was utilized).

Considering the chosen horizontal scale of the calculations (< 50 km), which spans several tens of kilometers, the RIMPUFF (Risø Mesoscale PUFF model), a Lagrangian mesoscale atmospheric dispersion model, was employed. Another reason of the uses of the RIMPUFF model was utilizing detailed in-stationary meteorological data (Thykier-Nielsen et al., 1999). The prognosis duration was set at 48 hours to accommodate the varying release durations specified in the selected source terms.

6.1.2 Source Terms

In NPP Dukovany, four units of the VVER-440/V213 type are in operation (SÚJB, 2019). In the presented research, a diverse range of source terms was employed to encompass a wide spectrum of potential accidents. These source terms were selected from the JRODOS library. Accordingly, five source terms with varying cesium isotope activities (^{134}Cs and ^{137}Cs) were selected for both DBA and SEV events. The selected source terms covered both small- and large-scale radionuclide releases, as well as a wide range of potential accident scenarios.

In the selected source terms, the total cesium activity differed by at least one order of magnitude. Other radionuclides, such as iodines and noble gases, were also included in the source terms; however, these were excluded from the analyses due to their shorter half-lives. Transuranium elements were not considered. Key parameters of the source terms, including the release height and duration, are presented in Table 4 (Raskob et al., 2011). Detailed source terms can be found in Appendix A – Source Terms..

The JRODOS simulations provide various outputs, such as information on the levels of surface deposition in affected areas. Deposited activities occur on different surfaces, including grassed areas, fields, trees, roads, and the walls and roofs of buildings (Andersson and Roed, 2006). Achieving such fine resolution in simulations is challenging due to the high demands on computational performance. However, knowledge of contamination on a large reference object, such as open grassed areas, can be used to recalculate activities on other surfaces (Andersson et al., 2002; Andersson and Roed, 2006).

In practical situations, detailed measurements are required, while simulations can serve as **supportive tools only** (Selivanova et al., 2022b).

Table 4. Parameters of source terms used in simulations (source: JRODOS, 2019 – extracted from software)

Source term	Description	Duration (h)	Height (m)	Activity of Cs (Bq)	Total Activity (Bq)	INES Scale
DBA1	Steam generator tube rupture (SGTR event), coolant bypass of containment, rupture of 3 tubes, release through the safety valve.	1	50	1.71E+10	1.51E+13	0
DBA4	SGTR event, collector cover opening, safety valve remains open, release through the safety valve.	1	50	1.60E+11	1.15E+14	4
SEV1	Containment leakage, leakage rate: 0.5 %/h, containment sprays off, gap release (uncovered 15-20 min).	6	120	3.90E+13	3.67E+15	5
SEV6	Containment coolant bypass, gap release (uncovered 15-20 min), steam generator: not partitioned, injection rate: 100 m^3/h.	3	40	3.99E+15	4.59E+17	7
SEV7	Core melt, coolant bypass of containment, steam generator: not partitioned, injection rate: 200 m^3/h.	6	40	3.97E+16	1.18E+19	7

6.1.3 Weather Data

To simulate atmospheric releases in the JRODOS tool, detailed meteorological records for NPP Dukovany were employed. The historical meteorological dataset was provided by the Czech Hydrometeorological Institute[6] (CHMI) and covered a continuous period of 14 months from 2011 to 2013. Additionally, the dataset was adjusted to meet the requirements of simulations (i.e., allowed stability classes) in JRODOS (Selivanova et al., 2023).

Subsequently, the most important parameters, especially the most frequent wind speed and wind direction, were analyzed. The typical wind speed ranged from 3 $m \cdot s^{-1}$ to 4 $m \cdot s^{-1}$, and the most common wind direction was within an interval of 300–330° (Northwest). Based on these estimates, 22 meteorological sequences were selected and then used in simulations for each source term. The corresponding wind rose is presented in Fig. 31. Consequently, for each of 5 source terms, 22 simulations with varying meteorological conditions were conducted, resulting in a total of 110 simulations (i.e., 5 source terms × 22 meteorological sequences).

[6] Czech Hydrometeorological Institute (CHMI), Na Šabatce 2050/17, 143 06 Prague, Czechia, https://www.chmi.cz/.

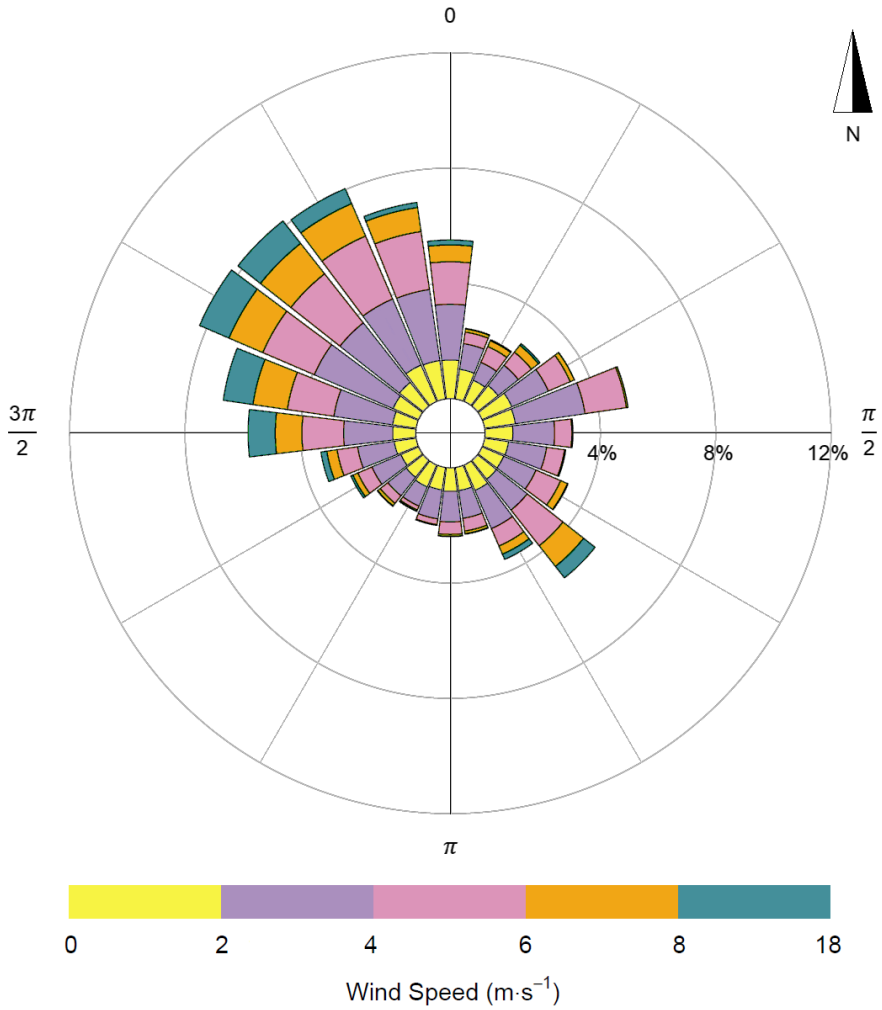

Fig. 31. Wind rose for Dukovany location (source: Selivanova, 2022: 327)

6.2 Initial Contamination

Using the chosen source terms (Table 4) all selected weather data, simulations were conducted in JRODOS. Thereafter, simulated layers with surface activities of ^{134}Cs and ^{137}Cs were extracted as shapefiles. Only the layers containing cesium isotopes were analyzed, due to the relatively longer half-lives of these radionuclides: ^{137}Cs with a half-life of 30.02 years and ^{134}Cs with a half-life of 2.06 years. Consequently, the output layers for each isotope were averaged within each cell, considering all selected meteorological cases.

The averaged layers for each radionuclide were then summed. The resulting layers of surface contamination with cesium isotopes were depicted using QGIS software (QGIS Development Team, 2021). To visualize towns, roads, fields, and forests, source layers provided by the OpenStreetMap database were added to the final output maps (OpenStreetMap contributors, 2021).

To estimate the scale of affected areas, the most typical types of contaminated objects and their corresponding extents within the EPZ were assessed. Objects such as buildings, fields/grassed areas, forests/shrubs, and roads were analyzed. Water bodies were excluded from the analysis due to their relatively small surface areas compared to the total areas of the other objects. Fields/grassed areas occur roughly on 48% of the EPZ. Forests/shrubs cover approximately 36% of the EPZ, being the most substantial objects in the EPZ requiring decontamination.

6.3 Population

To assess the gender and age representation of inhabitants, detailed analyses of towns within the EPZ were conducted. These estimates originated from the population census results in 2021. The data on inhabitants were provided by the Czech Statistical Office[7] (CZSO) (CZSO, 2021). The census results indicated that 104 277 individuals resided within the EPZ, including 51 913 men and 52 364 women. Detailed data are presented in Table 5.

According to ICRP (ICRP, 2006) and to the Czech legislation (SÚJB, 2016), three age categories are recommended to estimate a representative person:

- 0–5 years (infant),
- 6–15 years (child),
- 16–70 years (adult).

However, for practical purposes, these age cohorts can instead be represented by dose coefficients and habit descriptions for a 1-year-old child, a 10-year-old child, and an adult (ICRP, 2006). The CZSO provides data on other age cohorts divided into 5-year intervals. Therefore, the data were adapted and aggregated accordingly (CZSO, 2021).

Table 5. Description of population within EPZ

Age	0–5 years	6–15 years	≥16 years	Sum
Women	3 412	5 412	43 540	52 364
Men	3 616	5 580	42 717	51 913

[7] Czech Statistical Office (CZSO), Na padesátém 3268/81, 100 82 Prague, Czechia, https://www.czso.cz/.

6.4 Buildings

To estimate the most common parameters of buildings within the EPZ, data provided by the Czech Office for Surveying, Mapping, and Cadastre[8] (ČÚZK) were utilized (ČÚZK, 2023). Characteristics such as construction materials, number of floors, types of buildings were obtained from the ČÚZK database.

According to ČÚZK, 60 364 buildings are located in the EPZ. The detailed data are available for 59 570 buildings, or 99% of the overall records. The majority of the buildings (approximately 60%) is used for residential purposes. Therefore, these buildings are detached houses or apartment blocks. The most of the assumed buildings is made of bricks, stones, or concrete. The most common number of floors is one (ČÚZK, 2023).

6.5 Scenarios

In the EPZ, fields and forests are the most prevalent types of landscape. Consequently, countermeasures incorporated into the mathematical model of recovery were chosen to address these dominant environments. Considering fields, which represent the most frequently contaminated surfaces in the EPZ, three decontamination methods were selected: grass removal, soil stripping (removal of topsoil layers), and turf harvesting. For forests, pruning of trees and shrubs was anticipated as the primary decontamination technique.

Considering other surfaces potentially contaminated with radionuclides, the most common and effective decontamination methods were assumed. Hence, high-pressure water washing was planned for the clean-up of streets: houses, specifically roofs and walls, and roads.

Essential parameters such as working rates of different decontamination techniques, corresponding decontamination factors, and the number of personnel in teams were based on the guidelines by Nisbet et al. (Nisbet and Watson, 2018). Decontamination factors were primarily set to mean values for each technique. In cases of higher surface contamination levels (greater or equal 10 $MBq \cdot m^{-2}$), additional recovery efforts were anticipated, such as the removal of thicker soil layers. Consequently, slower working rates, increased radioactive organic waste production (e.g., soil and turf), and higher decontamination factors, as reported

[8] Czech Office for Surveying, Mapping and Cadastre (ČÚZK), Pod sídlištěm 1800/9, 182 11 Prague, Czechia, https://www.cuzk.cz/.

in the available sources, were applied in contrast to scenarios with contamination levels below 10 $MBq \cdot m^{-2}$.

Moreover, the recovery model contains such option as the access restriction, or demarcation of contaminated territories, in all decontamination scenarios, including the reference scenario. The reference scenario is a special case, which does not involve any decontamination strategies. The duration of implementation of the access restriction was set to 10 days in each scenario by default, due to the lack of specific information on the corresponding work rates.

Additionally, the mathematical model includes the collection of solid organic waste, its transport to a disposal site located 20 km from the decontaminated area, and the decontamination of workers and vehicles with water (Andersson et al., 2000; Nisbet and Watson, 2018). For completeness, the recovery model assesses the volumes of both solid organic waste (i.e., soil, turf, leaves and branches, grass) and liquid waste (generated during the cleaning of streets, roads and buildings). The model did not account to produce radioactive liquid waste in the vicinity of damaged reactors (in case of very severe accidents). The manipulation with such radioactive waste may potentially be included into the mathematical model of recovery in future studies.

6.6 Costs

Expenses related to decontamination included various items, such as the costs of materials, tools, equipment, labor, waste handling, and fixed capital. The original costs of the required items were from the period 2000–2021. All costs were derived from available sources and adjusted for inflation in 2022.

Detailed information about item costs is available in Appendix B – Costs. All costs are expressed in CZK. Subsequently, the total recovery costs in CZK were converted into EUR using the typical exchange rate for 2024–2025, where 1 EUR ≈ 25 CZK (CNB, 2025a).

6.6.1 Basic Items

With regard to the workers' equipment, the costs of personal protective equipment (PPE) included items such as protective suits (tyveks or tychems, depending on the contamination level), gloves, respirators, boots, and electronic personal dosimeters (EPD). For auxiliary tools and equipment, the costs of shovels, brooms, carts, chainsaws, axes, ladders, cutters,

fences, warning boards, tapes, and waste bags were included in the calculations (Andersson et al., 2000; Nisbet and Watson, 2018; U.S. EPA, 2016).

During the implementation of selected countermeasures, experienced operators of large machinery and their assistants (for manual works) were required. Consequently, workers' salaries were categorized using two wage rates. Additionally, expenses related to fuel and water consumption during the decontamination of workers and vehicles were incorporated into the model (Andersson et al., 2000; Selivanova, 2019).

6.6.2 Water Tie-down

Considering countermeasures such as topsoil removal (soil stripping) and turf harvesting, both methods were enhanced with a water tie-down process. The water tie-down process is intended to limit the resuspension of contaminated soil/dust particles during the removal of surfaces (Nisbet and Watson, 2018). This process requires two workers and specialized equipment to sprinkle the areas or objects of interest with water. The necessary equipment includes a sprinkler on a tripod and a hose reel (Nisbet and Watson, 2018).

The costs of the water tie-down process included items such as salaries, fuel and water consumption, and the wear of tractors, sprinklers, tripods, and hose reels. These costs were consistently added to the total costs of topsoil removal and turf harvesting.

6.6.3 Waste Handling

According to previous research, the waste produced during decontamination can significantly impact the total costs of recovery (Selivanova, 2020a; U.S. EPA, 2016). In the first version of the recovery model, a simplified approach to waste management was employed (Selivanova, 2020a, 2019). It was assumed that a disposal site located 20 km from the decontaminated area would be used. The waste handling cost of 20 EUR·m^{-3} was then adopted and corrected for inflation (Andersson et al., 2000; Selivanova, 2020a).

The current version of the waste handling sub-model, however, includes a detailed description of the entire process, including cost calculations. Real expenses associated with the collection and transportation of waste to disposal sites 20 km from the decontaminated area were assessed. These costs included personal protective equipment for workers, salaries, fuel and water consumption, and consumption of fixed capital (e.g., tractors or trucks). The updated waste sub-model also enabled the estimation of doses received by workers during waste handling (Nisbet and Watson, 2018; Selivanova, 2020b).

Comparing both the simplified and detailed approaches, the cost estimates were found to be of the same order of magnitude. Therefore, the detailed approach was adopted for the final version of the recovery model (Selivanova, 2020b).

Both approaches were dedicated to the handling of solid waste, including soil, turf, grass, leaves, and branches. The management of liquid waste produced during decontamination activities, such as the washing of surfaces or the decontamination of workers and vehicles, was not incorporated into the model due to the lack of specific information regarding the Czech environment. Nevertheless, water used for decontamination can probably be discharged if the corresponding volumetric activities are below the thresholds of 4 $MBq \cdot m^{-3}$ for sewers (or 20 MBq per 5 000 l) and 0.4 $MBq \cdot m^{-3}$ for watercourses (or 2 MBq per 5 000 l) (IAEA, 2000).

6.6.4 Fixed Capital

Consumption of fixed capital (or wear-off) was included in the total cost calculations, according to Roed et al. (1998). In the proposed mathematical model, fixed capital referred to heavy machinery such as tractors, excavators, trucks, and similar equipment. To assess these costs, it was necessary to assume the acquisition costs of heavy machinery, its expected annual usage (25 weeks per year), and its depreciation period (6 years) (Roed et al., 1998). In the model, total wear was estimated based on the duration of recovery and the number of operators (i.e., the number of heavy machinery units). All acquisition costs were also adjusted for inflation in 2022.

6.7 Mathematical Model

The mathematical model of recovery was created and developed using Vensim DSS (Ventana Systems, 2023a). The recovery model provides both dosimetry calculations, such as dose estimates, and economic assessments. Regarding dose modeling, the model allows for the calculation of doses for both inhabitants and workers (Selivanova et al., 2025).

The model is divided into 72 layers, each dedicated to specific tasks. It contains nearly 700 variables and parameters: 38 of these variables are stocks, representing the current states at specific times; approximately 480 are auxiliary variables, and the remaining are parameters.

6.7.1 Contaminated Objects

In the recovery model, five types of potentially contaminated objects are described, along with the physical processes following the deposition of radioactivity (Selivanova et al., 2025):

- Large grassed open areas (e.g., fields, playgrounds, recreational meadows),
- Shrubs or trees (e.g., gardens, forests),
- Roads (streets),
- Roofs of buildings,
- Walls of buildings.

To simplify dosimetry modeling for large urban and rural environments, large grassed open areas can be used **as reference contaminated areas**, along with the corresponding initial contamination levels, or surface activities (Andersson and Roed, 2006). Considering outdoor conditions, both radioactive decay and washout/weathering processes should be incorporated into the modeling. For subsequent decontamination efforts, the corresponding decontamination rates should be included (Ahn et al., 2014).

It should be noted that within the recovery modeling, assessments of surface contamination of the anticipated objects were based solely on simulations in JRODOS and on the use of equations (7)–(11). Under real conditions, actual levels of contamination will be determined based on real measurements (MEXT, 2011).

For contamination of large grassed areas, the modified formula was employed (Andersson and Roed, 2006):

$$A_{grass} = A_{0,grass}\, e^{-\lambda_r t} \left(0.575\, e^{-\lambda_{g1} t} + 0.425\, e^{-\lambda_{g2} t}\right), \quad (7)$$

where $A_{0,grass}$ is the initial contamination on the grassed surface (in Bq·m^{-2}), λ_r is the decay constant for cesium isotopes (^{137}Cs and ^{134}Cs), λ_{g1} and λ_{g2} are weathering rates for the weathering half-lives of 3.3 years and 21 years.

Considering contaminated roads (streets), the equation was adapted (Andersson and Roed, 2006):

$$A_{street} = 0.5\, A_{0,grass}\, e^{-\lambda_r t} \left(0.7\, e^{-\lambda_{s1} t} + 0.3\, e^{-\lambda_{s2} t}\right), \quad (8)$$

where $A_{0,grass}$ is the initial contamination of the reference grassed area, λ_r is the decay constant for ^{137}Cs or ^{134}Cs, λ_{s1} and λ_{s2} are weathering rates for the weathering half-lives of 120 days and 3 years.

In case of contamination of roofs, the modified formula below was utilized (Andersson and Roed, 2006):

$$A_{roofs} = 0.5\, A_{0,grass}\, e^{-\lambda_r t} \left(e^{-\lambda_{r1} t} + e^{-\lambda_{r2} t}\right), \quad (9)$$

where $A_{0,grass}$ is the initial contamination of the reference grassed surface, λ_r is the decay constant for the assumed cesium isotopes, λ_{r1} and λ_{r2} are weathering rates for the weathering half-lives of 4 years and 30 years.

For contamination deposited on walls, the equation was used (Andersson and Roed, 2006):

$$A_{walls} = 0.1\, A_{0,grass}\, e^{-\lambda_r t} \cdot e^{-\lambda_w t}, \quad (10)$$

where $A_{0,grass}$ is the initial contamination of the reference field/meadow, λ_r is the decay constant for ^{137}Cs or ^{134}Cs, λ_w is the weathering rate for the weathering half-life of 7 years.

Considering contamination of plants (shrubs or trees), the modified formula was employed (Andersson and Roed, 2006):

$$A_{trees} = 3\, A_{0,grass}\, e^{-\lambda_r t} \cdot e^{-\lambda_p t}, \quad (11)$$

where $A_{0,grass}$ is the initial contamination of the reference grassed object, λ_r is the decay constant for both cesium isotopes, λ_p is the weathering rate for the weathering half-life of 100 days.

6.7.2 MCNP Simulations

To obtain doses, equations (7)–(11) can be integrated over time and multiplied by the corresponding conversion coefficients, such as activity-to-dose-rate coefficients (Ahn et al., 2014; Andersson and Roed, 2006; Meckbach et al., 1988). For certain geometries, such coefficients are available (Nisbet and Watson, 2018). For example, considering large grassed surfaces, coefficients for cesium isotopes (^{137}Cs and ^{134}Cs) are listed in the Guide by Nisbet et al. (2018).

For other types of contaminated objects, the corresponding coefficients have been previously assessed using Monte Carlo methods (Meckbach et al., 1988). However, these coefficients cannot be applied in the current study due to differing approaches and due to differences in the expected geometries of irradiation. Consequently, new Monte Carlo simulations were conducted to calculate suitable conversion coefficients. All activity-to-dose-rate coefficients, both adopted and simulated, are presented in Table 6.

Monte Carlo simulations presented in the current study were performed using the MCNP code. MCNP is a general-purpose software package that enables three-

dimensional simulations of particle transport, including electrons, photons, neutrons, and others (Goorley et al., 2013). It can be applied in criticality calculations, medical physics, shielding and dosimetry assessments, detector response simulations, and various other fields. The code employs Monte Carlo methods based on nuclear data libraries, such as cross sections of interactions[9] (or probabilities). These methods were originally developed at Los Alamos National Laboratory (LANL) in the 1940s to address neutron transport problems (Goorley et al., 2013).

Considering the contamination of streets (i.e., roads and buildings) and vegetation (trees and shrubs), the required coefficients were obtained using the MCNP6.1 code (Goorley et al., 2013). The corresponding uncertainties of the Monte Carlo simulations were less than 0.2%. In the present study, only fresh deposition was assumed. Examples of the Monte Carlo tasks and the corresponding codes can be found in Appendix C – MCNP Simulations.

Streets and Buildings

To simulate contaminated street areas (e.g., roads), a simplified approach utilizing a quasi-infinite asphalt surface was employed. The material parameters, particularly for asphalt pavement, were adopted from the Material Compendium (McConn Jr et al., 2011).

Considering the contamination of surfaces (e.g., soil), the activity concentration decreases exponentially with depth and can be described using the concept of relaxation depth (UNSCEAR, 2000). The relaxation depth corresponds to the material thickness at which the surface activity decreases to $1/e$ of its initial surface value (Fig. 32). This parameter generally depends on the type of soil, its humidity, and its porosity (Kato et al., 2012; Takahashi et al., 2015). For older contamination (more than 1 year), a relaxation depth of 3 cm can be used, while for fresh contamination, a value of 1 mm is applicable.

The exponential distribution of activity concentration in soil can be expressed using the following equation (Beck, 1966):

$$A(h) = A_0 \cdot e^{-\alpha \cdot h}, \tag{12}$$

where $A(h)$ is the activity concentration depending on the depth h, A_0 is the surface activity concentration, and α is the inverse relaxation depth.

[9] Unlike the JRODOS tool, the MCNP code does not simulate aerosol transport/atmospheric dispersion using deterministic equations. The two codes are designed for fundamentally different purposes and employ distinct computational approaches.

Therefore, to simulate fresh deposition of both cesium isotopes, surface planar source geometries with a relaxation depth of 1 mm were utilized in the simulations (UNSCEAR, 2000). Weathering and washout phenomena were not considered in the Monte Carlo simulations. These effects, along with radioactive decay, were addressed in the recovery model. The source radius was set to 50 meters to simulate quasi-infinite surfaces, allowing for the tallying of more than 90% of the particles (Selivanova et al., 2019). To enhance the simulation results and to improve the statistical accuracy, variance reduction methods were employed, mainly the DXTRAN sphere technique (Selivanova et al., 2019; Wallace, 2013).

The scoring element was described as tally #6, which assesses the track length of energy deposition (Goorley et al., 2013). Tally #6 was positioned inside a small air sphere located 1 m above the source (Fig. 33). Subsequently, the simulation results required additional recalculations to convert the outputs into activity-to-dose-rate coefficients, in accordance with ICRP Publication 74 (ICRP, 1997).

The same methodology was applied to the simulations of contaminated buildings, particularly roofs and walls. The density and composition of the construction materials were based on the parameters of Portland concrete (McConn Jr et al., 2011).

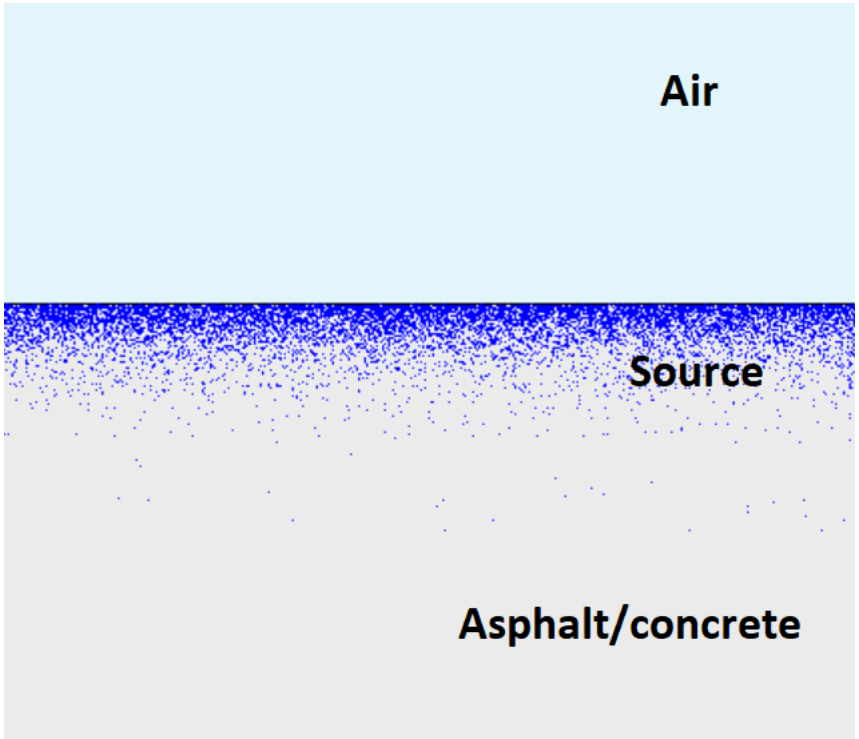

Fig. 32. Exponential source distribution in Monte Carlo simulations (source: own efforts)

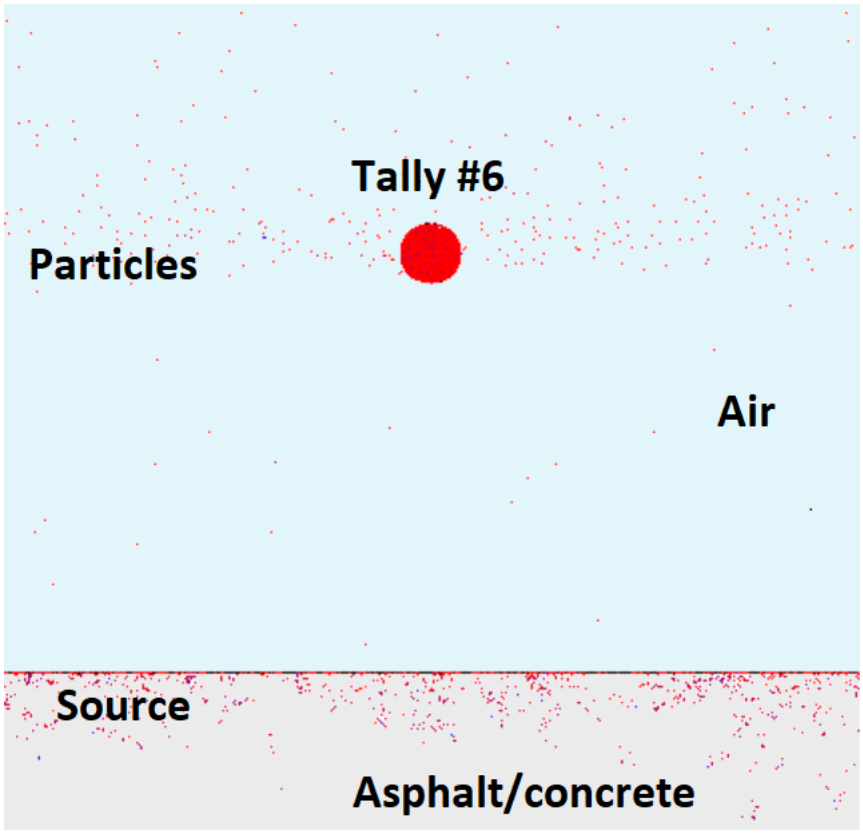

Fig. 33. Geometry of Monte Carlo simulations – surface source – road, buildings: walls and roofs (source: own efforts)

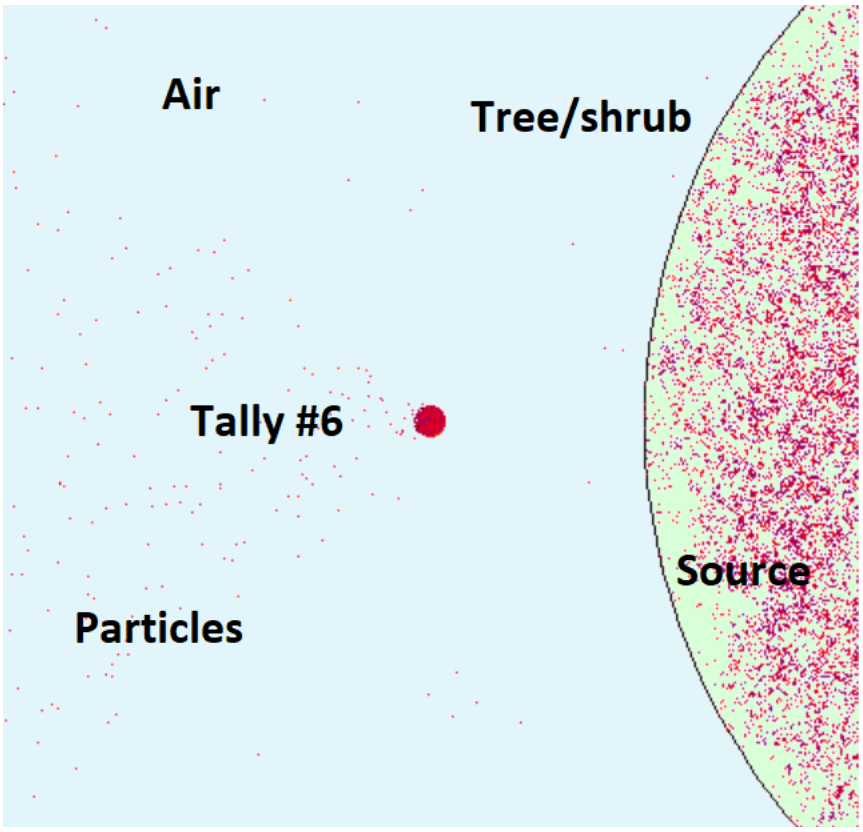

Fig. 34. Geometry of Monte Carlo simulations – surface source – trees and shrubs (source: own efforts)

Shrubs and Trees

To simulate contaminated vegetation, such as shrubs and trees, these objects were modeled as water spheres with a radius of 3 m (Fig. 34). The source of ^{134}Cs or ^{137}Cs, with a relaxation depth of 1 mm, was uniformly distributed on the surface of these spheres. For the vegetation, the activity-to-dose-rate conversion coefficients were derived in a manner similar to the procedure described in the previous paragraph.

Table 6. Conversion coefficients for various contaminated objects (source: Selivanova et al., 2025: 5)

Radionuclide	^{137}Cs	^{134}Cs
Type of object	Conversion coefficient for fresh deposition $((Sv \cdot h^{-1})/(Bq \cdot m^{-2}))$	
Fields	1.40E-12	3.60E-12
Roads	1.20E-12	2.30E-12
Buildings	1.22E-12	2.33E-12
Shrubs	6.93E-15	1.35E-14

6.7.3 Dose Assessments

To calculate the doses received by inhabitants (and workers) in the affected areas, equations (7)–(11), which describe the temporal changes in activity on various objects, were integrated and then summed. The dose assessments were conducted for a period of one year following the completion of the recovery process. The estimates took into account shielding provided by buildings and the time spent indoors and outdoors (Ahn et al., 2014).

Subsequently, a shielding factor of 0.2 was utilized, corresponding to single- or double-story block or brick structures (Ahn et al., 2014; IAEA, 2000). The selected shielding factor was consistent with information about buildings in the EPZ from the ČÚZK database (ČÚZK, 2023). Based on published data (Ahn et al., 2014; Nisbet and Watson, 2018), it was determined that inhabitants of the EPZ spend 90% of their time indoors.

The proposed approach to dose estimation for individuals living in the EPZ was simplified compared to the recommended parameters for a representative person as specified in Czech legislation (SÚJB, 2016). Nonetheless, further refinements can be made in subsequent research.

6.8 Tests of the Model

To verify the model and to ensure the accuracy of its calculations, three different tests were conducted. These tests were designed both to identify hidden bugs or missing units and to simulate doses and other outputs.

6.8.1 Units Check

The recovery model was evaluated for dimensional consistency using the *Units Check* option inbuilt within the Vensim software (Ventana Systems, 2023b). This test focuses on dimensional analysis and helps to identify errors within the mathematical equations. It also provides detailed information about the units employed in the model. The model was subsequently refined and successfully passed the *Units Check* test.

6.8.2 Dose Calculation

The dosimetry calculations were validated by comparing doses obtained from simulations in Vensim DSS with doses calculated independently from the model. The analytical or generic assessments were conducted using both empirical functions (Andersson and Roed, 2006) and simple time-dependent conversion coefficients (Nisbet and Watson, 2018).

For the test estimates, an open grassed area contaminated with cesium isotopes (^{137}Cs and ^{134}Cs) was considered, with a surface activity of each radionuclide set at 1 MBq·m^{-2}. In this test, no countermeasures were assumed. Subsequently, annual effective doses for both isotopes were simulated in the recovery model using Vensim DSS.

To perform the generic estimate, equation (7) was integrated over one year and multiplied by the corresponding conversion coefficient (Table 6). The second analytical assessment was based on a straightforward multiplication of initial surface activities by conversion coefficients, assuming a period of one year after surface contamination (Nisbet and Watson, 2018).

A comparison of all effective doses is summarized in Table 7. Differences between the Vensim simulations and the generic assessments were below 1%. For the second analytical approach, i.e., direct multiplication, the disparities between the simulated doses and the analytical calculations were under 3%. For both analytical approximations, the differences from the simulations were minimal and therefore considered acceptable.

Afterwards, the methodology for dose estimates developed in the recovery model was approved for subsequent simulations and analyses.

Table 7. Comparison of effective doses (source: Selivanova et al., 2025: 6)

Calculation mode	Model (Vensim simulation)	Analytical integration	Simple multiplication
Radionuclide	Annual effective dose (mSv)		
^{137}Cs	3.2	3.2	3.1
^{134}Cs	7.1	7.1	7.3

6.8.3 Waste Generation

To test waste generation in the recovery model, known parameters of contaminated objects and selected countermeasures were used. The results of simulations in the developed recovery model were then compared with published results (Hinrichsen et al., 2021).

In the simplified scenario, a contaminated soil surface of 3 000 m^2 was assumed. For this scenario, the removal of a 5 cm upper soil layer was anticipated. According to the simulations performed with the described setup, the generated waste volume was approximately 120 m^3. In the reference study (Hinrichsen et al., 2021), the generated waste volume was reported to be about 150 m^3.

Thus, both results were quite similar and of the same order of magnitude. The observed differences could be caused by the use of different parameters in the waste generation calculations (depends on parameters of decontaminated sites). The developed recovery model and its parameters were subsequently accepted.

6.9 Stock and Flow Diagrams

Changes in surface activities resulting from radioactive decay, weathering, and decontamination efforts are time-dependent processes, as is dose accumulation. Therefore, these variables can be conceptualized as definite integrals (stock variables or levels), while the rates of change correspond to flow variables (Albin, 2001; Selivanova and Krejčí, 2019).

Stock variables are typically represented as boxes, and flows are illustrated as arrows or pipes connecting these boxes (Sterman, 2000; Ventana Systems, 2023a). Thus, Stock and Flow Diagrams (SFDs) effectively illustrate the mathematical framework underlying the addressed problem (Sterman, 2000).

Equations (7)–(9) comprise two exponential components: fast and slow (Andersson and Roed, 2006). Consequently, the corresponding definite integrals consist of two parts, or

stock variables, which are aggregated in the computation of the total effective dose. An example of an SFD related to the conversion of surface activities of ^{137}Cs to accumulated effective doses obtained from fields is depicted in Fig. 35.

For completeness, selected SFDs illustrating changes in the surface activities ^{137}Cs and the corresponding dose accumulation for all assumed objects are provided in Appendix D – Stock and Flow Diagrams. Considering ^{134}Cs, the analogous SFDs are practically identical.

The boundaries of the model are summarized in Table 8, including the most important endogenous, exogenous and excluded variables. According to Sterman (2000), exogenous variables are stocks (time-dependent integrals) that are not described in the model explicitly. These variables originate outside the model boundaries (Torraco, 2003). For example, radionuclide releases are time-dependent and can be simulated, e.g., using JRODOS software (Ievdin et al., 2019). Another exogenous input is population data provided by census results (CZSO, 2021).

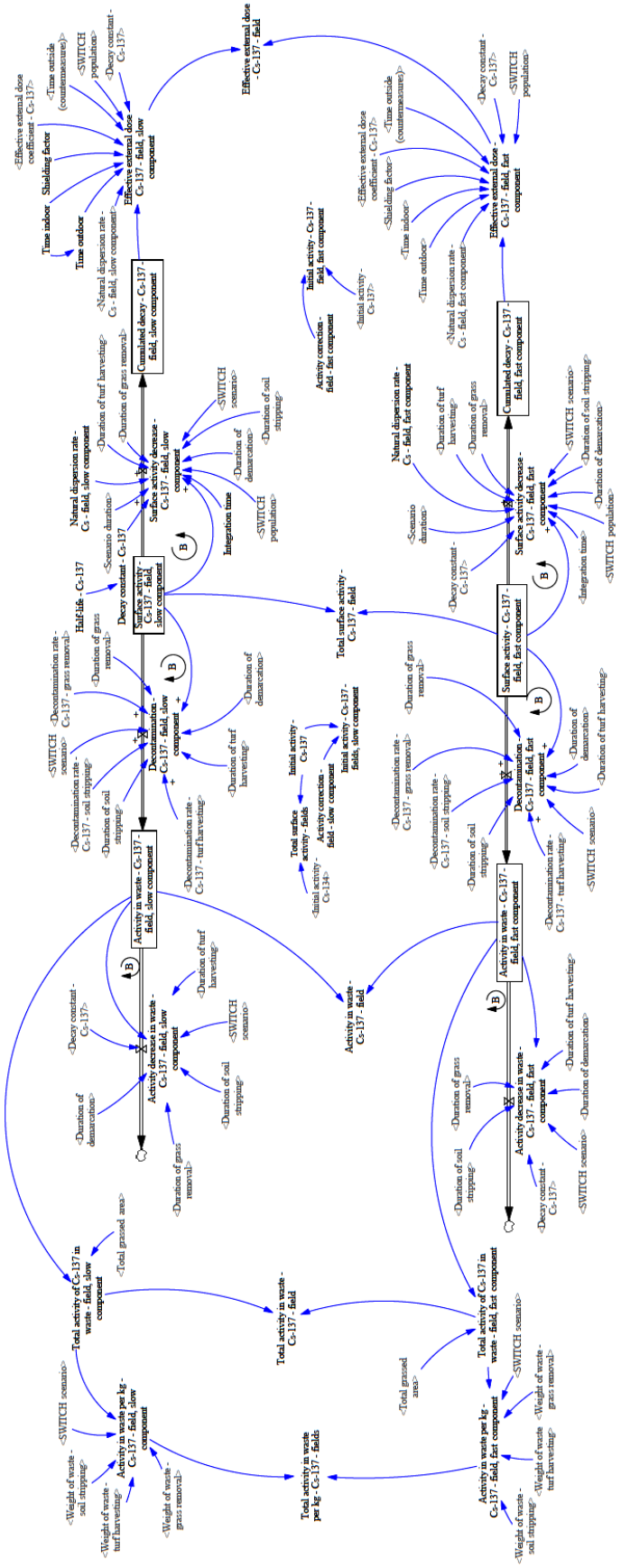

Fig. 35. SFD for contaminated fields: conversion of surface activity of ^{137}Cs to effective dose (source: Selivanova et al., 2025: 12)

Endogenous variables arise within the model itself (Sterman, 2000; Torraco, 2003). In the proposed models, key endogenous variables include obtained effective doses, the amount of produced radioactive waste, total recovery costs, and others. Excluded variables refer to aspects beyond the scope of this study. However, these issues may be addressed in future research. Nevertheless, the management of contaminated livestock and related measurements has already been solved by Bartusková et al. (2023).

Table 8. The key endogenous, exogenous, and excluded variables in the Recovery model (source: own efforts)

Endogenous variables	Exogenous variables	Excluded variables
Obtained doses	Radionuclide release	Early protective measures
Changes in surface activities	Scale of affected areas	Temporary relocation or permanent resettlement of inhabitants
Produced waste	Affected population	Restrictions on food and water consumption
Total costs of recovery	Available equipment	Management of contaminated livestock
Costs of countermeasure per m^2	Workers' productivity	Liquid waste management
Total benefits	Workers' wages	Meteorological and season conditions
Duration of recovery	Acquisition costs	Internal irradiation
	Inflation	

6.10 Simulations of Recovery Scenarios

In the model, the most typical decontamination methods were selected and implemented. For all assumed source terms (DBA1–SEV7), sequences of chosen decontamination techniques were proposed and then simulated using the Vensim DSS software (Ventana Systems, 2023a). The evaluations considered parameters such as decontamination duration, obtained effective doses, total recovery costs and benefits, and volumes of generated radioactive waste (solid and liquid) were assessed.

For each source term, a reference scenario was simulated under the assumption of no decontamination efforts. However, this scenario included access restrictions by demarcating affected areas with warning boards, tapes, or fences. The total cost of implementing the reference scenario ranged from approximately 70 000 to 300 000 EUR, depending on the extent of contamination, radioactivity levels, and the size of the restricted areas.

The mathematical model of recovery considers four scenarios of recovery:

1) A reference scenario without any recovery, including only access restriction,

2) A recovery scenario for lower levels of surface activities (e.g., several $kBq \cdot m^{-2}$), involving access restriction, grass cutting, and plants pruning (i.e., trees or shrubs),

3) A recovery scenario for higher levels of surface contamination (surface activities greater than 100 $kBq \cdot m^{-2}$), including access restriction, grass cutting, trees and shrubs pruning, removal up to 5 cm of topsoil (for fields), and high-pressure washing of streets with water (roads and buildings),

4) A recovery scenario for higher levels of contamination, similar to scenario 3), but with topsoil removal replaced by turf harvesting (removal of 1–2 cm of turf).

Subsequently, for DBA source terms, decontamination scenarios 1) and 2) were considered. For SEV source terms, recovery scenarios 1)–4) were simulated. However, decontamination scenario 2) was too demanding and proved inefficient for severe accidents (i.e., SEV source terms). Recovery scenario 2) was, therefore, excluded from the final assessments for severe accidents.

Additionally, recovery scenarios 3) and 4) included water tie-down or water sprinkling during soil/turf removal to minimize the resuspension of radioactive dust (Nisbet and Watson, 2018).

It should be highlighted that the chosen decontamination methods and proposed recovery scenarios are not the only relevant and possible options. Other methods, e.g., various techniques of deep ploughing, soil amendment (e.g., using fertilizers), and others, may be investigated in subsequent research.

Under real conditions, more comprehensive assessments of recovery, including the limitations of each recontamination technique, must be performed (Nisbet and Watson, 2018). Furthermore, this study concentrated solely on contamination within the EPZ, as comprehensive input data were available.

6.11 Application of Cost-Benefit Analysis

To evaluate the proposed recovery scenarios, a cost-benefit analysis is required. Within such analyses, the overall expenses of each scenario should be compared with the associated benefits (ICRP, 2006). The following steps are necessary to calculate these benefits:

- Simulate the effective doses originating from all contaminated objects in each scenario, including the reference scenario without any decontamination strategies.
- Sum all partial effective doses in each scenario.
- Estimate the collective effective doses (CEDs), which can be obtained by multiplying the simulated annual doses by the known number of inhabitants within the EPZ.

- Calculate the averted (or saved-up) CEDs, which can be assessed as the difference between the reference CEDs (i.e., from the reference scenario) and the CEDs obtained after the completion of decontamination.
- Multiply the averted CEDs by the corresponding financial coefficient for radiation accidents. This financial coefficient is 2.5 million CZK·manSv^{-1}, or roughly 100 000 EUR·manSv^{-1} (SÚJB, 2016). The financial expression of the averted CEDs then corresponds to the required benefits (ICRP, 2006; SÚJB, 2016).
- Subsequently, the most beneficial scenario should undergo further analysis to assess its suitability for implementation.

7 Results and Discussion

7.1 Initial Contamination

Fig. 36 – Fig. 40 show the averaged surface activity maps for ^{134}Cs and ^{137}Cs. These maps were obtained using the JRODOS system for selected source terms (DBA1–SEV7, Table 4) under typical historical weather conditions at the given location (NPP Dukovany). All presented maps depict the initial surface contamination, before any recovery scenarios.

Based on the simulated maps (Fig. 36–Fig. 40), sector #7 of the EPZ is most probably to be contaminated following hypothetical releases of radioactive matter, considering the most common historical weather data. The highest radionuclide concentrations in sector #7 occurred in both a small release (DBA1, Fig. 36) and a very significant release (SEV7, Fig. 40). These results are consistent with the wind rose in Fig. 31 and also with simulations of long-term discharges during normal operation of NPP Dukovany (Selivanova et al., 2023). Additionally, the results correspond to the wind rose data for the Dukovany site over longer time period (Amec Foster Wheeler s.r.o., 2017).

7.1.1 DBA Events

Considering both DBA events (Fig. 36 and Fig. 37), surface contamination was not observed across the overall EPZ. The radionuclide deposition occurred in specific sectors/segments only, being in a good agreement with the detailed weather records employed within the modeling in JRODOS.

DBA1 Event

In the case of source term DBA1 (Fig. 36), the surface activities of ^{137}Cs and ^{134}Cs were mostly in the range of tens of $Bq \cdot m^{-2}$, with maxima reaching several hundreds of $Bq \cdot m^{-2}$, particularly within 5 km from NPP Dukovany. These low activity levels are almost negligible, especially when compared to the cesium deposition in Czechia following the Chernobyl accident in 1986. In Czechia, the highest ^{137}Cs concentrations in soil samples were around 100 $kBq \cdot m^{-2}$ in 1986 (Bučina et al., 1996; Rulík and Helebrant, 2011). Taking into account radioactive decay, the current cesium concentrations from the Chernobyl fallout in Czechia could be up to 30 $kBq \cdot m^{-2}$, which is significantly greater (several orders of magnitude) than the surface activities from the simulated DBA1 event. When comparing the results of the simulated DBA1 event (Table 4) with the INES scale (Table 2), DBA1

appears to align roughly with Level 0, which is classified as below the scale and having no safety significance. However, the steam generator tube rupture (SGTR) event (Table 4) and the subsequent atmospheric release may require reclassification to a higher INES level within the JRODOS library.

Considering the Radiation Hazard Scale (CDC, 2021), categories 1 or 2 could be hypothetically applied to this case (Table 3). However, both scales were developed for communication purposes during radiation emergencies and not for assessments from a long-term perspective. **Therefore, subsequent discussions about accident levels or categories should be regarded as indicative only. In real conditions, accident classification requires real-time evaluation and should consider the presence of short-lived radionuclides, particularly iodine isotopes.**

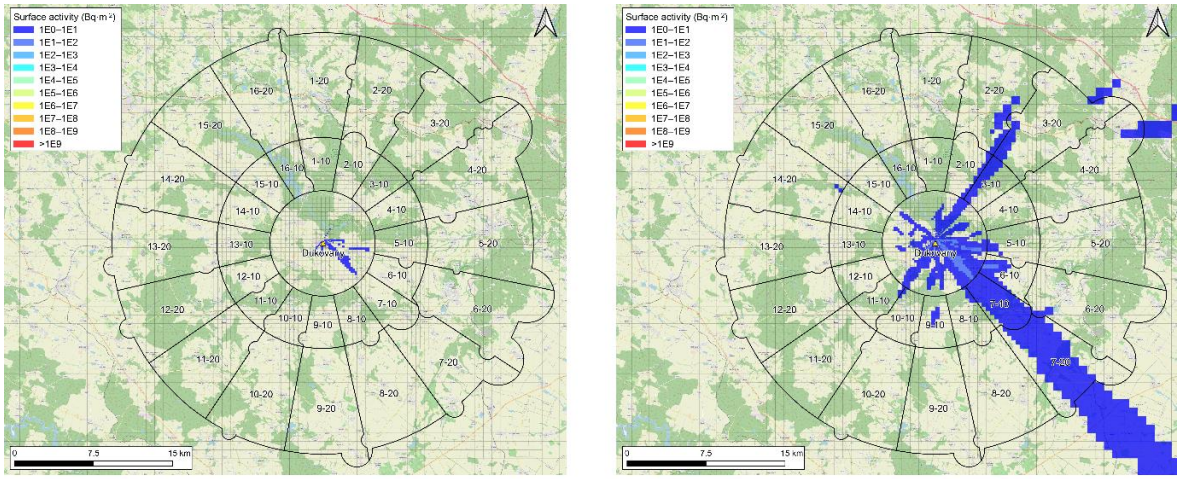

Fig. 36. Surface activities of cesium isotopes for the DBA1 source term: a) ^{134}Cs, b) ^{137}Cs (source: Selivanova et al., 2025: 7)

DBA4 Event

For DBA4 (Fig. 37), the surface deposition of ^{137}Cs and ^{134}Cs was primarily tens of Bq·m^{-2}, being similar to the case of DBA1 (Fig. 36). Surface activities of cesium isotopes in a range of hundreds of Bq·m^{-2} mainly occurred throughout sector #7. The cesium deposition of 1–10 kBq·m^{-2} was mostly found in sector #7, particularly within the inner ring of the EPZ, up to 10 km from the NPP. Nevertheless, these activities are still of the same order of magnitude as the existing cesium deposition in Czechia following the Chernobyl accident.

According to the description of the DBA4 event (Table 4), the corresponding INES level should be Level 4, which is classified as an accident with local consequences. However, the INES scale requires at least one radiation-related fatality for this level (Table 2), whereas the simulated results did not indicate any dangerous levels of irradiation. Therefore,

the description of the DBA4 event may need to be revised in the JRODOS database of source terms. Another reason for the discrepancy between the postulated INES level and the level derived from assessments may originate from the exclusion of iodine in the evaluations, owing to its shorter half-life from a long-term perspective.

As in the previous event (i.e., DBA1), categories 1 or 2 of the Radiation Hazard Scale may be applied to classify the current event, DBA4 (CDC, 2021).

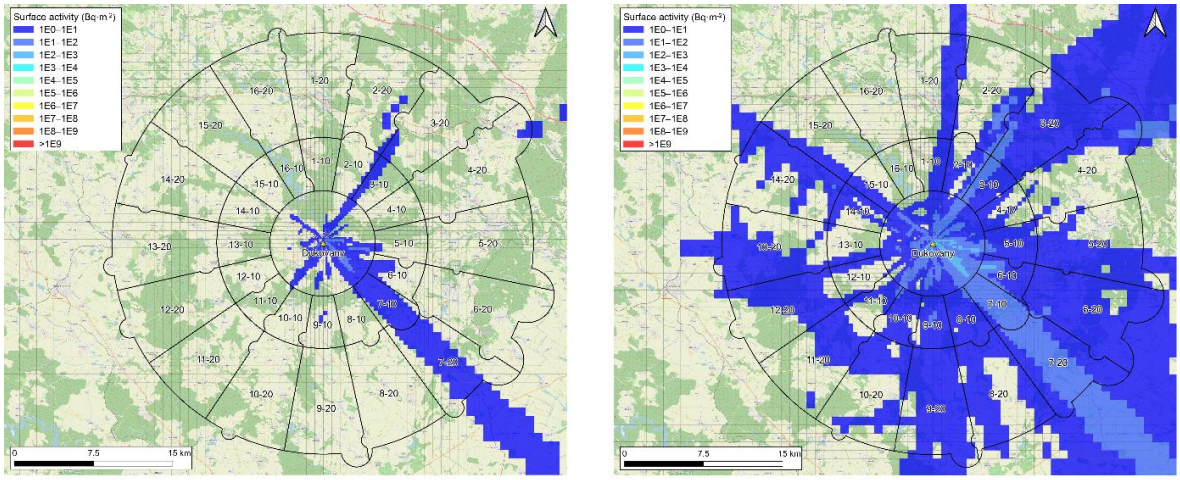

Fig. 37. Surface activities of cesium isotopes for the DBA4 source term: a) ^{134}Cs, b) ^{137}Cs (source: Selivanova et al., 2025: 8)

7.1.2 SEV Events

Considering SEV events, surface deposition of both cesium isotopes was observed across the entire EPZ (Fig. 38–Fig. 40).

SEV1 Event

For SEV1, surface activities of ^{134}Cs and ^{137}Cs reached several hundreds of kBq·m^{-2} (Fig. 38), being greater than the existing cesium fallout from Chernobyl in Czechia (Bučina et al., 1996). However, surface deposition higher than 10 kBq·m^{-2} occurred inside the EPZ only. Thereafter, several countermeasures can be expected to be implemented.

SEV1 is described as a Level 5 event (Table 4), classified as an Accident with Wider Consequences (Table 2). Level 5 typically corresponds to accidents involving multiple radiation-related fatalities (Table 2), whereas the simulation results did not indicate such high radiation levels. Therefore, a less conservative INES level may be more appropriate for this event in the JRODOS library. In addition, category 2 of the Radiation Hazard Scale may be applied to classify this accident (Table 3).

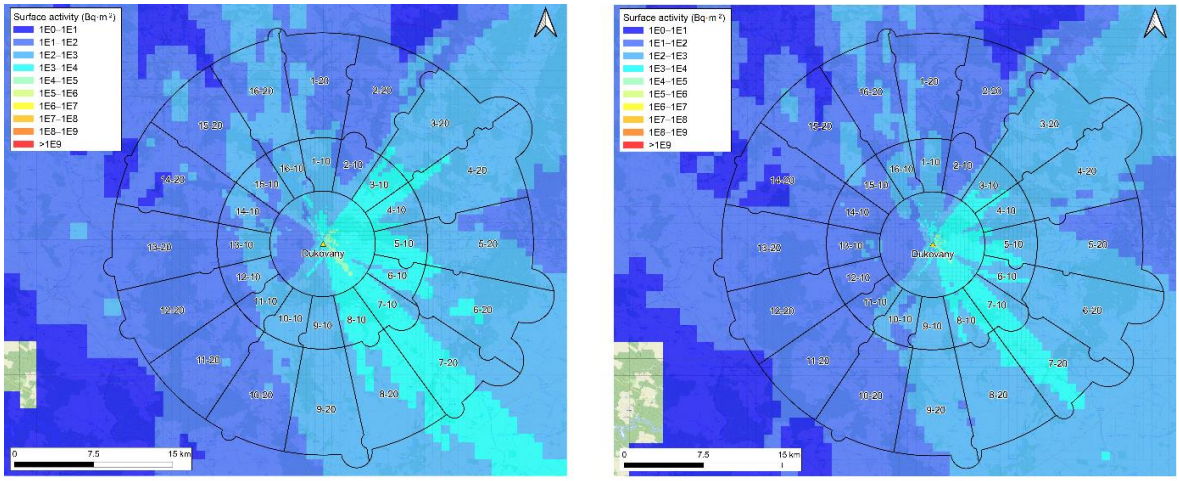

Fig. 38. Surface activities of cesium isotopes for the SEV1 source term: a) ^{134}Cs, b) ^{137}Cs (source: Selivanova et al., 2025: 8)

SEV6 and SEV7 Events

For source terms SEV6 (Fig. 39) and SEV7 (Fig. 40), more extensive and higher levels of contamination with ^{134}Cs and ^{137}Cs were observed. Anticipating event SEV6, surface activities were in a range from 1 kBq·m^{-2} to 10 MBq·m^{-2} (Fig. 39). Under conditions of the severest source term, SEV7 (Fig. 40), surface deposition of ^{137}Cs and ^{134}Cs reached up to hundreds of MBq·m^{-2}. However, the majority of the deposited radioactivity ranged from tens of kBq·m^{-2} to hundreds of kBq·m^{-2}. Surface activities of cesium isotopes (^{134}Cs and ^{137}Cs) exceeding 10 kBq·m^{-2} also occurred outside the EPZ.

Considering both events (i.e., SEV6 and SEV7), the highest contamination with cesium isotopes was comparable to the surface deposition of ^{134}Cs and ^{137}Cs observed in the surroundings of NPP Fukushima Daiichi shortly after the accident (MEXT, 2011), which necessitated large-scale recovery efforts in the affected areas (Nisbet and Watson, 2018; U.S. EPA, 2016).

In accordance with the descriptions of the SEV6 and SEV7 events, both correspond to Level 7 (Table 4), or a Major Accident, on the INES scale (Table 2), and are comparable to large historical accidents classified at the same INES level. According to the Radiation Hazard Scale, categories 3 and categories 4–5 would most likely be used to classify events SEV6 and SEV7, respectively (Table 3).

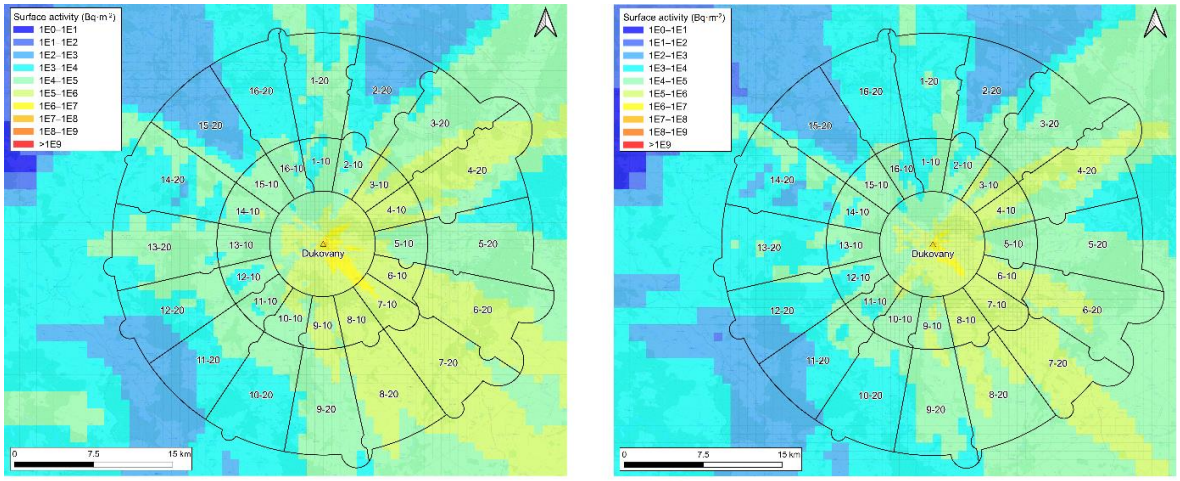

Fig. 39. Surface activities of cesium isotopes for the SEV6 source term: a) ^{134}Cs, b) ^{137}Cs (source: Selivanova et al., 2025: 9)

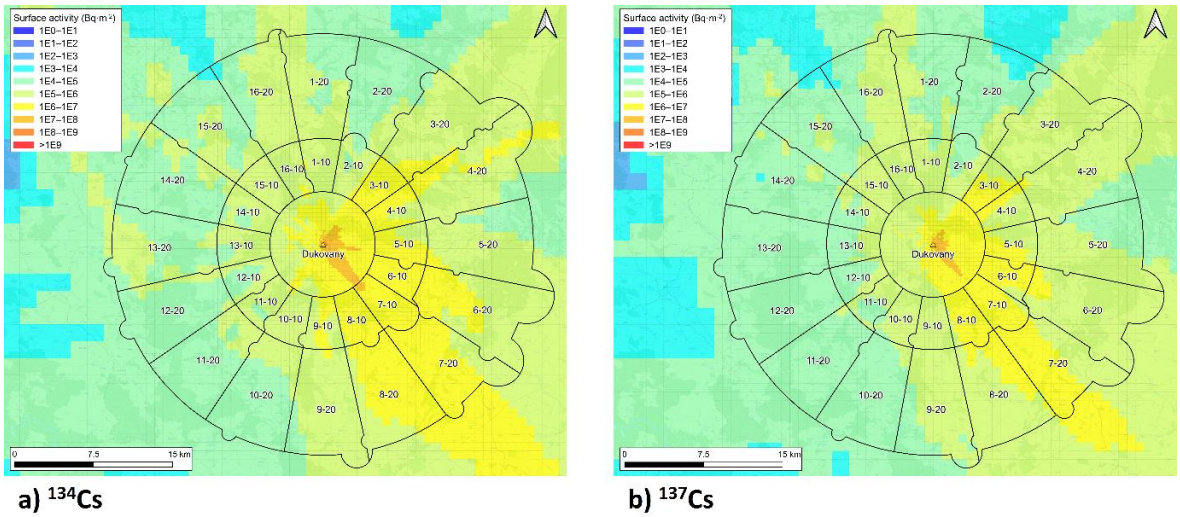

Fig. 40. Surface activities of cesium isotopes for the SEV7 source term: a) ^{134}Cs, b) ^{137}Cs (source: Selivanova et al., 2025: 9)

7.2 Recovery Scenarios

The results of mathematical modeling of recovery efforts in contaminated areas within the EPZ can be found in Table 9 – Table 12. These tables provide data on chosen decontamination techniques, simulated annual effective doses, total costs and benefits of decontamination, costs per m^2, and duration of decontamination. The results are discussed in detail in the paragraphs below, separately for DBA and SEV events.

An example of the accumulation of total effective doses over one year is illustrated in Fig. 41. All time courses of accumulation of effective doses over a one-year period, as simulated in the recovery model, are available in Appendix E – Dose Accumulation. This appendix also summarizes the effective dose accumulation from chosen rural and urban

objects with the highest surface contamination for each source term, representing the reference scenarios without decontamination.

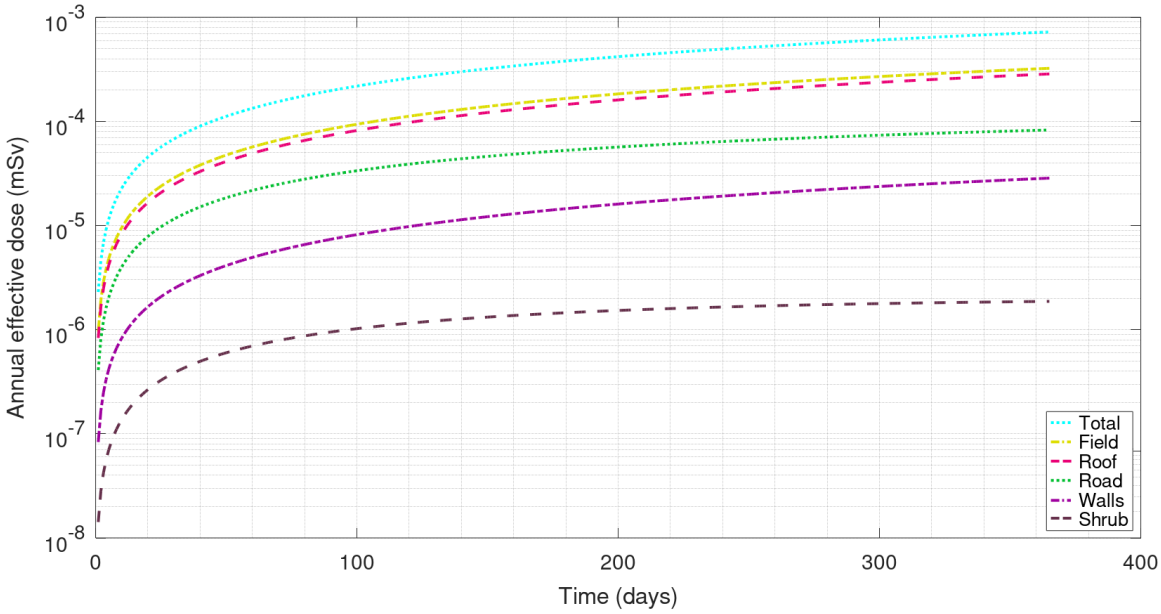

Fig. 41. Annual effective doses from different objects for DBA1 event, no decontamination (source: Selivanova et al., 2025: 17)

Nevertheless, recovery efforts following severe accidents should be initiated as promptly as possible due to the long-lasting negative socio-economic impacts on the well-being of inhabitants, which can persist for decades after the accidents (IAEA, 2001). Among the negative side effects of postponed decontamination in affected areas belong, e.g., secondary radionuclide dispersion caused by wildland fires (Kovalets et al., 2022; Masson et al., 2021; Talerko et al., 2021). For example, forest fires in Ukraine in 2020 led to a significant increase in airborne concentrations of ^{137}Cs, requiring the reconstruction of ^{137}Cs emissions (Tichý et al., 2025; Talerko et al., 2021).

7.2.1 DBA Events

According to the results of JRODOS simulations and owing to very low initial contamination with ^{134}Cs and ^{137}Cs (Fig. 36 and Fig. 37), it was anticipated that the DBA events would not require any recovery scenarios. However, for completeness, simplified decontamination procedures were designed, including grass removal and tree/shrub pruning. The estimated duration of decontamination ranged from one to two months (Table 9).

Effective Doses

Based on the simulations of decontamination of the both DBA events (Table 9), no substantial dose decrease to inhabitants occurred in the decontaminated parts of the EPZ, covering several hundred km^2. The chosen countermeasures and decontamination techniques, i.e., demarcation (access restriction), removal of grass, and tree/shrub pruning, in the proposed set-up were, therefore, not sufficiently effective. These results are consistent with conclusions summarized by Nisbet et al. (2018) and by the U.S. EPA (2016).

Considering the irradiation of workers involved in recovery in both scenarios DBA1 and DBA4, the total doses were practically negligible, ranging from several nSv to several μSv. Irradiation of workers was assessed using the same SFDs as for inhabitants, with changes in the irradiated group of interest (i.e., population or workers) managed via switches (Fig. 35). By setting specific values for the corresponding switch, the model calculates doses for the selected group. However, a disadvantage of this approach was the necessity of conducting several independent runs for each scenario. Therefore, further improvements in the assessment of worker doses should be considered in future research.

Produced Waste

In the designed decontamination scenarios (Table 9), only organic waste, including removed grass, leaves, and branches, was considered. The amount of produced radioactive waste was in an interval of 130–940 thousand m^3 for affected areas of 133–733 km^2. However, this approach was highly conservative and may not be applicable under real-world conditions due to the subsequent cost-benefit analysis (CBA).

CBA Analysis

According to the simulation results (Table 9), the cost of recovery per m^2 was in the range of hundredths of EUR. Nevertheless, the overall costs, reaching up to 30 million EUR, were significantly higher than the corresponding benefits, which amounted to only thousands of EUR. Hence, the proposed decontamination procedures were deemed unsuitable to be implemented. The associated annual effective doses to inhabitants were up to tens of μSv, being substantially below the public annual exposure limit of 1 mSv (SÚJB, 2016). Under these assumptions, no decontamination strategies would be necessary following such minimal atmospheric releases and low cesium isotope concentrations in the soil and on surfaces.

Nevertheless, the knowledge gained from the 1987 radiological accident involving the abandoned and then stolen medical ^{137}Cs source (Goiânia, Brazil) demonstrated that local authorities can face intense public and political pressure. These conditions may potentially result in the realization of extremely conservative recovery strategies (IAEA, 1988).

Based on these results, the analyses have the potential to be applied to small and medium-sized modular reactors (SMRs) in the future, which are currently under development. SMRs are defined as reactors with a generating capacity of up to 300 MWe (small) and 300–700 MWe (medium) (IAEA, 2021b). SMRs are expected to provide energy to remote locations where large nuclear power plants are not suitable. The primary advantages of SMRs include their smaller size, enhanced safety, simplified operation, and reduced capital investment for construction. Regarding the safety of SMRs, it is anticipated that, in the event of an accident, the quantity of released radioactive material would be minimal and would have a negligible impact on the health of local inhabitants (IAEA, 2021b; Murakami and Anbumozhi, 2021).

Taking into account the actual conditions in Czechia, the operator of both Czech NPPs, ČEZ Group, collaborates with Rolls-Royce SMR Limited (Rolls-Royce SMR) on the development and planning of small modular reactors (SMRs) in Czechia (ČEZ Group, 2024). Although this research was not conducted as part of this collaboration, its findings are expected to be of potential use to Czech stakeholders.

Table 9. Results of simulated decontamination for DBA1 and DBA4 source terms including cost-benefit analysis (source: Selivanova et al., 2025: 9)

Source term	DBA1	DBA4
Total decontaminated area	133 km^2	733 km^2
Maximum order of magnitude of **initial** surface cesium activities	100 $Bq \cdot m^{-2}$	10 $kBq \cdot m^{-2}$
Maximum annual effective dose **before recovery**	0.7 µSv	82 µSv
Maximum annual effective dose **after recovery**	0.7 µSv	82 µSv
Applied countermeasures	Access restriction, grass removal, tree/shrub pruning	
Duration of recovery	28 days	55 days
Organic waste	1.3E+05 m^3	9.4E+05 m^3
Total costs	5 mln. EUR	30 mln. EUR
Total benefits	2 ths. EUR	27 ths. EUR
Total costs per m^2	3.6E-02 $EUR \cdot m^{-2}$	4.0E-02 $EUR \cdot m^{-2}$

7.2.2 SEV Events

Annual Effective Doses

Following radiation accidents and subsequent contamination, affected areas can be classified into three zones in accordance with the Czech National Radiation Emergency Plan (SÚJB, 2020b):

1) *Danger zone*; permanent stay of inhabitants is prohibited except for workers implementing recovery countermeasures. Total effective doses of inhabitants are greater than 100 mSv per year.
2) *Restricted access zone*; access to this zone is permitted only in justified case. The implementation of specific protective measures and regulatory controls is required. Total effective doses of inhabitants are in a range of 20–100 mSv per year.
3) *Controlled stay zone*; permanent residence in this zone may be permitted under specified restrictions and regulations. Implementation of regime measures, regulation of drinking water consumption, and control of local agricultural product consumption is required. Total effective doses of inhabitants do not exceed 20 mSv per year.

The objective of the recovery process of affected areas is to systematically convert controlled stay zones into zones without limitations, to transform restricted access zones into controlled stay zones, and to change danger zones into restricted access zones after decontamination.

Considering radiation accidents corresponding to source term SEV1, the highest effective doses to inhabitants before decontamination were approximately 3 mSv per year (Table 10). According to the Czech National Radiation Emergency Plan (SÚJB, 2020b), areas with this level of radiation corresponded to the controlled stay zone. After decontamination, the maximum annual effective doses did not exceed 1 mSv, complying with the public exposure limit (SÚJB, 2016). In the case of worker irradiation, the corresponding doses were in a range of 56–85 μSv over the entire period of recovery works, being practically negligible.

For accidents characterized by source terms SEV6 and SEV7 (Table 11 and Table 12, respectively), the highest annual effective doses to inhabitants exceeded several hundreds of mSv prior to recovery. The corresponding affected areas should be classified as danger zones, according to the Czech National Radiation Emergency Plan (SÚJB, 2020b).

The proposed mathematical recovery model accounted for more extensive decontamination efforts, particularly for surface contamination exceeding 10 $MBq \cdot m^{-2}$.

Consequently, the simulated total effective doses to inhabitants were reduced by several orders of magnitude following the completion of decontamination in these areas. The maximum annual effective doses were then approximately up to 40 mSv. Areas with such dose levels following decontamination corresponded to the restricted access zone (SÚJB, 2020b). The annual effective dose of 40 mSv indicates that the implementation of additional countermeasures is necessary to gradually convert these areas into controlled stay zones. For example, deep ploughing, replacement of the contaminated topsoil layer, the use of fertilizers, and other techniques can be employed (Nisbet and Watson, 2018).

Considering the irradiation of workers and source term SEV6, the maximum effective doses were in a range of approximately 6–16 mSv over the total period of decontamination. These doses were below the reference level of 100 mSv for emergency responders (SÚJB, 2016). However, to reduce such doses, a larger number of workers can be employed, each performing shorter work periods.

In the case of source term SEV7, the highest effective doses obtained by workers were in a range of 6–56 mSv over the total recovery period. As with event SEV6, the doses did not exceed the reference level for emergency responders (SÚJB, 2016).

Decontamination Duration

The proposed recovery model was applied to accidents described by the DBA source terms and all affected areas with various levels of surface contamination. However, subsequent CBA analyses indicated that the extent of decontaminated territories should be reduced due to the overall effectiveness of the recovery process (Table 9). Consequently, during analyses of SEV events, areas with surface contamination of ^{134}Cs and ^{137}Cs below 10 $kBq \cdot m^{-2}$ per radionuclide were excluded from the evaluations. In addition, surface activities of tens of $kBq \cdot m^{-2}$ of ^{137}Cs were comparable to the current levels of Chernobyl fallout in Czechia (Bučina et al., 1996; Rulík and Helebrant, 2011). Therefore, areas with such low levels of surface activity were deemed insignificant in terms of the necessity for decontamination efforts.

Anticipating an accident corresponded to source term SEV1, the decontamination duration was approximately two months (48 days) for affected territories covering 4 km^2 (Table 10). Recovery efforts were conducted solely within the EPZ area. Additionally,

the reduction of decontaminated territories had a direct impact on radioactive waste production (Table 10). The decrease in generated waste volumes substantially reduced the overall costs of decontamination efforts (Selivanova, 2020a; U.S. EPA, 2016).

For radiation accidents being described by source terms SEV6 and SEV7 and affected areas inside the EPZ, the recovery duration of contaminated territories of 630–681 km^2 was about 1.6–1.7 years (Table 11 and Table 12, respectively). Nevertheless, the simulated contamination greater than 10 $kBq \cdot m^{-2}$ extended beyond the EPZ boundaries, necessitating decontamination efforts in these external areas as well. Consequently, the overall recovery process for all contaminated regions would be prolonged.

The simulations of decontamination did not account for seasonal variations, which may significantly impact the duration of the recovery process. For instance, during winter and severe cold meteorological conditions, soil or turf removal is not feasible due to frozen ground and low temperatures (Nisbet and Watson, 2018). Therefore, the complete decontamination and recovery process may require substantially more time. Notably, the decontamination efforts after the Fukushima accident and the Chernobyl accident are still in progress. Based on clean-up experiences from such severe accidents and large-scale contamination, the decontamination of affected territories is estimated to require more than a decade (IAEA, 2001; Schreurs, 2021).

Radioactive Waste

Considering decontamination works following SEV events, substantial amounts of solid and liquid radioactive waste were generated (Table 10–Table 12). For decontamination after event SEV1, the volumes of organic solid waste (turf, soil) from affected areas of 4 km^2 were approximately 58 thousand m^3 for turf harvesting and 120 thousand m^3 for topsoil removal (Table 10). The almost twofold difference originated from variations in the thickness of the removed topsoil layers: 1–2 cm for turf harvesting and approximately 5 cm for soil stripping (Nisbet and Watson, 2018).

For source term SEV1, approximately 5 000 m^3 of liquid waste was generated from high-pressure water washing of streets (Table 10). However, the mathematical recovery model does not consider the subsequent collection of contaminated water or the removal of cesium isotopes due to insufficient data specific to actual conditions in Czechia.

Assuming events SEV6 and SEV7 and subsequent decontamination, the amounts of solid organic waste ranged from approximately 7 million m^3 to 13 million m^3 for affected

territories of 630–681 km^2 (Table 11 and Table 12). In comparison, the estimated volume of solid radioactive waste generated during the Fukushima clean-up was 22 million m^3 (U.S. EPA, 2016). For Czechia, the simulated volumes of generated radioactive organic waste were of the same order of magnitude, demonstrating good agreement with the actual waste amounts originated from Fukushima.

Additionally, efforts have been made to develop optimal transportation patterns for transferring the generated solid waste to interim storage sites within the EPZ. To address this challenge, a routing methodology combined with linear optimization was proposed and tested (Hlavatý et al., 2024). However, further refinements of the proposed routing model will be required in future research.

Considering liquid waste produced during the high-pressure washing of streets (i.e., roads and buildings: walls and roofs), the total amount was approximately 2 million m^3 (Table 11 and Table 12). This liquid radioactive waste should be thoroughly collected and subsequently treated to separate radionuclides (U.S. EPA, 2016). However, the proposed mathematical decontamination model can address this aspect in future research.

Cost-Benefit Analysis

For source term SEV1, the total decontamination costs were approximately 16 million EUR for turf harvesting and 17 million EUR for topsoil removal (Table 10). The corresponding benefits for each scenario were 63 million EUR and 82 million EUR, respectively.

For accidents characterized by source terms SEV6 and SEV7, the overall recovery costs ranged from 3.2 to 3.4 billion EUR (Table 11 and Table 12, respectively). In the case of SEV6, the corresponding benefits were greater than 57 billion EUR (Table 11), while for SEV7, the benefits exceeded 100 billion EUR (Table 12).

Comparing the simulated total recovery costs with the corresponding benefits, decontamination costs were substantially lower than the benefits for all assumed severe radiation accidents (SEV1–SEV7). Therefore, for all SEV events (Table 10–Table 12), the selected decontamination techniques, including public access restriction, grass cutting, high-pressure water washing of streets, buildings and roads, tree and shrub pruning, turf harvesting, and topsoil removal, were collectively efficient and deemed suitable for implementation.

Regarding decontamination costs per square meter, the estimated costs ranged from approximately 4 to 5 EUR·m^{-2}, which is generally in good agreement with the costs of the Fukushima clean-up (U.S. EPA, 2016).

Regarding potential severe accidents in SMRs, such radiological consequences are not anticipated. According to available analyses, the probability of core melting and significant atmospheric releases is extremely low, even in the event of a station blackout (SBO) (Yin et al., 2016). However, these findings can be potentially utilized by Czech stakeholders in studies focused on the planning and construction of a new unit at the Dukovany NPP. Another potential application is their use in the hypothetical implementation of PSA Level 3 in Czechia in future.

Table 10. Results of simulated decontamination for SEV1 source term including cost-benefit analysis (source: Selivanova et al., 2025: 10)

Source term	SEV1	
Total decontaminated area	4 km^2	
Maximum order of magnitude of **initial** surface cesium activities	100 kBq·m^{-2}	
Maximum annual effective dose **before recovery**	2.8 mSv	
Maximum annual effective dose **after recovery**	0.3 mSv	
Applied countermeasures	Access restriction, grass removal, tree/shrub pruning, soil stripping, high-pressure washing of buildings and roads	Access restriction, grass removal, tree/shrub pruning, turf harvesting, high-pressure washing of buildings and roads
Duration of recovery	0.13 years	0.12 years
Soil and organic waste	1.2E+05 m^3	5.8E+04 m^3
Liquid waste	5.0E+03 m^3	
Total costs	17 mln. EUR	16 mln. EUR
Total benefits	82 mln. EUR	63 mln. EUR
Total costs per m^2	4.4 EUR·m^{-2}	4.1 EUR·m^{-2}

Table 11. Results of simulated decontamination for SEV6 source term including cost-benefit analysis (source: Selivanova et al., 2025: 10)

Source term	SEV6	
Total decontaminated area	630 km^2	
Maximum order of magnitude of **initial** surface cesium activities	10 $MBq \cdot m^{-2}$	
Maximum annual effective dose **before recovery**	284 mSv	
Maximum annual effective dose **after recovery**	38 mSv	
Applied countermeasures	Access restriction, grass removal, tree/shrub pruning, soil stripping, high-pressure washing of buildings and roads	Access restriction, grass removal, tree/shrub pruning, turf harvesting, high-pressure washing of buildings and roads
Duration of recovery	1.59 years	1.62 years
Soil and organic waste	1.3E+07 m^3	6.9E+06 m^3
Liquid waste	1.7E+06 m^3	
Total costs	3.3 bn. EUR	3.2 bn. EUR
Total benefits	72.3 bn. EUR	57.2 bn. EUR
Total costs per m^2	5.3 $EUR \cdot m^{-2}$	5.2 $EUR \cdot m^{-2}$

Table 12. Results of simulated decontamination for SEV7 source term including cost-benefit analysis (source: Selivanova et al., 2025: 10)

Source term	SEV7	
Total decontaminated area	681 km^2	
Maximum order of magnitude of **initial** surface Cs activities	100 $MBq \cdot m^{-2}$	
Maximum annual effective dose **before recovery**	3 Sv	
Maximum annual effective dose **after recovery**	40 mSv	
Applied countermeasures	Access restriction, grass removal, tree/shrub pruning, soil stripping, high-pressure washing of buildings and roads	Access restriction, grass removal, tree/shrub pruning, turf harvesting, high-pressure washing of buildings and roads
Duration of recovery	1.65 years	1.64 years
Soil and organic waste	1.3E+07 m^3	6.9E+06 m^3
Liquid waste	1.7E+06 m^3	
Total costs	3.4 bn. EUR	3.3 bn. EUR
Total benefits	124.1 bn. EUR	100.4 bn. EUR
Total costs per m^2	4.9 $EUR \cdot m^{-2}$	4.8 $EUR \cdot m^{-2}$

7.3 Sensitivity Analysis

According to Nisbet et al. (2018), DFs can vary widely and may change over time. Therefore, the DF for soil removal was examined. It can vary in an interval of 5–30 (Nisbet and Watson, 2018; U.S. EPA, 2016), while a default value of 10 was used in the model. For sensitivity

analyses performed in Vensim (Ventana Systems, 2025), DFs for soil removal were conservatively varied over an extended range of 1 to 50. This interval corresponded to a theoretical dose reduction ranging from 0% to nearly 98%. The initial surface activities of ^{137}Cs and ^{134}Cs were 1 $MBq \cdot m^{-2}$ and 1.57 $MBq \cdot m^{-2}$, respectively, assuming a severe accident. The results can be found in Fig. 42, where the annual effective doses from fields ranged from nearly 0 mSv to approximately 14 mSv following decontamination, aligning well with the expected dose reduction.

Considering turf harvesting, the corresponding DFs can be in a range of approximately 2–10 (Nisbet and Watson, 2018; U.S. EPA, 2016). Within the sensitivity analyses, the DF was changed in an interval of 1–20 for the same initial cesium surface activities described before. The results are presented in Fig. 43. According to the simulations, the effective doses were in a range of approximately 0–13 mSv per year, corresponding again to the dose reduction resulted from the decontamination.

Therefore, an earlier start of any recovery works would be significantly profitable than the delayed implementation, due to decline in the decontamination efficiency over time.

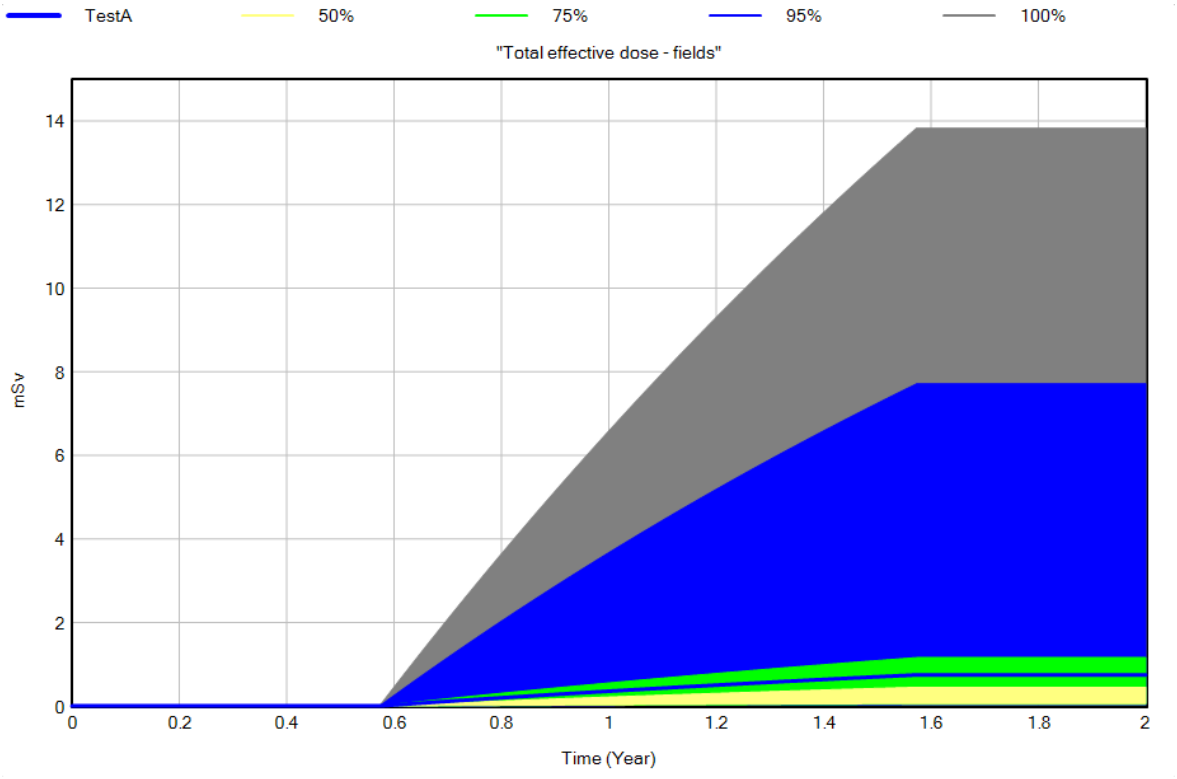

Fig. 42. Sensitivity analysis for effective doses from fields – soil stripping (source: own efforts)

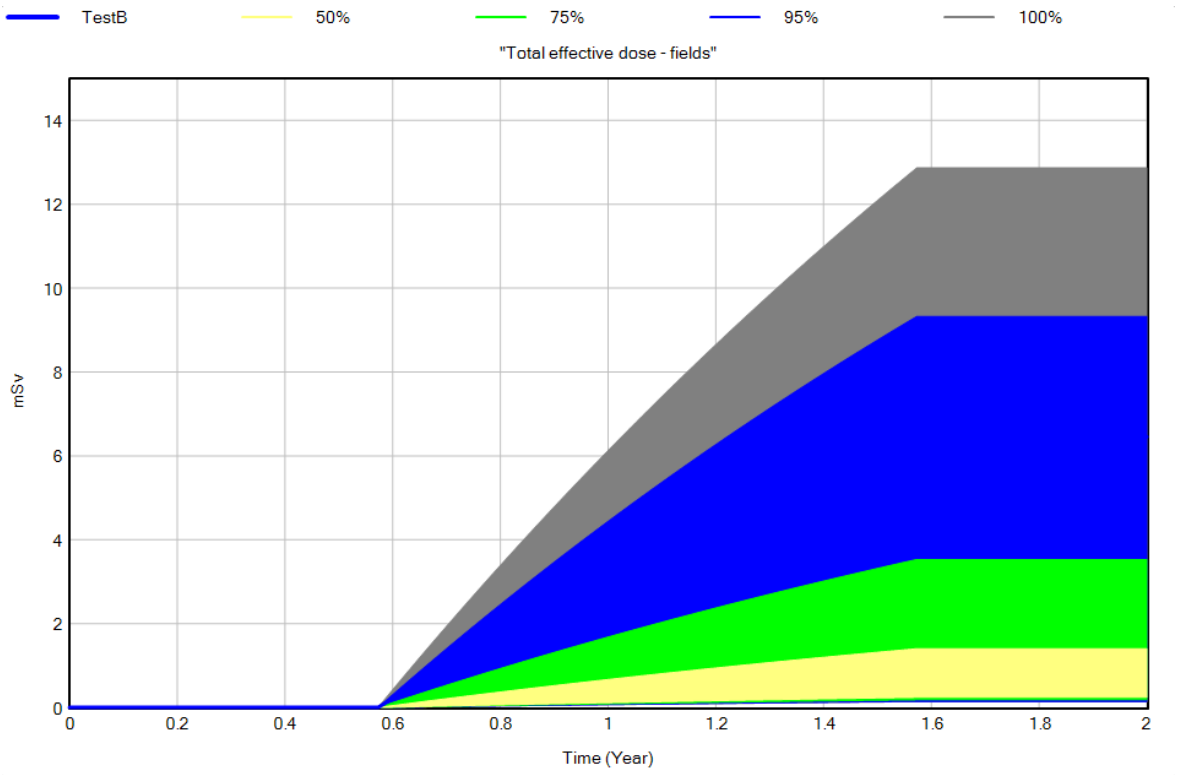

Fig. 43. Sensitivity analysis for effective doses from fields – turf harvesting (source: own efforts)

Considering sensitivity analysis, previous versions of the recovery model demonstrated that parameters such as initial surface activities, decontamination factors (DFs), and waste production can influence key model outputs. For example, waste production, or the total quantity of generated radioactive waste, was identified as the most influential parameter affecting the overall decontamination costs (Selivanova, 2020a). For example, a several-fold increase in waste production could result in a proportional increase in total recovery costs. This conclusion was consistent with previously published findings from the Fukushima clean-up and the Chernobyl experience (Nisbet and Watson, 2018; U.S. EPA, 2016).

Assuming initial surface activities of both cesium isotopes, the current version of the recovery model indicated that areas with total activity below 10 $kBq \cdot m^{-2}$ should be excluded from the decontamination process, as the implementation costs exceeded the associated benefits. This finding corresponded with results from the previous version of the model, in which the threshold for countermeasures such as grass removal was approximately in a range of several hundreds of $kBq \cdot m^{-2}$ and higher (Selivanova, 2020a).

For the removal of upper turf/soil layers, the current version of the model indicated a threshold for implementation of 100 $kBq \cdot m^{-2}$ and higher, whereas the previous version recommended a threshold of 1 $MBq \cdot m^{-2}$ and more (Selivanova, 2020a). This difference and the lower threshold in the current model can be attributed to the fact that the present study

considers significantly larger areas from several km^2 to hundreds of km^2, while the earlier version was applied to an area of only 0.06 km^2. Therefore, large-scale decontamination can be expected to be economically justified.

7.4 Potential Application and Extension of the Mathematical Model

Within the presented research, potential radiological consequences were assessed, including subsequent recovery scenarios. The model's findings may serve as a basis for the preparation of source materials for emergency response and long-term recovery planning. Therefore, the model can be applied in practice by decision-makers and policymakers involved in these activities. The results obtained from the developed model can also be utilized by various stakeholders and regulatory organizations.

The recovery model can be applied to other regions with appropriate modifications using actual site-specific input data. In such cases, demographic data, information on infrastructure and local topography, as well as current costs, should be updated. For example, up-to-date demographic parameters may be obtained from local statistical offices. Detailed information on infrastructure and topography can be sourced from cadastral services. Local costs, however, should be determined based on data from available suppliers. If such data are unavailable, currency conversion should be implemented directly within the model.

Regarding future improvements of the model, the following tasks should be solved:

- uses of actual source terms,
- analyses for various meteorological conditions (different wind directions and speeds, various precipitation rates, etc.),
- consideration of decontamination delays associated with seasonal variability (e.g., periods of severe winter conditions),
- analyses outside the EPZ if needed,
- inclusion of additional decontamination methods,
- extension of already implemented decontamination techniques,
- incorporation of internal dose calculations,
- integration of calculations for other radionuclides, e.g., iodine isotopes,
- inclusion of management of contaminated livestock,
- inclusion of management of contaminated water bodies,

- consideration of temporary relocation/permanent resettlement and restrictions on food and water consumption/production,
- optimization of solid waste collection, handling, and its disposal,
- inclusion of liquid waste management,
- implementation of legislative updates,
- inclusion of labor resources, supplies of PPE and auxiliary equipment,
- more detailed dose assessments for workers,
- consideration of social impacts.

8 Conclusion

Utilizing the System Dynamics methodology, the mathematical model for the recovery of affected areas was developed. The model was applied to potential cases of contamination following various accidents at the selected NPP and subsequent releases of radionuclides, taking into consideration actual conditions in Czechia. The model was tested within the EPZ of the NPP only due to the availability of input data. However, all presented analyses should be extended to areas beyond the EPZ, based on the results of atmospheric dispersion simulations in JRODOS.

Input data for the developed model were obtained from open sources and based on the results of own simulations performed using various software tools, i.e., JRODOS and MCNP. The presented study, therefore, integrates different simulation codes and links multiple fields to support emergency planning and decision-making in the field of radiation protection.

According to the results of simulations in the recovery model and subsequent analyses, minor atmospheric releases from the NPP would not necessitate any decontamination efforts. In such cases, surface activities of cesium isotopes would be of the same order of magnitude as the existing contamination after the Chernobyl accident. The corresponding levels of exposure would, therefore, be practically negligible, whereas the costs of decontamination are expected to significantly exceed the potential benefits.

In the case of severe accidents followed by large radionuclide releases (particularly involving cesium isotopes), decontamination works would be highly required. As part of the recovery of affected areas, agricultural fields, forests (trees and shrubs), buildings, gardens, roads, and other objects should be subject to decontamination. Grass cutting combined with topsoil removal proved to be highly effective for agricultural and grassed areas. High-pressure washing was sufficiently effective for buildings and roads. In such scenarios, the benefits of decontamination substantially exceeded the total costs.

A comparison between the results of the simulated decontamination and those of previously implemented clean-up activities in Fukushima showed good agreement in terms of total costs. However, further development and extension of the model would be required to enhance its comprehensiveness.

References

Ahn, J., Carson, C., Jensen, M., Juraku, K., 2014. Reflections on the Fukushima Daiichi Nuclear Accident: toward social-scientific literacy and engineering resilience. Springer Berlin Heidelberg, New York, NY. https://doi.org/10.1007/978-3-319-12090-4

Akleyev, A. V., Krestinina, L.Y., Degteva, M.O., Tolstykh, E.I., 2017. Consequences of the radiation accident at the Mayak production association in 1957 (the 'Kyshtym Accident'). J. Radiol. Prot. 37, R19–R42. https://doi.org/10.1088/1361-6498/aa7f8d

Albin, S., 2001. Generic Structures: First-Order Negative Feedback. Massachusetts Institute of Technology.

Amec Foster Wheeler s.r.o., 2017. New nuclear source at the Dukovany site, Environmental Report. CENIA - Czech Environmental Information Agency.

Andersson, K.G., Rantavaara, A., Roed, J., Rosén, K., Salbu, B., Skipperud, L., 2000. A Guide to Countermeasures for Implementation in the Event of a Nuclear Accident Affecting Nordic Food-Producing Areas. Nordic nuclear safety research, Roskilde.

Andersson, K.G., Roed, J., 2006. Estimation of doses received in a dry-contaminated residential area in the Bryansk region, Russia, since the Chernobyl accident. J. Environ. Radioact. 85, 228–240. https://doi.org/10.1016/j.jenvrad.2004.08.019

Andersson, K.G., Roed, J., Fogh, C.L., 2002. Weathering of radiocaesium contamination on urban streets, walls and roofs. J. Environ. Radioact. 62, 49–60. https://doi.org/10.1016/S0265-931X(01)00150-3

Assas, A.A., Gass, S.I., 2011. Profiles in Operations Research, International Series in Operations Research & Management Science. Springer US, Boston, MA. https://doi.org/10.1007/978-1-4419-6281-2

Asselt, E.D., Twenhöfel, C.J., Duranova, T., Smetsers, R.C., Bohunova, J., Müller, T., 2021. Facilitating the Decision-Making Process After a Nuclear Accident: Case Studies in the Netherlands and Slovakia. Integr. Environ. Assess. Manag. 17, 376–387. https://doi.org/10.1002/ieam.4375

Bartusková, M., Selivanova, A., Malátová, I., Hůlka, J., Škrkal, J., Rosmus, J., Kapyltsova, A., Rulík, P., 2023. A comparison of different detection techniques for 137Cs measurements of cattle in vivo. Radiat. Prot. Dosimetry. https://doi.org/10.1093/rpd/ncad252

Batorshin, G.S., Mokrov, Y.G., 2018. Experience and the results of emergency management

of the 1957 accident at the Mayak Production Association. J. Radiol. Prot. 38, R1–R12. https://doi.org/10.1088/1361-6498/aa9cf9

Beck, H.L., 1966. Environmental Gamma Radiation from Deposited Fission Products, 1960–1964. Health Phys. 12, 313–322. https://doi.org/10.1097/00004032-196603000-00002

Bennett, S., Pleasant, R., Cave, S., Woodham, E., 2017. Assessing the Future Workforce Supply for the UK Nuclear Sector, in: Proceedings of the 35th International Conference of the System Dynamics Society and 60th Anniversary of System Dynamics Celebration. System Dynamics Society, Cambridge, MA, USA.

Bertsch, V., Treitz, M., Geldermann, J., Rentz, O., Charnock, T., Benz, G., 2007. User guide for Web-HIPRE 2.0 with RODOS.

Bezhenar, R., Heling, R., Ievdin, I., Iosjpe, M., Maderich, V., Willemsen, S., de With, G., Dvorzhak, A., 2016. Integration of marine food chain model POSEIDON in JRODOS and testing versus Fukushima data. Radioprotection 51, S137–S139. https://doi.org/10.1051/radiopro/2016050

BfS, 2023. Phases of an emergency [WWW Document]. URL https://www.bfs.de/EN/topics/ion/accident-management/emergency/phases/phases.html (accessed 6.5.23).

Bier, A., 2011. Sensitivity Analysis Techniques for System Dynamics Models of Human Behavior. Proc. 29th Int. Conf. Syst. Dyn. Soc.

Bland, J., Potter, C., Homann, S., 2018. Radiological Exposure Devices (RED). Technical Basis for Threat Profile Sandia National Laboratories. Sandia National Laboratories, United States. https://doi.org/10.2172/1452666

Borgonovo, E., Plischke, E., 2016. Sensitivity analysis: A review of recent advances. Eur. J. Oper. Res. 248, 869–887. https://doi.org/10.1016/j.ejor.2015.06.032

Bossel, H., 2007a. System Zoo 1 Simulation Models – Elementary Systems, Physics, Engineering. Books On Demand, Norderstedt.

Bossel, H., 2007b. System Zoo 2 Simulation Models – Climate, Ecosystems, Resources. Books On Demand, Norderstedt.

Bossel, H., 2007c. System Zoo 3 Simulation Models – Economy, Society, Development. Books On Demand, Norderstedt.

Brent, R.J., 2006. Applied Cost–Benefit Analysis, 2nd editio. ed. Edward Elgar Publishing Limited, Cheltenham, UK.

Bučina, I., Drábová, D., Kunz, E., Malátová, I., 1996. Monitoring of post-Chernobyl contamination in the Czech Republic, in: Proceedings of the First International Conference "The Radiological Consequences of the Chernobyl Accident." International Atomic Energy Agency, Luxembourg, pp. 1045–1048.

Calábria, J.A.A., Morais, G.F., 2017. Agricultural countermeasure program - AGRICP: food and dose module in ARGOS- accident reporting and Guidance Operational System, in: INAC 2017: International Nuclear Atlantic Conference. Associação Brasileira de Energia Nuclear (ABEN), Belo Horizonte, MG (Brazil).

Cave, S., Peters, J., Walkingshaw, M., Gray, A., 2016. Simulation and analysis to support decision making in the treatment and handling of radioactive waste, in: 34th International Conference of the SDS, 17-21.7.2016. Delft, Netherlands.

CDC, 2021. Radiation Hazard Scale [WWW Document]. URL https://www.cdc.gov/radiation-emergencies/php/toolkit/hazard-scale.html (accessed 2.13.25).

ČEZ Group, 2024. Rolls-Royce SMR and ČEZ Group partner to deploy SMRs in UK and Czechia [WWW Document]. URL https://www.cez.cz/en/media/press-releases/rolls-royce-smr-and-cez-group-partner-to-deploy-smrs-in-uk-and-czechia-201775 (accessed 3.3.25).

ČEZ Group, 2023a. Nuclear Power Plants [WWW Document]. URL https://www.cez.cz/en/energy-generation/nuclear-power-plants (accessed 6.21.23).

ČEZ Group, 2023b. NPP Temelín [WWW Document]. URL https://www.cez.cz/en/energy-generation/nuclear-power-plants/temelin (accessed 12.5.23).

ČEZ Group, 2023c. NPP Dukovany [WWW Document]. URL https://www.cez.cz/en/energy-generation/nuclear-power-plants/dukovany (accessed 12.5.23).

ČEZ Group, 2022. CEZ launches a tender for the construction of a new nuclear power plant in Dukovany [WWW Document]. URL https://www.cez.cz/en/investors/inside-information/cez-launches-a-tender-for-the-construction-of-a-new-nuclear-power-plant-in-dukovany-156459 (accessed 6.14.23).

Charnes, A., Cooper, W.W., Rhodes, E., 1978. Measuring the efficiency of decision making units. Eur. J. Oper. Res. 2, 429–444. https://doi.org/10.1016/0377-2217(78)90138-8

Charnock, T., Landman, C., Trybushnyi, D., Ievdin, I., 2016. European model for inhabited areas - ERMIN 2. Radioprotection 51, S23–S25.

https://doi.org/10.1051/radiopro/2016006

Chia, E.S., Lim, C.K., Ng, A., Nguyen, N.H.L., 2015. The System Dynamics of Nuclear Energy in Singapore. Int. J. Green Energy 12, 73–86. https://doi.org/10.1080/15435075.2014.889001

CHMI, 2022. Czech Hydrometeorological Institute [WWW Document]. URL https://www.chmi.cz/ (accessed 6.20.22).

Cholteeva, Y., 2020. Making Chernobyl safe: a timeline. Power Technol.

Clarivate, 2023. Web of Science [WWW Document]. URL https://webofknowledge.com/ (accessed 6.23.23).

CNB, 2025a. Kurzy devizového trhu – měsíční průměry, EUR [Foreign exchange market rates – monthly averages, EUR] [WWW Document]. URL https://www.cnb.cz/cs/financni-trhy/devizovy-trh/kurzy-devizoveho-trhu/kurzy-devizoveho-trhu/prumerne_mena.html?mena=EUR (accessed 3.31.25).

CNB, 2025b. Kurzy devizového trhu – měsíční průměry, JPY [Foreign exchange market rates – monthly averages, JPY] [WWW Document]. URL https://www.cnb.cz/cs/financni-trhy/devizovy-trh/kurzy-devizoveho-trhu/kurzy-devizoveho-trhu/prumerne_mena.html?mena=JPY (accessed 3.31.25).

Crick, M.J., Linsley, G.S., 1984. An assessment of the radiological impact of the windscale reactor fire, october 1957. Int. J. Radiat. Biol. 46, 479–506. https://doi.org/10.1080/09553008414551711

ČÚZK, 2023. ČÚZK – Otevřená data [Open Data] [WWW Document]. URL https://www.cuzk.cz/Uvod.aspx (accessed 12.7.23).

ČÚZK, 2022. State Administration of Land Surveying and Cadastre [WWW Document]. URL https://www.cuzk.cz/ (accessed 6.20.22).

CZSO, 2024. Czech Statistical Office [WWW Document]. URL https://www.czso.cz/ (accessed 1.4.24).

CZSO, 2022. Inflation, Consumer Prices [WWW Document]. URL https://www.czso.cz/csu/czso/inflation_consumer_prices_ekon (accessed 6.20.22).

CZSO, 2021. Population Censuses [WWW Document]. URL https://www.czso.cz/csu/czso/population-censuses (accessed 1.4.24).

DHS, 2008. 73 FR 45029 - Planning Guidance for Protection and Recovery Following Radiological Dispersal Device (RDD) and Improvised Nuclear Device (IND) Incidents. Office of the Federal Register, National Archives and Records Administration,

Washington, D.C.

Di Giuli, M., Malicki, M., Dejardin, P., Corda, V., Swaidan, A.M., 2022. MELCOR 2.2-ASTEC V2.2 crosswalk study reproducing SBLOCA and CSBO scenarios in a PWR1000-like reactor part I: Analysis of RCS thermal-hydraulics and in-vessel phenomena. Nucl. Eng. Des. 387, 111248. https://doi.org/10.1016/j.nucengdes.2021.111248

Dunster, H.J., Howells, H., Templeton, W.L., 2007. District Surveys following the Windscale Incident, October 1957. J. Radiol. Prot. 27, 217–230. https://doi.org/10.1088/0952-4746/27/3/001

Duranova, T., van Asselt, E., Müller, T., Bohunova, J., Twenhöfel, C.J.W., Smetsers, R.C.G.M., 2020. MCDA stakeholder workshops. Radioprotection 55, S193–S196. https://doi.org/10.1051/radiopro/2020032

ENSI, 2011. Radiological Effects of the Nuclear Accidents in Fukushima on 11 March 2011. Swiss Federal Nuclear Safety Inspectorate (ENSI), Switzerland, Brugg.

EURATOM, 2016. Council Regulation (Euratom) 2016/52 of 15 January 2016 laying down maximum permitted levels of radioactive contamination of food and feed following a nuclear accident or any other case of radiological emergency, and repealing Regulation (Euratom) No 3954. Official Journal of the European Union.

European Central Bank, 2025. Japanese yen (JPY) [WWW Document]. URL https://www.ecb.europa.eu/stats/policy_and_exchange_rates/euro_reference_exchange_rates/html/eurofxref-graph-jpy.en.html (accessed 2.17.25).

Exchange-Rates.org, 2025. JPY To USD Exchange Rate History for 2022 [WWW Document]. URL https://www.exchange-rates.org/exchange-rate-history/jpy-usd-2022 (accessed 2.17.25).

FEMA, 2011. National Disaster Recovery Framework. Strengthening Disaster Recovery for the Nation. Federal Emergency Management Agency, Washington, D.C.

Forrester, J.W., 1961. Industrial Dynamics. MIT Press, Cambridge, Massachusetts.

Garland, J.A., Wakeford, R., 2007. Atmospheric emissions from the Windscale accident of October 1957. Atmos. Environ. 41, 3904–3920. https://doi.org/10.1016/j.atmosenv.2006.12.049

Gering, F., Raskob, W., Charnock, T., 2010. New model for agricultural countermeasures in RODOS and ARGOS. Radioprotection 45, S63–S76. https://doi.org/10.1051/radiopro/2010035

Glazner, C., Steckley, S., Lee, K., 2011. Nuclear Waste Management: Strategic Framework for Large-Scale Government Programs: Addressing Legacy Waste from the Cold War, in: Proceedings of the 29th International Conference of the System Dynamics Society. System Dynamics Society, Washington, D.C. USA.

Gong, S., Chen, L., Zhou, Q., Gao, X., Shen, F., 2025. Vulnerability evolution of critical infrastructures: A multidimensional environment-integrated system dynamics analysis. Reliab. Eng. Syst. Saf. 256, 110719. https://doi.org/10.1016/j.ress.2024.110719

Goorley, J., James, M., Booth, T., Brown, F., Bull, J., Cox, L., Durkee, Jr., J., Elson, J., Fensin, M., Forster, III, R., Hendricks, J., Hughes, III, H., Johns, R., Kiedrowski, B., Martz, R., Mashnik, S., McKinney, G., Pelowitz, D., Prael, R., Sweezy, J., Waters, L., Wilcox, T., Zukaitis, A., 2013. Initial MCNP6 Release Overview - MCNP6 version 1.0. Los Alamos, NM (United States). https://doi.org/10.2172/1086758

Guo, Xiaopeng, Guo, Xiaodan, 2016. Nuclear power development in China after the restart of new nuclear construction and approval: A system dynamics analysis. Renew. Sustain. Energy Rev. 57, 999–1007. https://doi.org/10.1016/j.rser.2015.12.190

Ham, G.J., 2009. The determination of Polonium-210 in urine following the Litvinenko incident. Radioprotection 44, 41–46. https://doi.org/10.1051/radiopro/20095014

Hämäläinen, R.P., Kettunen, E., 1994. HIPRE 3+ Group Link. User's Guide. Systems Analysis Laboratory, Helsinki University of Technology.

Hämäläinen, R.P., Mustajoki, J., 2007. Web-HIPRE.

Hanawa, K., 2023. Fukushima Anniversary: Fukushima cleanup costs swell with no end in sight. Nikkei Asia.

Harrison, J., Fell, T., Leggett, R., Lloyd, D., Puncher, M., Youngman, M., 2017. The polonium-210 poisoning of Mr Alexander Litvinenko. J. Radiol. Prot. 37, 266–278. https://doi.org/10.1088/1361-6498/aa58a7

He, S., Shi, S., Li, M., Lin, Z., Lu, Y., Li, H., 2025. Model of safety investment optimization in chemical industrial parks based on system dynamics. Reliab. Eng. Syst. Saf. 256, 110761. https://doi.org/10.1016/j.ress.2024.110761

Hinrichsen, Y., Finck, R., Martinsson, J., Rääf, C., 2021. Maximizing avertable doses with a minimum amount of waste for remediation of land areas around typical single family houses after radioactive fallout based on Monte Carlo simulations. Sci. Rep. 11, 1–9. https://doi.org/10.1038/s41598-021-84103-1

Hlavatý, R., Brožová, H., Selivanova, A., Sedlářová-Nehézová, T., 2024. Designing optimal

transportation patterns for radiation accident recovery, in: 42nd International Conference on Mathematical Methods in Economics (MME 2024) – Conference Proceedings. 11-13.9.2024, Ústí Nad Labem, Czech Republic. Czech Society for Operations Research, Ústí nad Labem, Czech Republic, pp. 126–131.

Hoe, S., McGinnity, P., Charnock, T., Gering, F., Jacobsen, S., Henrik, L., Havskov Sørensen, J., Andersson, K.G., Astrup, P., 2009. ARGOS Decision Support System for Emergency Management, in: Proceedings (Online). Argentine Radiation Protection Society.

Hofman, D., Monte, L., Boyer, P., Brittain, J., Donchyts, G., Gallego, E., Gheorghiu, D., Håkanson, L., Heling, R., Kerekes, A., Kocsy, G., Lepicard, S., Slavik, O., Slavnicu, D., Smith, J., Zheleznyak, M., 2011. Computerised Decision Support Systems for the management of freshwater radioecological emergencies: Assessment of the state-of-the-art with respect to the experiences and needs of end-users. J. Environ. Radioact. 102, 119–127. https://doi.org/10.1016/j.jenvrad.2010.11.002

Hostetter, M., Kranz, D.A., Seed, C., Terman, C., Ward, S., 1997. Curl: a gentle slope language for the Web. World Wide Web J. 2, 121–134.

Hsiao, C.T., Liu, C.S., Chang, D.S., Chen, C.C., 2018. Dynamic modeling of the policy effect and development of electric power systems: A case in Taiwan. Energy Policy 122, 377–387. https://doi.org/10.1016/j.enpol.2018.07.001

Humphries, L.L., Beeny, B.A., Gelbard, F., Louie, D.L., Phillips, J., 2017. MELCOR Computer Code Manuals. Vol.2: Reference Manual, Version 2.2.9541. SAND2017-0876 O.

IAEA, 2021a. Country Nuclear Power Profiles: Czech Republic [WWW Document]. URL https://cnpp.iaea.org/countryprofiles/CzechRepublic/CzechRepublic.htm (accessed 6.20.22).

IAEA, 2021b. Benefits and Challenges of Small Modular Fast Reactors. Proceedings of a Technical Meeting. IAEA-TECDOC-1972, Benefits and Challenges of Small Modular Fast Reactors. International Atomic Energy Agency, Vienna, Austria.

IAEA, 2015a. The Fukushima Daiichi Accident. Report by the Director General. International Atomic Energy Agency, Vienna, Austria.

IAEA, 2015b. The Fukushima Daiichi Accident: Radiological Consequences, The Fukushima Daiichi Accident Vol. 4/5. International Atomic Energy Agency, Vienna, Austria.

IAEA, 2014. Experiences and Lessons Learned Worldwide in the Cleanup and Decommissioning of Nuclear Facilities in the Aftermath of Accidents, IAEA nuclear energy series No. NW-T-2.7. International Atomic Energy Agency, Vienna, Austria.

IAEA, 2013a. IAEA Report on Decommissioning and Remediation after a Nuclear Accident. International Atomic Energy Agency, Vienna, Austria.

IAEA, 2013b. Guidelines for Remediation Strategies to Reduce the Radiological Consequences of Environmental Contamination., Technical Reports Series No. 475. International Atomic Energy Agency, Vienna, Austria.

IAEA, 2013c. INES: The International Nuclear and Radiological Event Scale. User's Manual. Vienna, Austria.

IAEA, 2012. The Chernobyl I-131 Release: Model Validation and Assessment of the Countermeasure Effectiveness. International Atomic Energy Agency, Vienna, Austria.

IAEA, 2011. Historical collections of the Chernobyl accident [WWW Document]. URL https://www.flickr.com/photos/iaea_imagebank/5612553615/in/photostream/ (accessed 11.24.23).

IAEA, 2010. IAEA USIE – Unified System for Information Exchange in Incidents and Emergencies [WWW Document]. URL https://iec.iaea.org/usie/actual/LandingPage.aspx (accessed 9.5.23).

IAEA, 2008a. Derivation of the Source Term and Analysis of the Radiological Consequences of Research Reactor Accidents (Safety Reports Series No. 53). International Atomic Energy Agency, Vienna, Austria.

IAEA, 2008b. INES – The international nuclear and radiological event scale. 08-26941/E.

IAEA, 2008c. CHERNOBYL: Looking Back to Go Forward, in: Proceedings of an International Conference on Chernobyl: Looking Back to Go Forward. International Atomic Energy Agency, Vienna.

IAEA, 2007. Arrangements for Preparedness for a Nuclear or Radiological Emergency. Safety Guide No. GS-G-2.1. International Atomic Energy Agency, Vienna, Austria.

IAEA, 2006. Environmental Consequences of the Chernobyl Accident and their Remediation: Twenty Years of Experience, Report of the Chernobyl Forum Expert Group 'Environment.' International Atomic Energy Agency, Vienna.

IAEA, 2001. Present and future environmental impact of the Chernobyl accident. IAEA-TECDOC-1240. International Atomic Energy Agency, Vienna, Austria.

IAEA, 2000. Generic procedures for assessment and response during a radiological

emergency. IAEA-TECDOC-1162.

IAEA, 1999. State of the Art Technology for Decontamination and Dismantling of Nuclear Facilities, Technical Reports Series No. 395. International Atomic Energy Agency, Vienna.

IAEA, 1996. Procedures for Conducting Probabilistic Safety Assessments of Nuclear Power Plants (Level 3). Off-Site Consequences and Estimation of Risks to the Public: A Safety Practice. International Atomic Energy Agency, Vienna, Austria.

IAEA, 1994. Guidelines for Agricultural Countermeasures Following an Accidental Release of Radionuclides. A joint undertaking by the IAEA and FAO, Technical Reports Series No. 363. International Atomic Energy Agency, Vienna, Austria.

IAEA, 1993. Generic intervention levels for protecting the public in the event of a nuclear accident or radiological emergency. IAEA-TECDOC-698. International Atomic Energy Agency, Vienna, Austria.

IAEA, 1988. The Radiological Accident in Goiânia. International Atomic Energy Agency, Vienna, Austria.

ICRP, 2007. ICRP Publication 103. The 2007 Recommendations of the International Commission on Radiological Protection, Annals of the ICRP. Elsevier Ltd.

ICRP, 2006. ICRP Publication 101. Assessing Dose of the Representative Person for the Purpose of Radiation Protection of the Public and The Optimisation of Radiological Protection: Broadening the Process, Annals of the ICRP. Elsevier Ltd. https://doi.org/10.1016/j.icrp.2006.09.007

ICRP, 1997. ICRP Publication 74. Conversion Coefficients for use in Radiological Protection against External Radiation, Annals of the ICRP. Pergamon.

Ievdin, I., Trybushnyi, D., Landman, C., 2017. JRodos Customization Guide Version 3.01 (JRodos February 2017).

Ievdin, I., Trybushnyi, D., Staudt, C., Landman, C., 2019. JRODOS User Guide.

Ievdin, I.O., Khalchenkov, O. V., Kovalets, I. V., Raskob, W., Trybushnyi, D., Zheleznyak, M.J., 2012. Application of decision support system JRODOS for assessments of atmospheric dispersion and deposition from Fukushima Daiichi Nuclear Power Plant Accident. Int. J. Energy a Clean Environ. 13, 179–190. https://doi.org/10.1615/InterJEnerCleanEnv.2013006151

Ismail, I., Failler, P., March, A., Thorpe, A., 2022. A System Dynamics Approach for Improved Management of the Indian Mackerel Fishery in Peninsular Malaysia.

Sustainability 14, 14190. https://doi.org/10.3390/su142114190

Jacobsen, L.H., Andersson, K.G., Charnock, T., Kaiser, J.C., Gering, F., Hoe, S.C., Juul Larsen, L., 2010. Implementation in ARGOS of ERMIN and AGRICP. Radioprotection 45, 191–198. https://doi.org/10.1051/radiopro/2010025

Jacobson, J.J., Yacout, A.M., Matthern, G.E., Piet, S.J., Shropshire, D.E., Jeffers, R.F., Schweitzer, T., 2010. Verifiable Fuel Cycle Simulation Model (VISION): A Tool for Analyzing Nuclear Fuel Cycle Futures. Nucl. Technol. 172, 157–178. https://doi.org/10.13182/NT172-157

Jiang, W., Marggraf, R., 2021. The origin of cost–benefit analysis: a comparative view of France and the United States. Cost Eff. Resour. Alloc. 19, 74. https://doi.org/10.1186/s12962-021-00330-3

Ju, H., Hwang, I.S., 2018. Systematic model for estimation of future inadvertent human intrusion into deep rad-waste repository by domestic groundwater well drilling. Nucl. Eng. Des. 327, 38–50. https://doi.org/10.1016/j.nucengdes.2017.12.005

Kang, K.M., Jae, M., 2008. Development of radiation risk assessment simulator using system dynamics methodology. J. Nucl. Sci. Technol. 45, 728–731. https://doi.org/10.1080/00223131.2008.10875958

Kato, H., Onda, Y., Teramage, M., 2012. Depth distribution of 137Cs, 134Cs, and 131I in soil profile after Fukushima Dai-ichi Nuclear Power Plant Accident. J. Environ. Radioact. 111, 59–64. https://doi.org/10.1016/j.jenvrad.2011.10.003

Khalil, M.Y., Nagy, M.S., Talha, K.A., Hassan, M.I., 2006. Effect of iodine chemical form on thyroid doses during a severe accident. Int. J. Low Radiat. 3, 105–116. https://doi.org/10.1504/IJLR.2006.010014

Kim, Y. Il, Woo, T.H., 2017. Safety assessment for the ultimate heat sink (UHS) system with non-injection concept in nuclear power plants (NPPs). J. Nucl. Sci. Technol. 54, 39–46. https://doi.org/10.1080/00223131.2016.1204255

Kim, S. yeop, Bixler, N.E., Ahn, K. Il, Hwang, S.W., 2020. An approach to incorporate multiple forms of iodine in radiological consequence analysis. J. Environ. Radioact. 213, 106139. https://doi.org/10.1016/j.jenvrad.2019.106139

KIT, 2025. Helmholtz MCDA Tool (HELDA).

KIT, 2024. Decision analysis tool for a sustainable energy transition [WWW Document]. URL https://www.itas.kit.edu/english/2024_028.php (accessed 4.1.25).

Kovalets, I. V., Robertson, L., Persson, C., Didkivska, S.N., Ievdin, I.A., Trybushnyi, D.,

2014. Calculation of the far range atmospheric transport of radionuclides after the Fukushima accident with the atmospheric dispersion model MATCH of the JRODOS system. Int. J. Environ. Pollut. 54, 101. https://doi.org/10.1504/IJEP.2014.065110

Kovalets, I. V., Romanenko, O., Synkevych, R., 2020. Adaptation of the RODOS system for analysis of possible sources of Ru-106 detected in 2017. J. Environ. Radioact. 220–221, 106302. https://doi.org/10.1016/j.jenvrad.2020.106302

Kovalets, I. V., Talerko, M., Synkevych, R., Koval, S., 2022. Estimation of Cs-137 emissions during wildfires and dust storm in Chernobyl Exclusion Zone in April 2020 using ensemble iterative source inversion method. Atmos. Environ. 288, 119305. https://doi.org/10.1016/j.atmosenv.2022.119305

Kubanyi, J., Lavin, R.B., Serbanescu, D., Toth, B., Wilkening, H., 2008. Risk Informed Support of Decision Making in Nuclear Power Plant Emergency Zoning. Generic Framework towards Harmonising NPP Emergency Planning Practices, JRC Scientific and Technical Reports. European Communities.

Kunsch, P.L., Friesewinkel, J., 2014. Nuclear energy policy in Belgium after Fukushima. Energy Policy 66, 462–474. https://doi.org/10.1016/j.enpol.2013.11.035

Lai, D., Wahba, R., 2001. System Dynamics Model Correctness Checklist. Massachusetts Institute of Technology.

Landman, C., Päsler-Sauer, J., Raskob, W., 2014. RODOS and the Fukushima Accident, in: The Risks of Nuclear Energy Technology. Science Policy Reports. Springer Berlin Heidelberg, pp. 349–352. https://doi.org/10.1007/978-3-642-55116-1_22

Lepicard, S., Heling, R., Maderich, V., 2004. POSEIDON/RODOS models for radiological assessment of marine environment after accidental releases: Application to coastal areas of the Baltic, Black and North Seas. J. Environ. Radioact. 72, 153–161. https://doi.org/10.1016/S0265-931X(03)00197-8

Lidovky.cz, 2016. Výlet k reaktoru smrti za 350 eur [Trip to the Reactor of Death for 350 Euros] [WWW Document]. URL https://www.lidovky.cz/svet/neolizujte-si-ruce-hlavni-je-se-nebat-vylet-k-reaktoru-smrti-za-350-eur.A160425_144700_ln_zahranici_msl (accessed 3.3.25).

Liu, A., Chen, K., Huang, X., Li, D., Zhang, X., 2021. Dynamic risk assessment model of buried gas pipelines based on system dynamics. Reliab. Eng. Syst. Saf. 208, 107326. https://doi.org/10.1016/j.ress.2020.107326

Liu, J., Zou, Y., Wang, W., Zhang, L., Liu, X., Ding, Q., Qin, Z., Čepin, M., 2021. Analysis

of dependencies among performance shaping factors in human reliability analysis based on a system dynamics approach. Reliab. Eng. Syst. Saf. 215. https://doi.org/10.1016/j.ress.2021.107890

Maloney, S., Sterman, J.D., 1982. Policy analysis of the low-level radioactive waste disposal problem in the USA. Nucl. Saf. 23, 300–309.

Margvelashvily, N., Maderich, V., Zheleznyak, M., 1997. THREETOX - A Computer Code to Simulate Three-Dimensional Dispersion of Radionuclides in Stratified Water Bodies. Radiat. Prot. Dosimetry 73, 177–180. https://doi.org/10.1093/oxfordjournals.rpd.a032128

Masayuki, I., 2012. Report of the results of the decontamination model projects: analysis and evaluation of the results of the decontamination model projects – decontamination technologies. Fukushima, Japan.

Masson, O., Romanenko, O., Saunier, O., Kirieiev, S., Protsak, V., Laptev, G., Voitsekhovych, O., Durand, V., Coppin, F., Steinhauser, G., De Vismes Ott, A., Renaud, P., Didier, D., Boulet, B., Morin, M., Hýža, M., Camps, J., Belyaeva, O., Dalheimer, A., Eleftheriadis, K., Gascó-Leonarte, C., Ioannidou, A., Isajenko, K., Karhunen, T., Kastlander, J., Katzlberger, C., Kierepko, R., Knetsch, G.J., Kónyi, J.K., Mietelski, J.W., Mirsch, M., Møller, B., Nikolić, J.K., Rusconi, R., Samsonov, V., Simion, E., Steinmann, P., Stoulos, S., Suarez-Navarro, J.A., Wershofen, H., Zapata-García, D., Zorko, B., 2021. Europe-Wide Atmospheric Radionuclide Dispersion by Unprecedented Wildfires in the Chernobyl Exclusion Zone, April 2020. Environ. Sci. Technol. 55, 13834–13848. https://doi.org/10.1021/acs.est.1c03314

McConn Jr, R.J., Gesh, C.J., Pagh, R.T., Rucker, R.A., Williams III, R.G., 2011. Compendium of Material Composition Data for Radiation Transport Modeling - Revision 1, PIET-43741-TM963, PNNL-15870 Rev. 1.

McKnight, U.S., Finkel, M., 2013. A system dynamics model for the screening-level long-term assessment of human health risks at contaminated sites. Environ. Model. Softw. 40, 35–50. https://doi.org/10.1016/j.envsoft.2012.07.007

McKnight, U.S., Funder, S.G., Rasmussen, J.J., Finkel, M., Binning, P.J., Bjerg, P.L., 2010. An integrated model for assessing the risk of TCE groundwater contamination to human receptors and surface water ecosystems. Ecol. Eng. 36, 1126–1137. https://doi.org/10.1016/j.ecoleng.2010.01.004

Meadows, D.H., 1999. Leverage Points: Places to Intervene in a System. The Sustainability

Institute, Hartland, USA.

Meadows, D.H., Meadows, D.L., Randers, J., Behrens, W.W., 1972. The Limits to Growth: A Report for the Club of Rome's Project on the Predicament of Mankind. Universe Books, New York.

Meadows, D.H., Wright, D., 2008. Thinking in Systems: a Primer. Earthscan, Londin, Sterling, VA.

Meckbach, R., Jacob, P., Paretzke, H.G., 1988. Gamma Exposures due to Radionuclides Deposited in Urban Environments. Part II: Location Factors for Different Deposition Patterns. Radiat. Prot. Dosimetry. https://doi.org/10.1093/oxfordjournals.rpd.a080370

Meng, H., Liu, X., Xing, J., Zio, E., 2022. A method for economic evaluation of predictive maintenance technologies by integrating system dynamics and evolutionary game modelling. Reliab. Eng. Syst. Saf. 222, 108424. https://doi.org/10.1016/j.ress.2022.108424

MEXT, 2011. Results of Airborne Monitoring by the MEXT and the U.S. Department of Energy (May 6, 2011).

Mildeová, S., Vojtko, V., 2008. Systémová dynamika [System Dynamics], Vyd. 2., p. ed. Oeconomica, Praha.

Mishan, E.J., Quah, E., 2020. Cost-Benefit Analysis. Routledge, Sixth edition. | Milton Park, Abingdon, Oxon ; New York : Routledge, 2020. https://doi.org/10.4324/9781351029780

Miyahara, K., Tokizawa, T., Nakayama, S., 2012. Overview of the Results of Fukushima Decontamination Pilot Projects, IAEA International Experts' Meeting on Decommissioning and Remediation after a Nuclear Accident. International Atomic Energy Agency, Vienna, Austria.

MOE, 2013. Decontamination Guidelines, 2nd Ed.

Monte, L., Brittain, J.E., Gallego, E., Håkanson, L., Hofman, D., Jiménez, A., 2009. MOIRA-PLUS: A decision support system for the management of complex fresh water ecosystems contaminated by radionuclides and heavy metals. Comput. Geosci. 35, 880–896. https://doi.org/10.1016/j.cageo.2008.03.008

Monte, L., Brittain, J.E., Haakanson, L., Gallego, E., 1999. MOIRA models and methodologies for assessing the effectiveness of countermeasures in complex aquatic systems contaminated by radionuclides. ENEA, Centro Ricerche Casaccia, Rome, Italy.

Müller, T., Bai, S., Raskob, W., 2020. MCDA handling uncertainties. Radioprotection 55,

S181–S185. https://doi.org/10.1051/radiopro/2020030

Müller, T., Möhrle, S., Bai, S., Raskob, W., 2021. Multi Criteria Decision Analysis: Uncertainties and Combining Decision Making Methods. Annu. Rep. 2019 Inst. Nucl. Energy Technol. 7759, 39–47. https://doi.org/10.5445/IR/1000131287

Murakami, T., Anbumozhi, V., 2021. Safety and Economics of Small Modular Reactors. Jakarta, Indonesia.

Mustajoki, J., Hämäläinen, R.P., 2000. Web-Hipre: Global Decision Support By Value Tree And AHP Analysis. INFOR Inf. Syst. Oper. Res. 38, 208–220. https://doi.org/10.1080/03155986.2000.11732409

Naeem, K., Aloui, S., Zghibi, A., Mazzoni, A., Triki, C., Elomri, A., 2024. A system dynamics approach to management of water resources in Qatar. Sustain. Prod. Consum. 46, 733–753. https://doi.org/10.1016/j.spc.2024.03.024

Napier, B.A., Schmieman, E.A., Voitsekovitch, O., 2007. Radioactive waste management and environmental contamination issues at the Chernobyl site. Health Phys. 93, 441–451. https://doi.org/10.1097/01.HP.0000279602.34009.e3

Naseri-Rad, M., Berndtsson, R., Aminifar, A., McKnight, U.S., O'Connor, D., Persson, K.M., 2022. DynSus: Dynamic sustainability assessment in groundwater remediation practice. Sci. Total Environ. 832, 154992. https://doi.org/10.1016/j.scitotenv.2022.154992

National Research Council, 2014. Lessons Learned from the Fukushima Nuclear Accident for Improving Safety of U.S. Nuclear Plants. National Academies Press, Washington, D.C. https://doi.org/10.17226/18294

NCRP, 2014. Report No. 175 – Decision Making For Late-Phase Recovery From Major Nuclear Or Radiological Incidents. National Council on Radiation Protection and Measurements, Bethesda, Maryland.

NEA, 2018. Status of Practice for Level 3 Probabilistic Safety Assessments. OECD Nuclear Energy Agency (NEA), Paris, France.

Nisbet, A., Brown, J., Cabianca, T., Jones, A.L., Andersson, K.G., Hänninen, R., Ikäheimonen, T., Kirchner, G., Bertsch, V., Hiete, M., 2010. Generic handbook for assisting in the management of contaminated inhabited areas in Europe following a radiological emergency, Version 2. ed.

Nisbet, A., Watson, S., 2018. UK Recovery Handbooks for Radiation Incidents 2015. Inhabited Areas Handbook. Version 4.1. Public Health England, Chilton, Didcot,

Oxfordshire.

NRC, 2014. The Science of Responding to a Nuclear Reactor Accident: Summary of a Symposium. National Academies Press (US), Washington, D.C.

OpenStreetMap contributors, 2021. OpenStreetMap [WWW Document]. URL https://www.openstreetmap.org (accessed 1.26.21).

Pappas, C., Ikonomopoulos, A., Sfetsos, A., Andronopoulos, S., Varvayanni, M., Catsaros, N., 2014. Derivation of the source term, dose results and associated radiological consequences for the Greek Research Reactor – 1. Nucl. Eng. Des. 274, 100–117. https://doi.org/10.1016/j.nucengdes.2014.04.008

Park, Y., Park, D.J., 2024. System dynamics approach for assessing the performance of safety management systems in petrochemical plants. J. Loss Prev. Process Ind. 90, 105324. https://doi.org/10.1016/j.jlp.2024.105324

Peníze.cz, 2023. Kalkulačka inflace: jak se znehodnocuje česká koruna? [Inflation calculator: how does the Czech crown depreciate?] [WWW Document]. URL https://www.penize.cz/kalkulacky/znehodnoceni-koruny-inflace (accessed 11.20.23).

QGIS Development Team, 2021. QGIS.

Qiao, Y., Gao, X., Ma, L., Chen, D., 2024. Dynamic human error risk assessment of group decision-making in extreme cooperative scenario. Reliab. Eng. Syst. Saf. 249, 110194. https://doi.org/10.1016/j.ress.2024.110194

R Core Team, 2022. R: A language and environment for statistical computing.

Raskob, W., Landman, C., Trybushnyi, D., 2016. Functions of decision support systems (JRodos as an example): overview and new features and products. Radioprotection 51, S9–S11. https://doi.org/10.1051/radiopro/2016015

Raskob, W., Trybushnyi, D., Ievdin, I., Zheleznyak, M., 2011. JRODOS: Platform for improved long term countermeasures modelling and management. Radioprotection 46, 731–736. https://doi.org/10.1051/radiopro/20116865s

Robinson, R., 1993. Cost-benefit analysis. BMJ 307, 924–926. https://doi.org/10.1136/bmj.307.6909.924

RODOS team, 2013. Working with the ERMIN 2 model.

Roed, J., Andersson, K.G., Barkovsky, A.N., Fogh, C.L., Mishine, A.S., 1998. Mechanical decontamination tests in areas affected by the Chernobyl accident. Risø National Laboratory, Roskilde.

Rooney, M., Nuttall, W.J., Kazantzis, N., 2015. A dynamic model of the global uranium

market and the nuclear fuel cycle. Resour. Policy 43, 50–60. https://doi.org/10.1016/j.resourpol.2014.11.003

Rosenthal, J.J., de Almeidat, C.E., Mendonca, A.H., 1991. The Radiological Accident in Goiania: the initial remedial actions. Health Phys. 60, 7–15. https://doi.org/10.1097/00004032-199101000-00001

Rulík, P., Helebrant, J., 2011. Mapa kontaminace půdy České republiky 137Cs po havárii JE Černobyl [The map of contaminated soil with 137Cs in Czechia after the Chernobyl accident].

Rutledge, G.K., Alpert, J., Stouffer, R., Lawrence, B., 2003. The NOAA Operational Model Archive and Distribution System (NOMADS), in: Realizing Teracomputing. World Scientific, pp. 106–129. https://doi.org/10.1142/9789812704832_0009

Schneider, T., Gering, F., Charron, S., Zhelezniak, M., Andronopoulos, S., Heriard-Dubreuil, G., Camps, J., Raskob, W., 2017. Nuclear and radiological preparedness: The achievements of the European research project PREPARE. Radiat. Prot. Dosimetry 173, 151–156. https://doi.org/10.1093/rpd/ncw318

Schreurs, M.A., 2021. Reconstruction and revitalization in Fukushima a decade after the "triple disaster" struck: Striving for sustainability and a new future vision. Int. J. Disaster Risk Reduct. 53, 102006. https://doi.org/10.1016/j.ijdrr.2020.102006

Selivanova, A., 2022. Application of a System Dynamics Model of Recovery, in: Vojáčková, H. (Ed.), 40th International Conference on Mathematical Methods in Economics (MME 2022) – Conference Proceedings. 7-9.9.2022, Jihlava, Czech Republic. College of Polytechnics Jihlava, Jihlava, Czech Republic, pp. 325–330.

Selivanova, A., 2021. The System Dynamics approach to creation of a recovery model of an urban object, in: Hlavatý, R. (Ed.), 39th International Conference on Mathematical Methods in Economics (MME 2021) – Conference Proceedings. 8-10.9.2021, Prague, Czech Republic. Czech University of Life Sciences Prague, Prague, Czech Republic, pp. 429–434.

Selivanova, A., 2020a. Sensitivity Analysis of a System Dynamics Decontamination Model, in: Kapounek, S., Vránová, H. (Eds.), 38th International Conference on Mathematical Methods in Economics (MME 2020) – Conference Proceedings. 9-11.9.2020, Brno, Czech Republic. Mendel University in Brno, Brno, Czech Republic, pp. 523–529.

Selivanova, A., 2020b. Creation of a Model of Waste Handling Within Recovery After a Nuclear Accident Using the System Dynamics Approach, in: ICRP International

Conference on Recovery After Nuclear Accidents. Radiological Protection Lessons from Fukushima and Beyond, 1-4.12.2020, on-Line.

Selivanova, A., 2019. Cost-benefit analysis of decontamination in late-phase recovery from a nuclear accident. Czech University of Life Sciences Prague.

Selivanova, A., Ferretto, D., Mazzini, G., Hrehor, M., 2022a. Simulace následků dlouhodobé ztráty napájení bloku VVER-1000 Záporožské jaderné elektrárny [Simulations of Consequences of a Long-Term Station Blackout in a VVER-1000 in of Zaporizhzhya Nuclear Power Plant]. Jad. Energ. 4, 10–15.

Selivanova, A., Hůlka, J., Kotík, L., Kuča, P., Helebrant, J., Rubovič, P., Malátová, I., Koc, J., Vlček, O., 2022b. Pilot study of simulations of routine atmospheric discharges transport using the JRODOS system. Prague, Czech Republic.

Selivanova, A., Hůlka, J., Kotík, L., Kuča, P., Rubovič, P., Malátová, I., Helebrant, J., Koc, J., Rulík, P., Vlček, O., 2023. Advanced simulation techniques for the transport of routine atmospheric discharges using the JRODOS system. Prog. Nucl. Energy 157. https://doi.org/10.1016/j.pnucene.2023.104596

Selivanova, A., Hůlka, J., Vrba, T., Češpírová, I., 2019. Efficiency calibration of a CZT detector and MDA determination for post accidental unmanned aerial vehicle dosimetry. Appl. Radiat. Isot. 154, 108879. https://doi.org/10.1016/j.apradiso.2019.108879

Selivanova, A., Krejčí, I., 2019. Simulations of decontamination scenarios using the system dynamics approach, in: 5th NERIS Workshop Proceedings – Key Challenges in the Preparedness, Response and Recovery Phase of a Nuclear or Radiological Emergency. 3-5 April 2019, Roskilde, Denmark. Centre d'étude sur l'Evaluation de la Protection (CEPN), pp. 38–43.

Selivanova, A., Krejčí, I., Sedlářová-Nehézová, T., 2022c. The dynamical model of recovery after radioactive contamination, in: Proceedings of the 40th International System Dynamics Conference, July 18-22, 2022. System Dynamics Society, Frankfurt, Germany.

Selivanova, A., Krejčí, I., Sedlářová-Nehézová, T., Hůlka, J., Češpírová, I., Kuča, P., 2025. Creation of a System Dynamics model of recovery of affected areas after radioactive contamination. Reliab. Eng. Syst. Saf. 260, 111031. https://doi.org/10.1016/j.ress.2025.111031

Severa, J., Bár, J., 1985. Kontaminace radioaktivními látkami a dekontaminace

[Contamination with radioactive substances and decontamination]. Československá komise pro atomovou energii, Prague.

Steinhauser, G., Brandl, A., Johnson, T.E., 2014. Comparison of the Chernobyl and Fukushima nuclear accidents: A review of the environmental impacts. Sci. Total Environ. 470–471, 800–817. https://doi.org/10.1016/j.scitotenv.2013.10.029

Sterman, J.D., 2000. Business Dynamics: Systems Thinking and Modeling for a Complex World. McGraw-Hill Education, Boston.

SÚJB, 2021. IAEA Advisory Mission: Nuclear security in the Czech Republic is robust [WWW Document]. URL https://www.sujb.cz/en/news/detail/iaea-advisory-mission-nuclear-security-in-the-czech-republic-is-robust (accessed 6.20.22).

SÚJB, 2020a. Monitorování radiační situace.

SÚJB, 2020b. National Radiation Emergency Plan. State Office for Nuclear Safety, Prague, Czech Republic.

SÚJB, 2019. The Czech Republic National Report under the Convention on Nuclear Safety. Prague, Czech Republic.

SÚJB, 2016. Implementing decree 422/2016 Coll., on Radiation Protection and Security of a Radioactive Source.

SÚJB, 2010. Pravděpodobnostní hodnocení bezpečnosti. Bezpečnostní návod JB-1.6 [Probabilistic safety assessments. Safety instructions JB-1.6].

System Dynamics Society, 2024. System Dynamics Society [WWW Document]. URL https://www.systemdynamics.org/ (accessed 3.17.25).

System Dynamics Society, 2023. System Dynamics Bibliography [WWW Document]. URL https://www.systemdynamics.org/bibliography (accessed 6.23.23).

Takahashi, J., Tamura, K., Suda, T., Matsumura, R., Onda, Y., 2015. Vertical distribution and temporal changes of 137 Cs in soil profiles under various land uses after the Fukushima Dai-ichi Nuclear Power Plant accident. J. Environ. Radioact. 139, 351–361. https://doi.org/10.1016/j.jenvrad.2014.07.004

Taylor, T.R.B., Ford, D.N., Reinschmidt, K.F., 2012. Impact of Public Policy and Societal Risk Perception on U.S. Civilian Nuclear Power Plant Construction. J. Constr. Eng. Manag. 138, 972–981. https://doi.org/10.1061/(ASCE)CO.1943-7862.0000516

The Asahi Shimbun, 2022. Radioactive waste stuck at 830 sites with nowhere to go [WWW Document]. URL https://www.asahi.com/ajw/articles/14562951 (accessed 7.26.23).

The Guardian, 2019. Fukushima grapples with toxic soil that no one wants [WWW

Document]. URL https://www.theguardian.com/world/2019/mar/11/fukushima-toxic-soil-disaster-radioactive (accessed 7.26.23).

The Guardian, 2012. The story of Sellafield nuclear power station – in pictures [WWW Document]. URL https://www.theguardian.com/environment/gallery/2012/mar/12/sellafield-nuclear-power-energy-in-pictures (accessed 11.24.23).

The Japan Times, 2022. Japan finish radioactive soil transfer to interim storage site [WWW Document]. URL https://nuclear-news.net/2022/03/14/japan-to-finish-radioactive-soil-transfer-to-interim-storage-site/ (accessed 7.26.23).

The Japan Times, 2015. Delivery of radioactive soil to interim storage begins in Fukushima [WWW Document]. URL https://www.japantimes.co.jp/news/2015/03/13/national/delivery-of-radioactive-soil-to-interim-storage-begins-in-fukushima/ (accessed 11.24.23).

Thykier-Nielsen, S., Deme, S., Mikkelsen, T., 1999. Description of the atmospheric dispersion module RIMPUFF.

Tichý, O., Evangeliou, N., Selivanova, A., Šmídl, V., 2025. Inverse modeling of 137Cs during Chernobyl 2020 wildfires without the first guess. Atmos. Pollut. Res. 16, 102419. https://doi.org/10.1016/j.apr.2025.102419

Torraco, R.J., 2003. Exogenous and Endogenous Variables in Decision Making and the Implications for HRD Research and Practice. Adv. Dev. Hum. Resour. 5, 423–439. https://doi.org/10.1177/1523422303257286

U.S. EPA, 2016. Current and Emerging Post-Fukushima Technologies, and Techniques, and Practices for Wide Area Radiological Survey, Remediation, and Waste Management. Office of Research and Development, Homeland Security Research Center, Washington, DC.

U.S. NRC, 2023. Regulatory Guide (RG) 1.183, Revision 1. Alternative Radiological Source Terms for Evaluating Design Basis Accidents at Nuclear Power Reactors. U.S. Nuclear Regulatory Commission (NRC).

U.S. NRC, 2003. Regulatory Guide (RG) 1.195. Methods and Assumptions for Evaluating Radiological Consequences of Design Basis Accidents at Light-Water Nuclear Power Reactors. U.S. Nuclear Regulatory Commission (NRC).

Uatom, 2023. Дезактивация [Decontamination] [WWW Document]. URL https://www.uatom.org/ru/yadernaya-y-radyatsyonnaya-bezopasnost/dezaktivatsiya

(accessed 11.24.23).

UNSCEAR, 2000. Sources and Effects of Ionizing Radiation. Official Records of the General Assembly UNSCEAR 2000 Report to the General Assembly, with Scientific Annexes. ANNEX A – Dose Assessment Methodologies. United Nations, New York.

UNSCEAR, 1988. Sources and Effects of Ionizing Radiation. 1988 Report to the General Assembly, with annexes. ANNEX D Exposures from the Chernobyl accident.

Ventana Systems, 2025. Vensim Help: Sensitivity Simulations (Monte-Carlo) [WWW Document]. URL https://www.vensim.com/documentation/sensitivity.html (accessed 3.7.25).

Ventana Systems, 2023a. Vensim. Vensim Softw.

Ventana Systems, 2023b. Vensim Help: Units Checking [WWW Document]. URL https://www.vensim.com/documentation/ref_units_check.html (accessed 6.20.23).

Wade, D.C., Yacout, A.M., Van Den Durpel, L., 2006. DANESS: a system dynamics code for the holistic assessment of nuclear energy system strategies, in: Proceedings of the 24th International Conference of the System Dynamics Society. System Dynamics Society, Nijmegen, The Netherlands.

Wallace, J.D., 2013. Monte Carlo modelling of large scale NORM sources using MCNP. J. Environ. Radioact. 126, 55–60. https://doi.org/10.1016/j.jenvrad.2013.06.009

Webb, G.A.M., Anderson, R.W., Gaffney, M.J.S., 2006. Classification of events with an off-site radiological impact at the Sellafield site between 1950 and 2000, using the International Nuclear Event Scale. J. Radiol. Prot. 26, 33–49. https://doi.org/10.1088/0952-4746/26/1/002

WENRA, 2014. Guidance Document. Issue F: Design Extension of Existing Reactors.

Womer, N.K., Bougnol, M.-L., Dula, J.H., Retzlaff-Roberts, D., 2006. Benefit-cost analysis using data envelopment analysis. Ann. Oper. Res. 145, 229–250. https://doi.org/10.1007/s10479-006-0036-5

Woo, T.H., 2018. Climate change modelling for nuclear industry in the aspect of energy consumption using system dynamics method. Int. J. Glob. Warm. 16, 136. https://doi.org/10.1504/IJGW.2018.10015778

Woo, T.H., 2014. Real time analysis for atmospheric dispersions for Fukushima nuclear accident: Mobile phone based cloud computing assessment. Ann. Nucl. Energy 63, 255–260. https://doi.org/10.1016/j.anucene.2013.07.020

Woodham, E., Cave, S., Gray, A., 2016. Simulation of the management and disposal of Low

Level Radioactive Waste in the United Kingdom, in: Proceedings of the 36th International Conference of the System Dynamics Society. System Dynamics Society, Reykjavík, Iceland.

Yin, S., Zhang, Y., Tian, W., Qiu, S., Su, G.H., Gao, X., 2016. Simulation of the small modular reactor severe accident scenario response to SBO using MELCOR code. Prog. Nucl. Energy 86, 87–96. https://doi.org/10.1016/j.pnucene.2015.10.007

Zemanová, J., Zykmund, Z., Sedláčková, V., Rafaelová, L., 2011. Česko neplánuje ochranná opatření kvůli jaderné krizi v Japonsku [The Czech Republic is not planning protective measures due to the nuclear crisis in Japan]. iRozhlas.

Zheleznyak, M., Dontchits, G., Dzjuba, N., Giginyak, V., Lyashenko, G., Marinets, A., Tkalich, P., 2003. RIVTOX–One dimensional model for the simulation of the transport of radionuclides in a network of river channels, RODOS Report WG4-TN (97) 05. https://doi.org/10.13140/RG.2.1.4071.8241

Zheleznyak, M., Heling, R., Raskob, W., 2002. Hydrological dispersion module of the decision support system RODOS. Radioprotection 37, C1-683-C1-688. https://doi.org/10.1051/radiopro/2002188

Talerko, M., Kovalets, I., Lev, T., Igarashi, Y., Romanenko, O., 2021. Simulation study of radionuclide atmospheric transport after wildland fires in the Chernobyl Exclusion Zone in April 2020. Atmos. Pollut. Res. 12, 193–204. https://doi.org/10.1016/j.apr.2021.01.010

Appendix A – Source Terms

Table A. 1. Source terms for VVER-440/V213 reactors (source: JRODOS, 2019 – extracted from software)

Source term	VVER440DBA1	VVER440DBA4	VVER440SEV1	VVER440SEV6	VVER440SEV7
Radionuclide			Activity (Bq)		
Ba-140	5.38E+08	5.22E+09	0	0	0
Cs-134	1.27E+09	1.19E+10	2.38E+13	2.43E+15	2.42E+16
Cs-137	1.58E+10	1.48E+11	1.52E+13	1.56E+15	1.55E+16
I-131	2.42E+12	2.90E+13	2.66E+14	2.72E+16	3.80E+17
I-132	2.12E+12	2.50E+13	3.82E+14	3.88E+16	5.44E+17
I-133	2.22E+12	2.64E+13	5.44E+14	5.54E+16	7.74E+17
I-134	4.06E+11	4.42E+12	6.00E+14	6.12E+16	8.57E+17
I-135	1.31E+12	1.56E+13	4.76E+14	4.86E+16	6.79E+17
Kr-85	5.34E+08	1.02E+09	2.41E+12	3.69E+14	7.76E+15
Kr-85m	7.54E+10	2.10E+11	1.02E+14	1.55E+16	5.90E+17
Kr-87	2.72E+10	9.66E+10	1.02E+14	3.11E+16	1.18E+18
Kr-88	1.31E+11	3.96E+11	2.93E+14	4.47E+16	1.69E+18
La-140	1.27E+07	1.17E+08	0	0	0
Sr-89	1.42E+08	1.37E+09	0	0	0
Sr-90	6.38E+05	6.18E+06	0	0	0
Xe-133	4.88E+12	9.42E+12	7.25E+14	1.11E+17	4.20E+18
Xe-135	1.48E+12	4.22E+12	1.39E+14	2.14E+16	8.11E+17
Total sum (Bq)	1.51E+13	1.15E+14	3.67E+15	4.59E+17	1.18E+19
Cs isotopes (Bq)	1.71E+10	1.60E+11	3.90E+13	3.99E+15	3.97E+16
Iodines (Bq)	8.47E+12	1.00E+14	2.27E+15	2.31E+17	3.23E+18
Noble gases (Bq)	6.59E+12	1.43E+13	1.36E+15	2.24E+17	8.48E+18

Appendix B – Costs

Table B. 1. Costs of items required for decontamination (source: own efforts)

Category	Item	Cost (rounded)		Year
Personal protective equipment	Dosimeter	13 ths.	CZK	2019
	Tyvek	220	CZK	2019
	Tychem	800	CZK	2019
	Respirator	100	CZK	2019
	Helmet	300	CZK	2019
	Mask	1.3 ths.	CZK	2019
	Filters	600	CZK	2019
	Goggles	400	CZK	2019
	Cotton gloves	5	CZK	2019
	Rubber gloves	50	CZK	2019
	Rubber boots	160	CZK	2019
	Reflective vest	50	CZK	2019
Access restriction (demarcation) equipment	Tape	160	CZK	2019
	Board	50	CZK	2019
	Fence	1 ths.	CZK	2019
Auxiliary equipment	Waste bag	300	CZK	2019
	Shovel	220	CZK	2019
	Broom	200	CZK	2019
	Garden cart	1.2 ths.	CZK	2019
	Chainsaw	21 ths.	CZK	2022
	Chainsaw charger	3.5 ths.	CZK	2022
	Chainsaw battery	7 ths.	CZK	2022
	Ladder	2.2 ths.	CZK	2022
	Axe	300	CZK	2022
	Cutters	1.5 ths.	CZK	2022
Resources	Cost of fuel	35	CZK/l	2019
	Cost of water	50	CZK/m^3	2019
	Wage for machinery operation under demanding conditions	500	CZK/h	2019
	Wage for manual labor under demanding conditions	400	CZK/h	2019
Agricultural machinery	Tractor	1.9 mln.	CZK	2019
	Excavator	1.5 mln.	CZK	2012
	Turf harvester	2.5 mln.	CZK	2014
	Tractor Zetor	877 ths.	CZK	2011
	Hose reel	39 ths.	CZK	2011
	Tripod	5 ths.	CZK	2021
	Pressure washer	1 mln.	CZK	2021
	Tatra	8 mln.	CZK	2020

Appendix C – MCNP Simulations

Code C 1. Monte Carlo task to calculate conversion coefficients for ^{137}Cs source located on building surfaces

```
Air sphere with r 5cm, Cs-137, building, h 1m, relax 1 mm, AKR
C ----------------Cells specification---------------------------------------------------
C ----------------Quasi-detector--------------------------------------------------------
1   6  -1.205e-3 -1                          $ sphere
C ----------------Envir-----------------------------------------------------------------
500 6  -1.205e-3 -500 499 #1                    $ air
501 10 -2.3   -500 -499                         $ building
900 0            500                          $ void

C ----------------Surface specif--------------------------------------------------------
1 sph  0 0 0  5                               $ sphere
499 pz -100                                   $ building surface
500 rpp -4000 4000  -4000 4000  -200 200          $ total env

C ----------------Task specification----------------------------------------------------
mode p
C ----------------Source----------------------------------------------------------------------
sdef par=2 pos 0 0 -101.000001 erg=0.661657 rad=d2 axs=0 0 1 ext=d4 cel=501
si2 0 5000
sp2 -21 1
si4 0 1
sp4 -31 10
C ----------------Importance------------------------------------------------------------
imp:p 1 1 1 0
C ----------------Tallies---------------------------------------------------------------
fc6 AKR
f6:p 1             $ Kerma
fm6 5.7672e-7      $ 1.602e-10 Gy.g/MeV x 3600 s/h -> in Gy/h/source prt
C
fc16 Ambient dose equi rate (ICRP 74)
f16:p 1            $ Kerma
fm16 5.8819e-7     $ AKR x yield x 1.2 -> in Sv/h/source prt
C
fc26 Effective dose rate (ICRP 74, ISO field)
f26:p 1            $ Kerma
fm26 3.4311e-7     $ AKR x yield x 0.7 -> in Sv/h/source prt
C ----------------Materials-------------------------------------------------------------
m6  6000 -0.000124   &
    7000 -0.755268   &
    8000 -0.231781   &
   18000 -0.012827       $ air, 4
m10 1000 -0.010000   &
    6000 -0.001000   &
    8000 -0.529107   &
   11000 -0.016000   &
   12000 -0.002000   &
   13000 -0.033872   &
   14000 -0.337021   &
   19000 -0.013000   &
   20000 -0.044000   &
   26000 -0.014000       $ Portland concrete, 98
C ----------------Other params----------------------------------------------------------
DXT:p 0 0 0   6 7   100 1e-15
prdmp 1e9  1e9  1
print
ctme 500
```

Code C 2. Monte Carlo task to calculate conversion coefficients for ^{134}Cs source located on building surfaces

```
Air sphere with r 5cm, Cs-134, building, h 1m, relax 1 mm, AKR
C ----------Cells specification----------
C ----------Quasi-detector----------
1   6  -1.205e-3 -1                          $ sphere
C ----------Envir----------
500 6  -1.205e-3 -500 499 #1                 $ air
501 10 -2.3   -500 -499                      $ building
900 0          500                           $ void

C ----------Surface specif----------
1 sph  0 0 0  5                              $ sphere
499 pz -100                                  $ building surface
500 rpp -4000 4000  -4000 4000  -200 200     $ total env

C ----------Task specification----------
mode p
C ----------Source----------
sdef par=2 pos 0 0 -101.000001 erg=d1 wgt=1.831 rad=d2 axs=0 0 1 ext=d4 cel=501
si1 l 0.60472 0.79586
sp1 d 0.9763 0.8547
si2 0 5000
sp2 -21 1
si4 0 1
sp4 -31 10
C ----------Importance----------
imp:p 1 1 1 0
C ----------Tallies----------
fc6 AKR
f6:p 1          $ Kerma
fm6 5.7672e-7   $ 1.602e-10 Gy.g/MeV x 3600 s/h -> in Gy/h/source prt
C
fc16 Ambient dose equi rate (ICRP 74)
f16:p 1         $ Kerma
fm16 5.8819e-7  $ AKR x yield x 1.2 -> in Sv/h/source prt
C
fc26 Effective dose rate (ICRP 74, ISO field)
f26:p 1         $ Kerma
fm26 3.4311e-7  $ AKR x yield x 0.7 -> in Sv/h/source prt
C ----------Materials----------
m6  6000 -0.000124   &
    7000 -0.755268   &
    8000 -0.231781   &
   18000 -0.012827       $ air, 4
m10 1000 -0.010000   &
    6000 -0.001000   &
    8000 -0.529107   &
   11000 -0.016000   &
   12000 -0.002000   &
   13000 -0.033872   &
   14000 -0.337021   &
   19000 -0.013000   &
   20000 -0.044000   &
   26000 -0.014000       $ Portland concrete, 98
C ----------Other params----------
DXT:p 0 0 0   6 7   100 1e-15
prdmp 1e9  1e9  1
print
ctme 500
```

Code C 3. Monte Carlo task to calculate conversion coefficients for ^{137}Cs source located on road surfaces

```
Air sphere with r 5cm, Cs-137, road, h 1m, relax 1 mm, AKR
C ----------Cells specification----------
C ----------Quasi-detector----------
1   6  -1.205e-3 -1                          $ sphere
C ----------Envir----------
500 6  -1.205e-3 -500 499 #1                 $ air
501 10 -2.5784   -500 -499                   $ asphalt
900 0            500                         $ void

C ----------Surface specif----------
1 sph  0 0 0  5                              $ sphere
499 pz -100                                  $ asphalt
500 rpp -4000 4000  -4000 4000  -200 200     $ total env

C ----------Task specification----------
mode p
C ----------Source----------
sdef par=2 pos 0 0 -101.000001 erg=0.661657 rad=d2 axs=0 0 1 ext=d4 cel=501
si2 0 5000
sp2 -21 1
si4 0 1
sp4 -31 10
C ----------Importance----------
imp:p 1 1 1 0
C ----------Tallies----------
fc6 AKR
f6:p 1           $ Kerma
fm6 5.7672e-7    $ 1.602e-10 Gy.g/MeV x 3600 s/h -> in Gy/h/source prt
C
fc16 Ambient dose equi rate (ICRP 74)
f16:p 1          $ Kerma
fm16 5.8819e-7   $ AKR x yield x 1.2 -> in Sv/h/source prt
C
fc26 Effective dose rate (ICRP 74, ISO field)
f26:p 1          $ Kerma
fm26 3.4311e-7   $ AKR x yield x 0.7 -> in Sv/h/source prt
C ----------Materials----------
m6  6000 -0.000124   &
    7000 -0.755268   &
    8000 -0.231781   &
   18000 -0.012827       $ air, 4
m10 1000 -0.007781   &
    6000 -0.076175   &
    7000 -0.000363   &
    8000 -0.459103   &
   11000 -0.011659   &
   12000 -0.021757   &
   13000 -0.051009   &
   14000 -0.231474   &
   16000 -0.002804   &
   19000 -0.017058   &
   20000 -0.084471   &
   22000 -0.003403   &
   23000 -0.000024   &
   25000 -0.000362   &
   26000 -0.031375   &
   28000 -0.000002   &
   82000 -0.001179       $ asphalt pavement, 19
C ----------Other params----------
DXT:p 0 0 0   6 7   100 1e-15
prdmp 1e9  1e9  1
print
ctme 500
```

Code C 4. Monte Carlo task to calculate conversion coefficients for ^{134}Cs source located on road surfaces

```
Air sphere with r 5cm, Cs-134, road, h 1m, relax 1 mm, AKR
C ----------Cells specification----------
C ----------Quasi-detector----------
1   6  -1.205e-3 -1                          $ sphere
C ----------Envir----------
500 6  -1.205e-3 -500 499 #1                 $ air
501 10 -2.5784   -500 -499                   $ asphalt
900 0            500                         $ void

C ----------Surface specif----------
1 sph  0 0 0  5                              $ sphere
499 pz -100                                  $ asphalt
500 rpp -4000 4000  -4000 4000  -200 200     $ total env

C ----------Task specification----------
mode p
C ----------Source----------
sdef par=2 pos 0 0 -101.000001 erg=d1 wgt=1.831 rad=d2 axs=0 0 1 ext=d4 cel=501
si1 l 0.60472 0.79586
sp1 d 0.9763 0.8547
si2 0 5000
sp2 -21 1
si4 0 1
sp4 -31 10
C ----------Importance----------
imp:p 1 1 1 0
C ----------Tallies----------
fc6 AKR
f6:p 1           $ Kerma
fm6 5.7672e-7    $ 1.602e-10 Gy.g/MeV x 3600 s/h -> in Gy/h/source prt
C
fc16 Ambient dose equi rate (ICRP 74)
f16:p 1          $ Kerma
fm16 5.8819e-7   $ AKR x yield x 1.2 -> in Sv/h/source prt
C
fc26 Effective dose rate (ICRP 74, ISO field)
f26:p 1          $ Kerma
fm26 3.4311e-7   $ AKR x yield x 0.7 -> in Sv/h/source prt
C ----------Materials----------
m6  6000 -0.000124   &
    7000 -0.755268   &
    8000 -0.231781   &
   18000 -0.012827       $ air, 4
m10 1000 -0.007781   &
    6000 -0.076175   &
    7000 -0.000363   &
    8000 -0.459103   &
   11000 -0.011659   &
   12000 -0.021757   &
   13000 -0.051009   &
   14000 -0.231474   &
   16000 -0.002804   &
   19000 -0.017058   &
   20000 -0.084471   &
   22000 -0.003403   &
   23000 -0.000024   &
   25000 -0.000362   &
   26000 -0.031375   &
   28000 -0.000002   &
   82000 -0.001179       $ asphalt pavement, 19
C ----------Other params----------
DXT:p 0 0 0   6 7   100 1e-15
prdmp 1e9  1e9  1
print
ctme 500
```

Code C 5. Monte Carlo task to calculate conversion coefficients for ^{137}Cs source located on vegetation

```
Air sphere with r 5cm, Cs-137, tree, r 3m, h 1m, relax 1 mm, AKR
C ----------Cells specification----------
C ----------Quasi-detector----------
1   6  -1.205e-3 -1                          $ sphere
C ----------Tree-source----------
2   7  -0.998207 -2                          $ tree
C ----------Envir----------
500 6  -1.205e-3 -500 #1 #2                  $ air
900 0            500                         $ void

C ----------Surface specif----------
1 sph  0 0 0  5                              $ sphere AKR
2 sph  400 0 0 300                           $ tree
500 rpp -2000 2000  -2000 2000  -1000 1000   $ total env

C ----------Task specification----------
mode p
C ----------Source----------
C ----------Source----------
sdef par=2 pos 400 0 0 erg=0.661657 rad=d2 cel=2
si2 0 299.999999
sp2 -21 2
C ----------Importance----------
imp:p 1 1 1 0
C ----------Tallies----------
fc6 AKR
f6:p 1            $ Kerma
fm6 5.7672e-7     $ 1.602e-10 Gy.g/MeV x 3600 s/h -> in Gy/h/source prt
C
fc16 Ambient dose equi rate (ICRP 74)
f16:p 1           $ Kerma
fm16 5.8819e-7    $ AKR x yield x 1.2 -> in Sv/h/source prt
C
fc26 Effective dose rate (ICRP 74, ISO field)
f26:p 1           $ Kerma
fm26 3.4311e-7    $ AKR x yield x 0.7 -> in Sv/h/source prt
C ----------Materials----------
m6  6000 -0.000124    &
    7000 -0.755268    &
    8000 -0.231781    &
   18000 -0.012827      $ air, 4
m7  1000 -0.111894    &
    8000 -0.888106      $ water, 354
C ----------Other params----------
DXT:p 0 0 0   6 7   100 1e-15
prdmp 1e9  1e9  1
print
ctme 500
```

Code C 6. Monte Carlo task to calculate conversion coefficients for ^{134}Cs source located on vegetation

```
 Air sphere with r 5cm, Cs-134, tree, r 3m, h 1m, relax 1 mm, AKR
C ----------------Cells specification---------------------------------------------------
C ----------------Quasi-detector---------------------------------------------------------
1   6  -1.205e-3 -1                          $ sphere
C ----------------Tree-source------------------------------------------------------------
2   7  -0.998207 -2                          $ tree
C ----------------Envir------------------------------------------------------------------
500 6  -1.205e-3 -500 #1 #2                    $ air
900 0            500                         $ void

C ----------------Surface specif---------------------------------------------------------
1 sph  0 0 0  5                              $ sphere AKR
2 sph  400 0 0 300                           $ tree
500 rpp -2000 2000  -2000 2000  -1000 1000          $ total env

C ----------------Task specification-----------------------------------------------------
mode p
C ----------------Source-----------------------------------------------------------------
sdef par=2 pos 400 0 0 erg=d1 wgt=1.831 rad=d2 cel=2
si1 l 0.60472 0.79586
sp1 d 0.9763 0.8547
si2 0 299.999999
sp2 -21 2
C ----------------Importance-------------------------------------------------------------
imp:p 1 1 1 0
C ----------------Tallies----------------------------------------------------------------
fc6 AKR
f6:p 1             $ Kerma
fm6 5.7672e-7       $ 1.602e-10 Gy.g/MeV x 3600 s/h -> in Gy/h/source prt
C
fc16 Ambient dose equi rate (ICRP 74)
f16:p 1             $ Kerma
fm16 5.8819e-7       $ AKR x yield x 1.2 -> in Sv/h/source prt
C
fc26 Effective dose rate (ICRP 74, ISO field)
f26:p 1             $ Kerma
fm26 3.4311e-7       $ AKR x yield x 0.7 -> in Sv/h/source prt
C ----------------Materials--------------------------------------------------------------
m6  6000 -0.000124    &
    7000 -0.755268    &
    8000 -0.231781    &
   18000 -0.012827        $ air, 4
m7  1000 -0.111894    &
    8000 -0.888106        $ water, 354
C ----------------Other params-----------------------------------------------------------
DXT:p 0 0 0   6 7   100 1e-15
prdmp 1e9  1e9  1
print
ctme 500
```

Appendix D – Stock and Flow Diagrams

Fig. D 1. Conversion of surface activity of ^{137}Cs to effective dose from fields (source: Selivanova et al., 2025: 12)

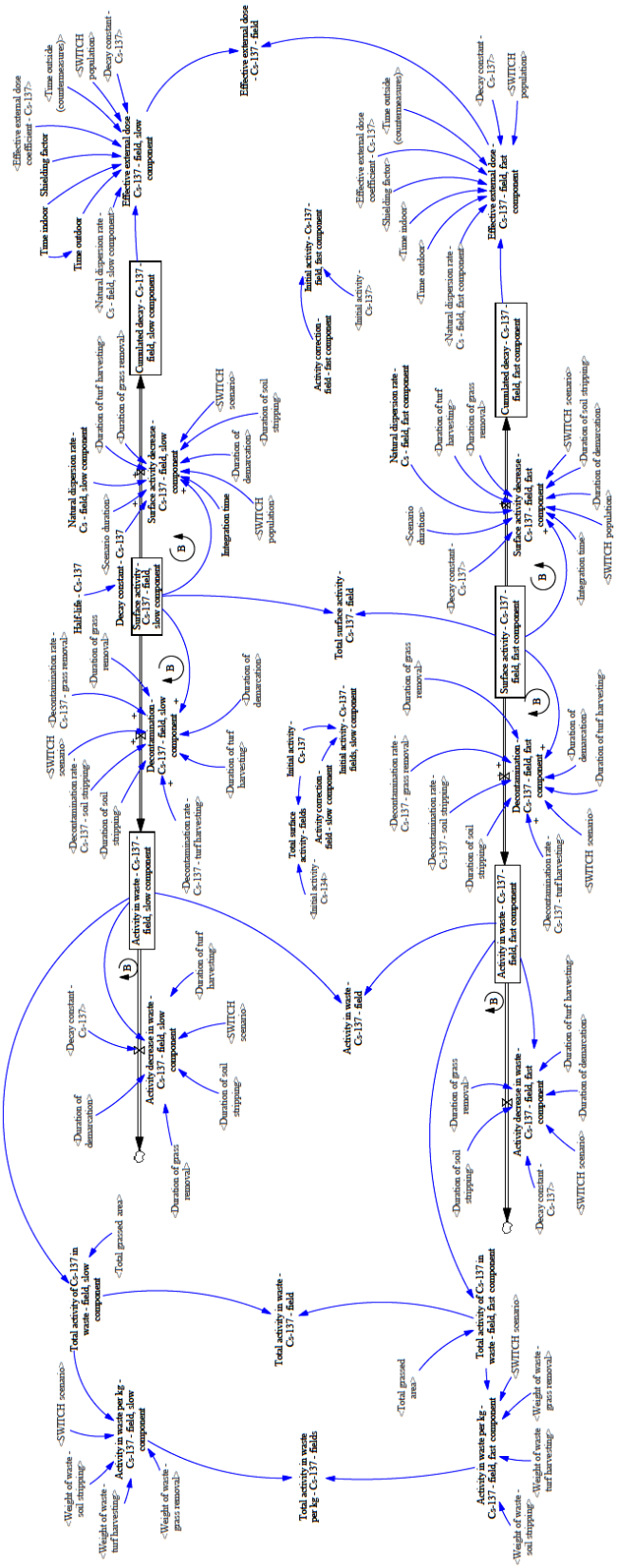

Fig. D 2. Conversion of surface activity of ^{137}Cs to effective dose from roads (source: Selivanova et al., 2025: 13)

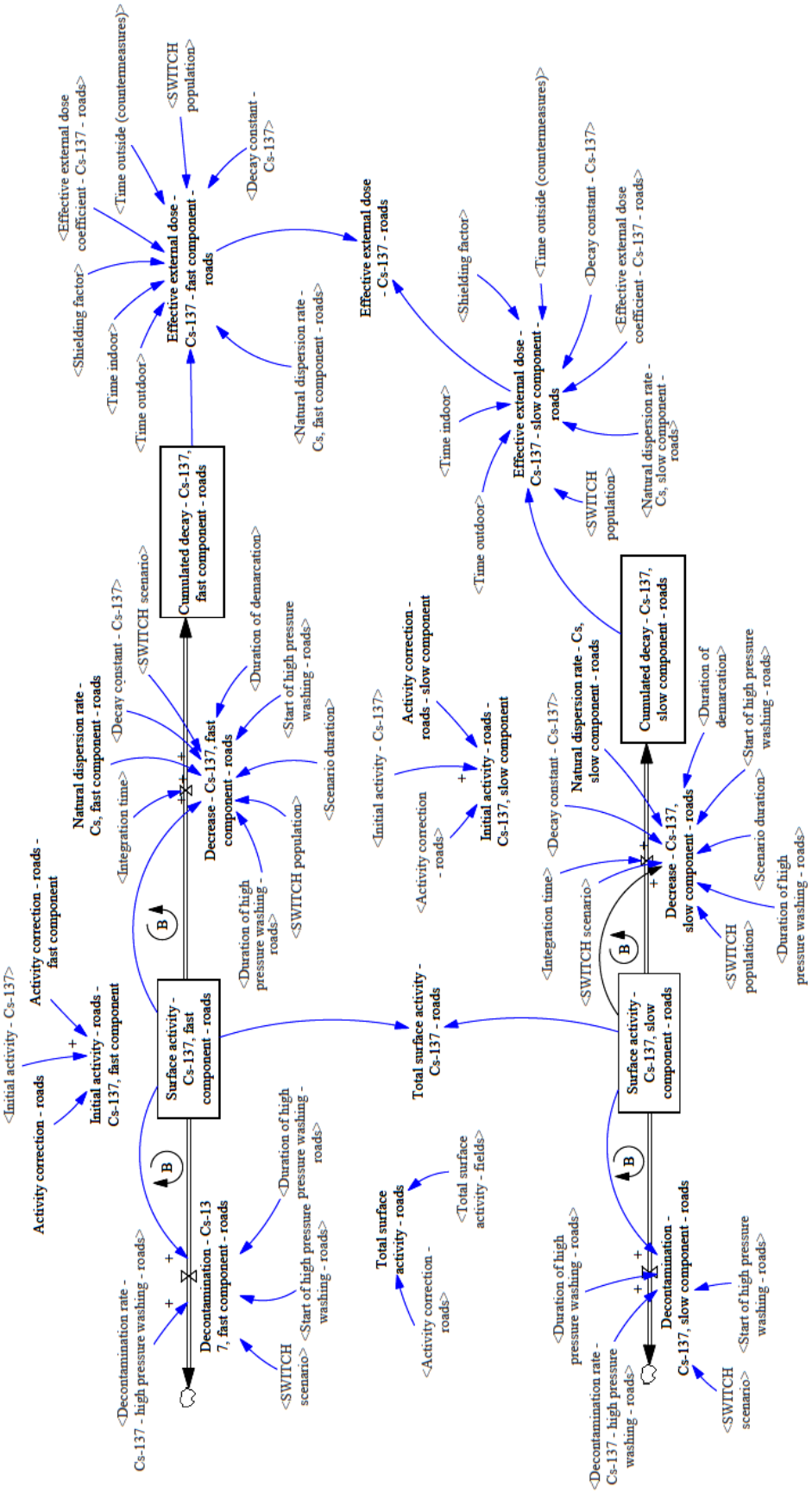

Fig. D 3. Conversion of surface activity to effective dose from shrubs/trees, a) ^{134}Cs, b) ^{137}Cs (source: Selivanova et al., 2025: 14)

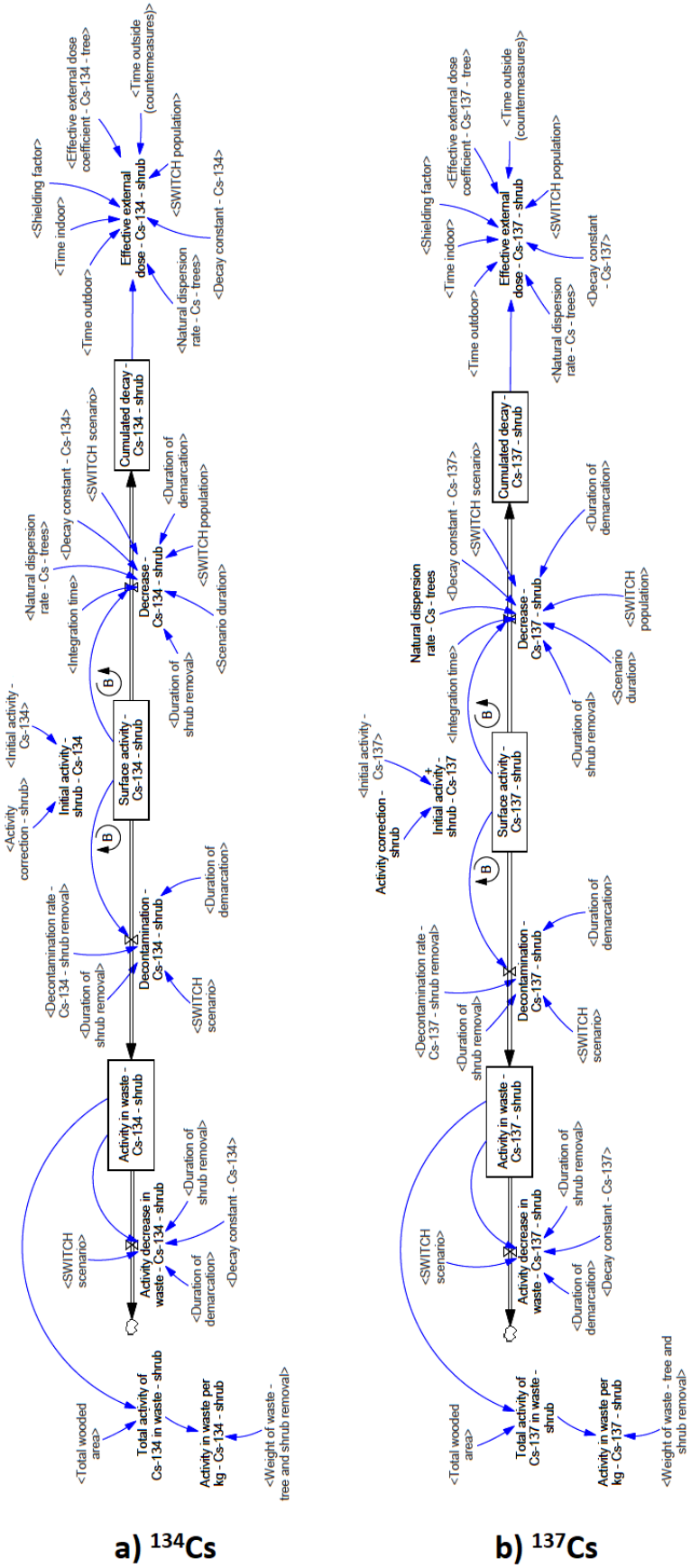

Fig. D 4. Conversion of surface activity of ^{137}Cs to effective dose from roofs (source: Selivanova et al., 2025: 15)

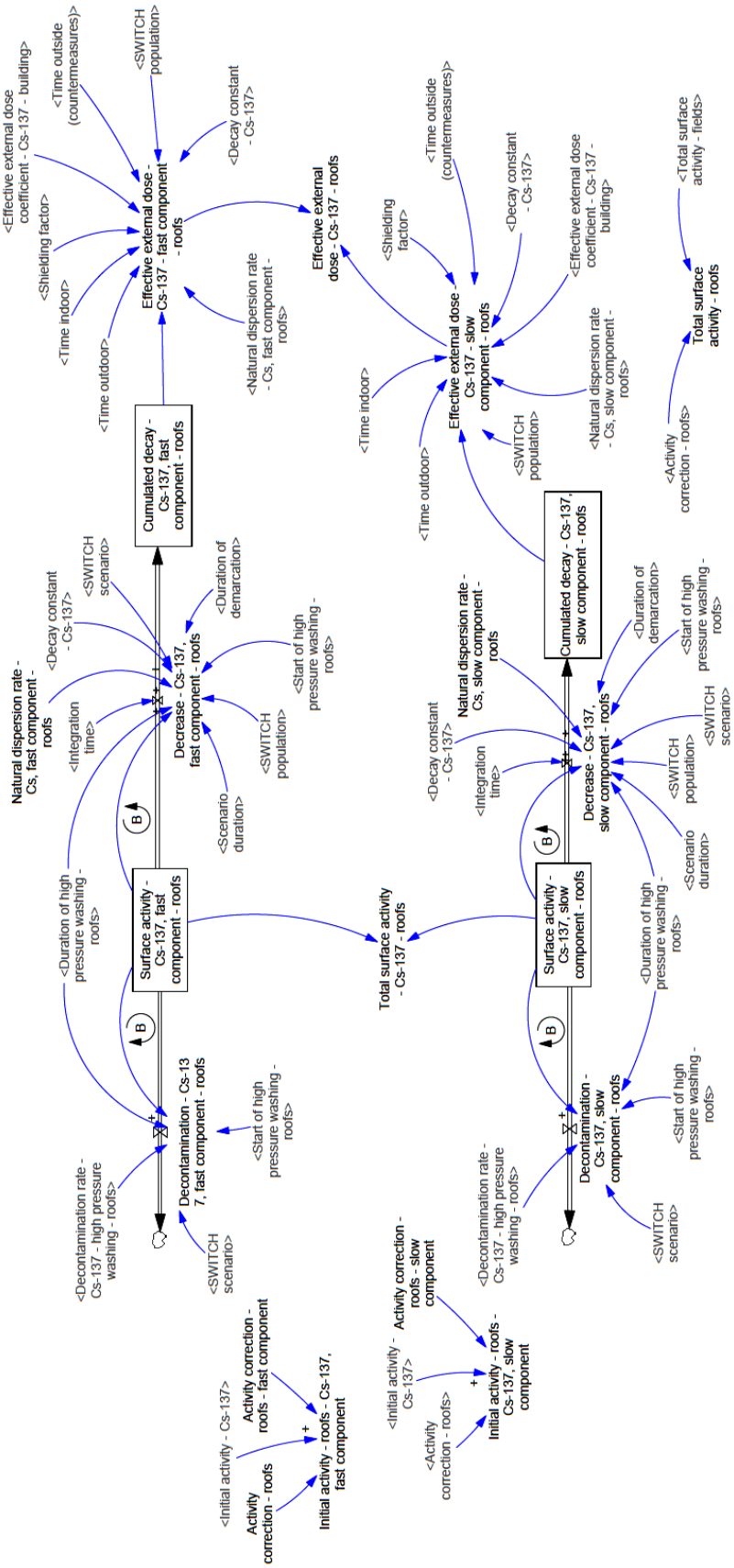

Fig. D 5. Conversion of surface activity to effective dose from walls, a) ^{134}Cs, b) ^{137}Cs (source: Selivanova et al., 2025: 16)

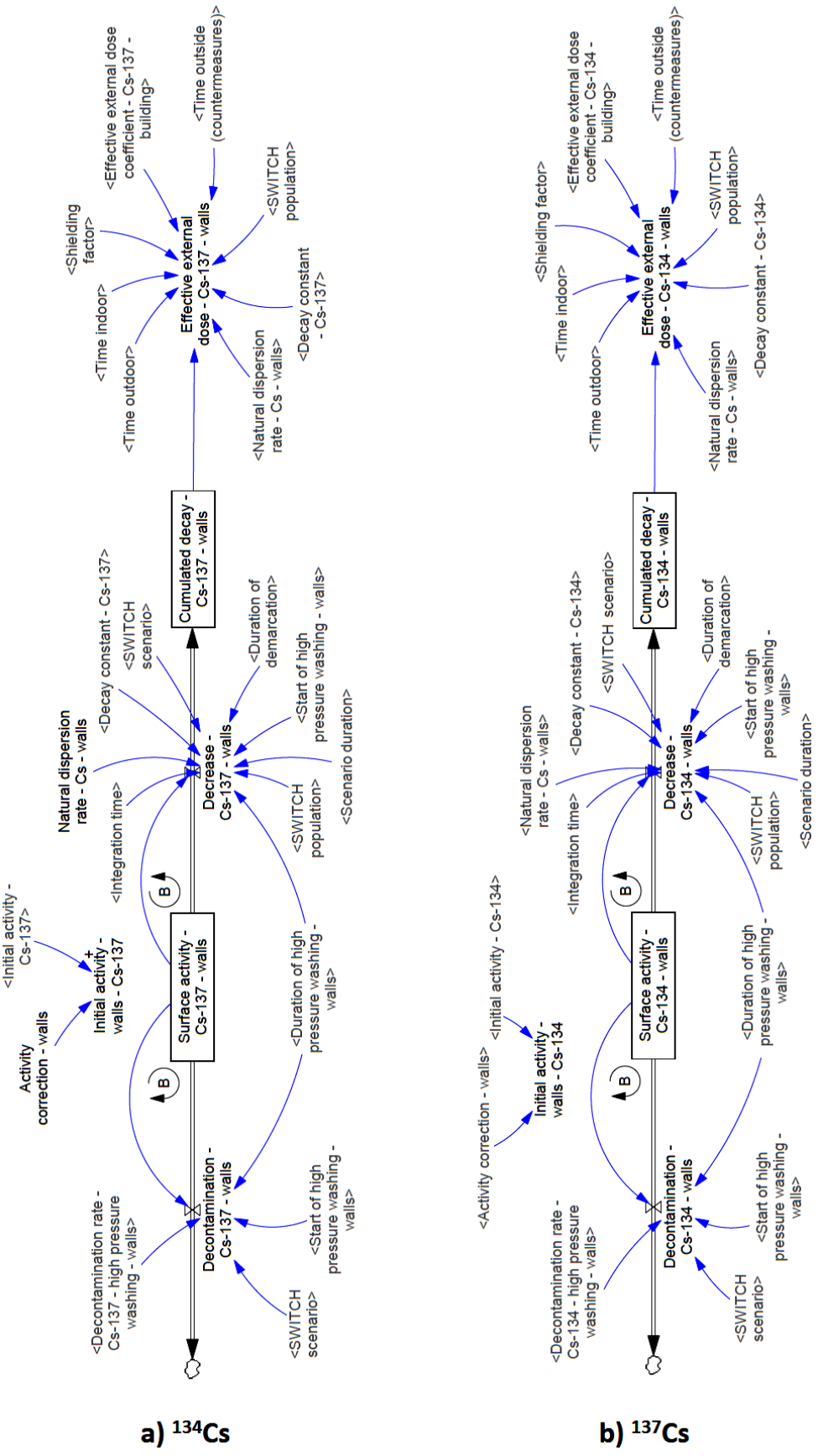

Appendix E – Dose Accumulation

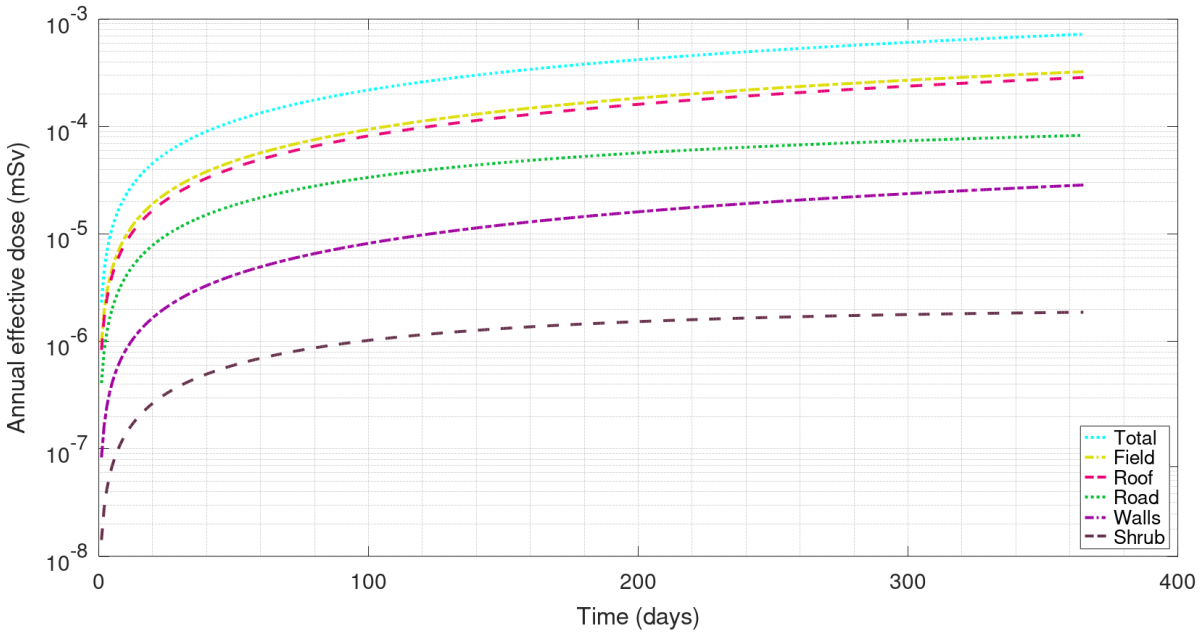

Fig. E 1. Maximum effective doses from selected urban and agricultural objects for DBA1 event, integrated over 1 year and simulated in the recovery model (no decontamination) (source: Selivanova et al., 2025: 17)

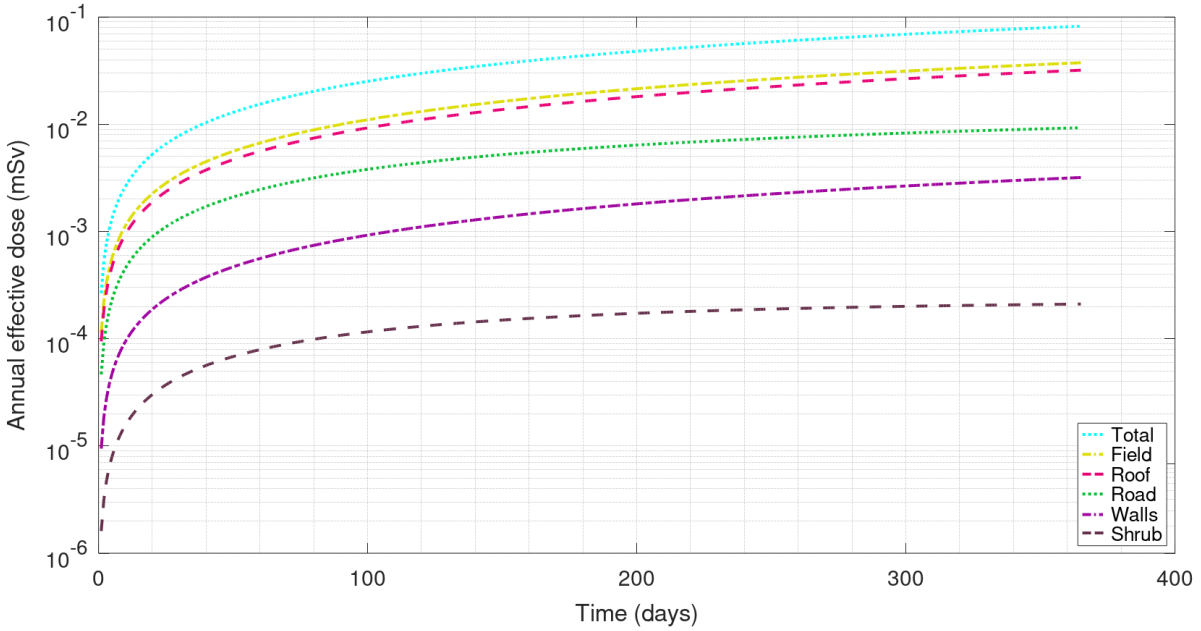

Fig. E 2. Maximum effective doses from selected urban and agricultural objects for DBA4 event, integrated over 1 year and simulated in the recovery model (no decontamination) (source: Selivanova et al., 2025: 17)

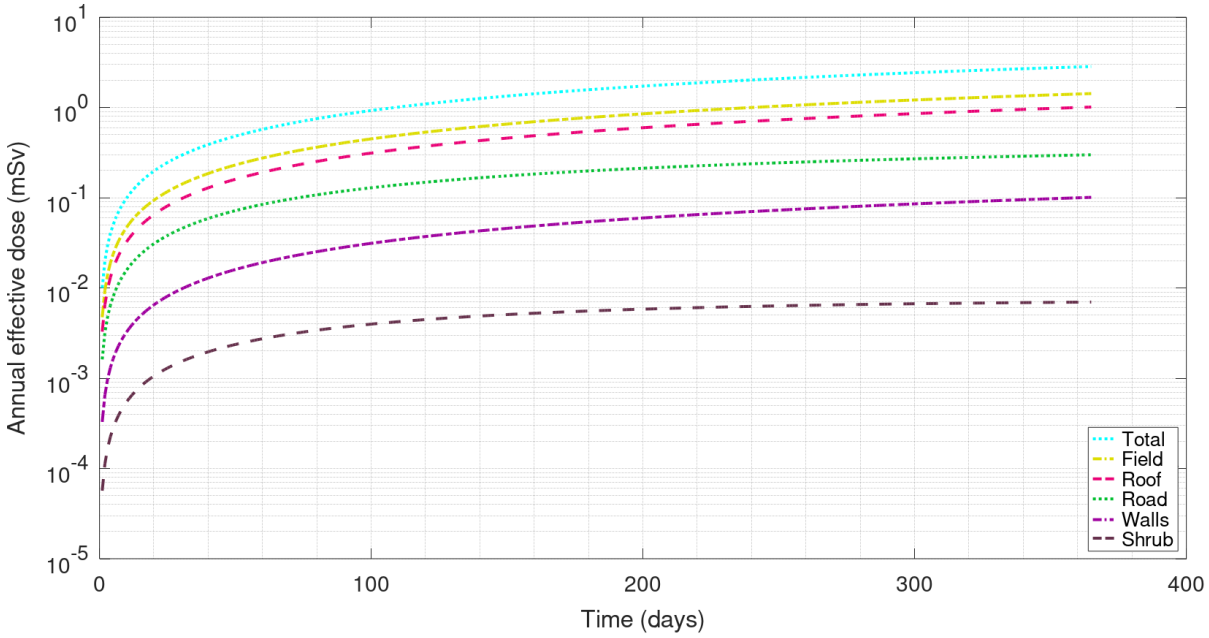

Fig. E 3. Maximum effective doses from selected urban and agricultural objects for SEV1 event, integrated over 1 year and simulated in the recovery model (no decontamination) (source: Selivanova et al., 2025: 18)

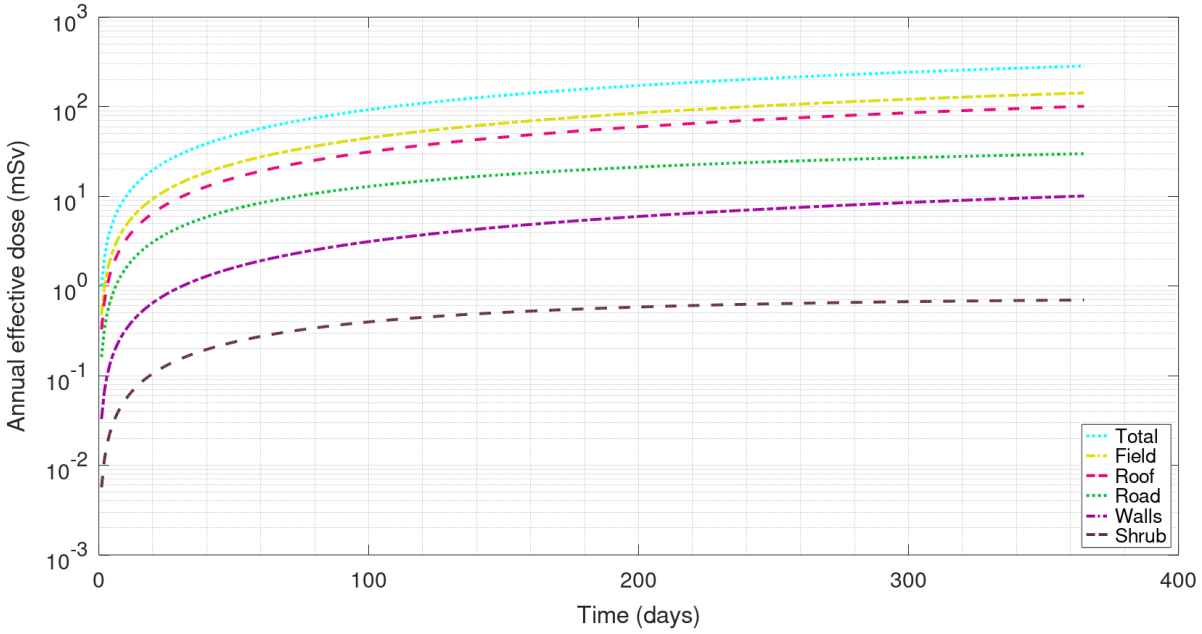

Fig. E 4. Maximum effective doses from selected urban and agricultural objects for SEV6 event, integrated over 1 year and simulated in the recovery model (no decontamination) (source: Selivanova et al., 2025: 18)

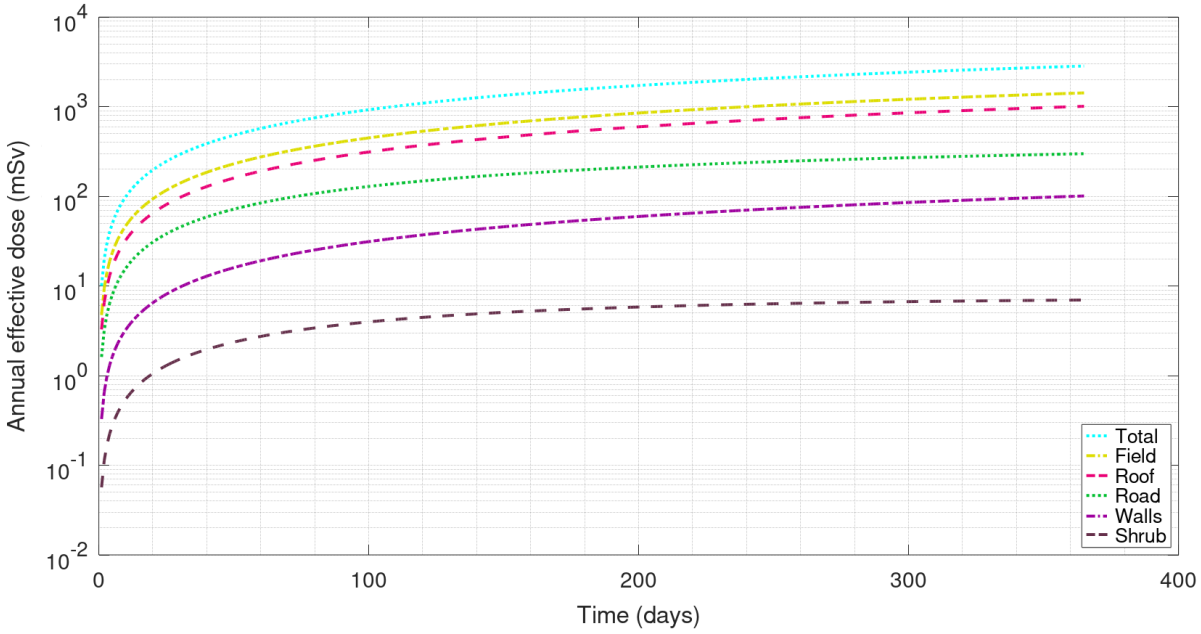

Fig. E 5. Maximum effective doses from selected urban and agricultural objects for SEV7 event, integrated over 1 year and simulated in the recovery model (no decontamination) (source: Selivanova et al., 2025: 19)

List of Figures

List of Tables

List of Acronyms

ADM	Atmospheric Dispersion Module
AgriCP	Agricultural Countermeasure Program
AHP	Analytic Hierarchy Process
ARGOS	Accident Reporting and Guiding Operational System
BfS	Bundesamt für Strahlenschutz
BWR	Boiling Water Reactor
CBA	Cost-Benefit Analysis
CDC	U.S. Centers for Disease Control and Prevention
CED	Collective Effective Dose
CEZ	Chernobyl Exclusion Zone
CI	Critical Infrastructure
CIP	Chemical Industrial Park
CLD	Causal Loop Diagram
CNB	Czech National Bank
CZSO	Czech Statistical Office
ČÚZK	State Administration of Land Surveying and Cadastre
DBA	Design Basis Accident
DEA	Data Envelopment Analysis
DEC	Design Extension Conditions
DF	Decontamination Factor
DHS	Department of Homeland Security
DMU	Decision Making Unit
DRR	Dose Rate Reduction
DSS	Decision Support System
ENSI	Swiss Federal Nuclear Safety Inspectorate
EPD	Electronic Personal Dosimeter
EPZ	Emergency Planning Zone
ERMIN	European Model for Inhabited Areas
EURATOM	European Atomic Energy Community
EURT	East Urals Radioactive Trace
FDNPP	Fukushima Daiichi Nuclear Power Plant

FEMA	Federal Emergency Management Agency
FHA	Fuel Handling Accidents
HDM	Hydrological Dispersion Module
HELDA	Helmholtz MCDA Tool
HEP	Human Error Probability
HRA	Human Reliability Analysis
CHMI	Czech Hydrometeorological Institute
IAEA	International Atomic Energy Agency
ICRP	International Commission on Radiological Protection
IDA	Intelligent Data Analysis
IGA FEM	Internal Grant Agency of Faculty of Economics and Management CZU Prague
IND	Improvised Nuclear Device
INES	International Nuclear and Radiological Event Scale
JRODOS	Java-based Real-time On-line Decision Support
KIT	Karlsruhe Institute of Technology
LANL	Los Alamos National Laboratory
LOCA	Loss-of-Coolant Accident
LP	Linear Program
MAVT	Multi-Attribute Value Theory
MCDA	Multi-Criteria Decision Analysis
MCNP	Monte Carlo N-Particle Transport Code
MELCOR	Methods of Estimation of Leakages and Consequences of Releases
MEXT	Ministry of Education, Culture, Sports, Science and Technology of Japan
MOE	Ministry of the Environment, Government of Japan
MOIRA-PLUS	MOdel-based Computerised System for Management Support to Identify Optimal Remedial Strategies for Restoring Radionuclide Contaminated Aquatic Ecosystems and Drainage Areas
NAPL	Non-Aqueous Phase Liquid
NCRP	National Council on Radiation Protection and Measurements

NFA	No Further Action
NOMADS	NOAA Operational Model Archive and Distribution System
NPP	Nuclear Power Plant
NRC	Nuclear Regulatory Commission
PPE	Personal Protective Equipment
PROMETHEE	Preference Ranking for Organization Method for Enrichment Evaluation
PSA	Probabilistic Safety Assessment
PSF	Performance Shaping Factor
RBMK	High-Power Channel-Type Reactor
RCS	Reactor Coolant System
RDD	Radiological Dispersal Device
RED	Radiological Exposure Device
RIMPUFF	Risø Mesoscale PUFF model
SA	Sensitivity Analysis
SDB	System Dynamics Bibliography
SD-EGT	System Dynamics and Evolutionary Game Theory
SEV	Severe Accident
SFD	Stock and Flow Diagram
SGTR	Steam Generator Tube Rupture
SMART	Simple Multi Attribute Rating Technique
SMR	Small Modular Reactor
SMS	Safety Management System
SPAR-H	Standardized Plant Analysis of Risk-Human Reliability Analysis
SÚJB	State Office for Nuclear Safety
SÚRO	National Radiation Protection Institute
SWING	Stakeholder Weighted Interactions and Negotiated Group
TCE	Trichloroethylene
TOPSIS	Technique for Order of Preference by Similarity to Ideal Solution
U.S. EPA	U.S. Environmental Protection Agency

U.S. NRC	U.S. Nuclear Regulatory Commission
UNSCEAR	United Nations Scientific Committee on the Effects of Atomic Radiation
USIE	Unified System for Information Exchange in Incidents and Emergencies
VIKOR	Multicriteria Optimization and Compromise Solution Method
VVER	Water-Water Energetic Reactor
WEB-HIPRE	Hierarchical preference analysis software
WENRA	Western European Nuclear Regulators' Association
WOS	Web of Science
WRM	Water Resource Management